

Fluid Jet Polishing

- possibilities and limitations of a new fabrication technique -

Fluid Jet Polishing

- possibilities and limitations of a new fabrication technique -

Proefschrift

ter verkrijging van de graad van doctor
aan de Technische Universiteit Delft,
op gezag van de Rector Magnificus prof.dr.ir. J.T. Fokkema,
voorzitter van het College voor Promoties,
in het openbaar te verdedigen

op maandag 22 september 2003 om 10.30 uur

door

Silvia Maria BOOIJ

natuurkundig ingenieur
geboren te Delft.

Dit proefschrift is goedgekeurd door de promotor:
Prof.dr.ir. J.J.M. Braat

Samenstelling promotiecommissie:

Rector Magnificus,	voorzitter
Prof.dr.ir. J.J.M. Braat	Technische Universiteit Delft, promotor
Prof.dr. S.D. Jacobs	University of Rochester, USA
Prof.dr. H.P. Herzig	University of Neuchâtel, Switzerland
Dr.Dipl.Phys. O.W. Föhnle	FISBA-Optik, Switzerland
Dr.ir. H. van Brug	TNO-TPD, Nederland
Prof.dr.ing. habil. B. Karpuschewski	Technische Universiteit Delft
Prof.dr.ir. L.J. van Vliet	Technische Universiteit Delft

Cover: Pieces of broken glass bottles rounded off by the erosive effect of the tidal movement of the sea.

ISBN 90-9017012-X

Copyright 2003 by S.M. Booij

All rights reserved. No part of the material protected by this copyright notice may be reproduced or utilised in any form or by any means, electronic or mechanical, including photocopying, recording or by any information storage and retrieval system, without priori written permission from the author: S.M. Booij, Delft, the Netherlands.

Printed in the Netherlands by PrintPartners IPSkamp B.V., Enschede

Table of contents

Table of contents	v
Chapter 1 Introduction	1
1.1 Scope and goal of the research	1
1.2 History of glass discovery, production and shaping	2
1.3 Outline of the thesis	3
Chapter 2 Production of optics - traditional and with FJP	5
2.1 Existing grinding and polishing techniques	7
2.1.1 Classical grinding and Preston's equation	7
2.1.2 Abrasive jet cutting	8
2.1.3 Water-jet cutting	8
2.1.4 Abrasive blasting	9
2.1.5 Classical polishing	10
2.1.6 Bowl feed polishing	11
2.1.7 Magneto Rheological Finishing	11
2.1.8 Ion beam assisted etching	11
2.2 Fluid Jet Polishing	12
2.2.1 The origin of FJP	12
2.2.2 Possible setup components	12
2.2.3 The experimental setup	13
2.2.4 Comparison between FJP and classical grinding or polishing	16
2.2.5 Advantages and risks of the FJP method	17
Chapter 3 Measurements	19
3.1 Surface characterisation parameters	19
3.2 Existing measurement techniques	21
3.2.1 Test plate	22
3.2.2 Line-scanning method	23
3.2.3 Nomarski microscope	23
3.2.4 Profilometer and interferometer	24
3.2.5 Scanning electron microscope	25
3.3 In-process roughness measurements using iTIRM	26
3.4 In-process shape measurements	28
3.4.1 Measurement setup	28
3.4.2 Temporal Phase Unwrapping	29

3.4.3 Experimental verification	31
3.4.4 Conclusions	33
Chapter 4 Models for FJP	35
4.1 Definitions	35
4.2 Crack formation	36
4.3 Theoretical pressure distribution in the slurry jet	38
4.4 Computation of the position of impacting particles in a flow	40
4.4.1 Computation of free streamlines under an angle	41
4.4.2 Computing intermediate streamlines	44
4.4.3 Computing the velocity from the stream function	46
4.4.4 Computing particle trajectories in the slurry	46
4.5 Microscopic model of material removal by one single slurry particle	50
4.5.1 Finite element approach	50
4.5.2 Simple estimation	50
4.5.3 Finnie's estimation	52
4.6 Removal profile over an area larger than the footprint	55
4.6.1 Theoretical influence of translation or rotation	55
4.6.2 Surface errors in the center of the work piece	58
4.6.3 Application - nozzle design	61
4.7 Final surface state (micro roughness)	62
Chapter 5 FJP process parameters	69
5.1 Description of the slurry	69
5.1.1 Particle concentration	69
5.1.2 Type and size of abrasive particles	70
5.1.3 Slurry temperature	74
5.1.4 Particle velocity measured with an LDA	74
5.2 Stand-off distance	78
5.3 Processing time	79
5.4 Processed material	81
5.5 Impact angle	83
5.6 Influence of the nozzle shape	85
Chapter 6 Implementation of FJP	89
6.1 Reproducibility	89
6.2 Homogeneity of a translating spot	91
6.3 Slurry degradation	93
6.4 Ripple formation / mid-spatial frequencies	94
6.5 Ductile or brittle removal?	97
6.6 Shaping	99
6.6.1 Rotation only	99
6.6.2 Flat center area	100
6.6.3 Producing some typical prescribed surfaces	104
6.7 Polishing	109

6.7.1 Roughness as a function of time and initial roughness	109
6.7.2 Roughness as a function of the pressure	112
6.7.3 Surface structure	113
6.7.4 Best roughness obtained	116
Chapter 7 Conclusions and suggestions	117
7.1 Conclusions	117
7.2 Alternative setup 1: Chemically assisted FJP etching	123
7.3 Alternative setup 2: The Jules Verne setup	124
7.3.1 Principle of material removal	126
7.3.2 Advantages and disadvantages of Jules Verne	127
7.3.3 Simulation of the flow	127
7.3.4 Initial experiments with JV	130
Appendix I Proof that the particle velocity equals the slurry velocity	133
Appendix II Glass and abrasive properties	135
II.1 Properties of glasses	135
II.2 Properties of abrasives	137
Appendix III Process parameters	141
Appendix IV Finnie's model for material removal	143
Index of symbols and subscripts	147
References	151
Summary	157
Samenvatting	159
Acknowledgements	161
Biography and publications	163

1 Introduction

Since glass was discovered and man learnt how to make lenses out of it, lenses have been applied in many devices like telescopes, microscopes, and spectacles. The areas in which lenses are used continue to grow. Many modern machines make use of lenses in some way, like computers, CD players, and digital cameras. The demands on the accuracy of their shape and on the quality of their surfaces also continue to grow. The use of aspherical surfaces and free-form surfaces is growing due to higher demands on image quality and this is made possible by the extra effort of designers and the increased computation power available for the design programs. Making surfaces that increasingly deviate from the spherical shape is a big challenge. The classical polishing technique is no longer capable of finishing the surface when the deviation from a spherical surface becomes too large. Some alternative techniques are available that can polish these surfaces, like magnetho-rheological finishing and stressed lap polishing. Another technique capable of polishing these extreme surfaces is the new technique that is the subject of this thesis: Fluid Jet Polishing (FJP).

This introductory chapter begins with the scope and goal of the research. Then a historical overview of the discovery, the production and the shaping of glass is given. This chapter concludes with the outline of the thesis, which is meant as a guide to the chapters most interesting to the reader.

1.1 Scope and goal of the research

The goal of this thesis is to investigate the possibilities and limitations of the Fluid Jet Polishing technique. The technique's current possibilities of both shaping and polishing will be presented. A more solid understanding of the process itself will be gained by models that have been developed for the process. Experiments will be presented to validate the relations between the adjustable parameters and the material removal rate and the roughness in the FJP process. Finally, some remarks will be made on the future abilities of the technique based on the presented experiments combined with an improved setup. Since measuring is essential for the accurate production of surfaces, adequate measuring techniques are also discussed. Two in-process measuring techniques will be presented, one for shape and one for roughness.

1.2 History of glass discovery, production and shaping

Natural glass has existed since the beginning of time. The definition of glass and some properties are given in Appendix II. Glass is formed when certain types of rock melt (e.g. by volcanic eruptions or lightning strikes) and then cool rapidly. Stone-age men are believed to have used cutting tools made of naturally occurring glass. Phoenician merchants transporting stone are said to have become aware of the existence of glass in the region of Syria around 5000 BC. They accidentally melted nitrite blocks placed by their fires, which then mixed with the sand of the beach and formed an opaque liquid [www1].

The first accounts of man-made glass objects date back to 3500 BC when non-transparent glass beads were made in Egypt and Eastern Mesopotamia. In the third millennium BC, in central Mesopotamia glazes were made to cover pots and vases, presumably to improve their water tightness. The production of hollow glass shapes started around the sixteenth century BC in Mesopotamia, Egypt, Greece, China and North Tyrol. The first glass-making manual dates back to around 650 BC. Instructions on how to make glass are contained in tablets from the library of the Assyrian king Ashurbanipal.

The discovery of glass blowing (between 27 BC and 14 AD) and the combination with using moulds increased the number of produceable shapes of glass. The Romans were the first to use glass for architectural purposes around 100 AD. From the year 1000 AD soda glass was gradually replaced by potash glass. Soda glass contains soda ash (sodium carbonate) which is usually derived from burnt marine vegetation, whereas potash glass contains potassium carbonate (usually derived from wood ash). Soda glass is cheaper but more soluble in water than potash glass.

The invention of spectacles by Salvino d'Armati degli Armati in about 1285 is an important event for the production of optics. In the early part of the seventeenth century the telescope and the microscope were invented and the production of spherical lenses therefore became an important factor in scientific development. The production process progressed from a primitive manual one to a lathe based one. Some of the lenses for Galilei's instruments were made in Florence between 1623 and 1653 using this new lathe-based approach. In 1671 the book by Père Chérubin d'Orléans titled 'La Dioptrique oculaire, ou la Théorique, la positive et la mécanique de l'oculaire dioptrique en toutes ses espèces' appeared. In this book he accurately describes the process of lens making and the various machines he has invented to reduce the labour intensity of the process.

The imaging properties of non-spherical surfaces were already known to Descartes (1596-1650), Huygens (1629-1695) and Newton (1643-1727), but the fabrication technology had not been developed far enough yet to produce useful aspheres in the seventeenth century [hor72]. Driven by the need to improve the imaging properties of telescopes, aspheres were proposed to be used. But it was not until the beginning of the twentieth century that the first large telescopes based on aspheres like the Ritchey-Chrétien design were built [twy42].

Whereas the window production had been done by pouring out molten glass onto a special table and rolling it out flat, and subsequently grinding and polishing it, a big invention for glass production for windows came in 1905 when a Belgian named Fourcault managed to draw a continuous sheet of glass from a tank. And the currently used process of float glass production was developed after the Second World War by Britain's

Pilkington Brothers Ltd. In this process molten glass is poured across a bath of molten tin, from which it is drawn horizontally. This process results in a homogeneous thickness and a surface finish acceptable for windows, so no post polishing is necessary.

Only very recently the asphere design and manufacturing has taken a high flight, driven by the need to accurately and cheaply produce small plastic objectives for optical disc players (Compact disk, DVD system). As time progresses the production of aspheres becomes cheaper and faster. A very large market for aspheres is that for the production of spectacle glasses.

1.3 Outline of the thesis

Since the work described in this thesis is meant for use in the regime of the optical world the terms that are used in this work correspond to the definitions of the optical world. When the term ‘grinding’ is used, this is not limited to the mechanical definition of a removal process that involves bonded abrasives [koe96], but loose abrasive grinding is also included. In order to judge the merits of the Fluid Jet Polishing (FJP) technique for shaping, shape corrections and surface roughness reduction, it is essential to know the capabilities of a number of existing techniques for grinding and polishing. How accurately can we shape or how finely can we polish with the existing techniques, and what are the limitations of those techniques? Therefore, Chapter 2 starts with a description of some existing grinding and polishing techniques. The chapter ends with a description of the Fluid Jet Polishing origin, setup and its advantages over existing techniques.

Since measuring is very important in the optical fabrication world, Chapter 3 is devoted to this subject. It starts with the definition of some surface characterisation parameters, then some existing shape and roughness measurement methods will be described that are currently in use in the optical industry. Contrary to the existing techniques it would be desirable to have a technique that measures in-process. Therefore this chapter will conclude with a description of two in-process techniques for measuring the roughness (iTIRM) and the shape of a surface (a custom-built interferometric setup). Both techniques have been developed at the same time as the FJP research was done, and could therefore be used in combination with FJP.

In order to get a better understanding of the FJP process, some of its aspects have been analysed and numerically evaluated in Chapter 4. In order to understand the difference between ductile and brittle mode material removal, an analysis for crack formation is quoted from the literature in Section 4.2. Two models from the literature for the pressure distribution in a slurry jet are presented in Section 4.3; from one of these models the shape of the stationary footprint of a cylindrical nozzle is deduced. The next section shows the computation of the position of impact of single particles when they are released in a typical FJP jet. In Section 4.5 three analyses are highlighted that describe the material removal at the microscopic level. Section 4.6 describes the material removal over areas larger than the footprint, and ends with an application of this model to the design of a nozzle with a specific footprint. The roughness of a surface is also an important issue. The simulation that has been carried out for the prediction of this roughness is presented in Section 4.7.

Experiments that have been carried out with the FJP setup are described in Chapters 5 and 6. Chapter 5 focuses on the effect the process parameters have on the resulting surface shape and roughness. The effects of the slurry, the processing time, the processed material, the impact angle and the nozzle shape are treated consecutively. Chapter 6 describes the experiments that show the potential applications of the process. First the reproducibility is investigated, followed by the homogeneity of a translating spot, then the degradation of the slurry is monitored, and the formation and removal of ripples or mid-spatial frequencies is treated. In Section 6.5 some arguments are presented with which the distinction between ductile and brittle material removal can be made. The last two sections of the chapter, Section 6.6 and Section 6.7, respectively, treat the shaping and polishing capabilities of the FJP system.

In the final chapter, Chapter 7, conclusions will be drawn on the possibilities of FJP and its limitations and suggestions for alternative setup components will be made. A new fabrication technique that is similar to FJP will also be presented as an alternative setup. This technique is called Jules Verne. Some initial experiments that have been carried out with this setup will be discussed.

Appendix I shows the calculations that prove that the velocity of the particles in the slurry have the same velocity as the slurry itself in the case of FJP. For the properties of glasses and abrasives Appendix II can be consulted. Appendix III consists of a table with an overview of all the important process parameters and some of their typical values. Appendix IV describes Finnie's model for material removal in more detail than mentioned in the main text of this thesis.

2 Production of optics - traditional and with FJP

In many areas of our daily life there is a need for transparent components with a specific shape. In this thesis we limit ourselves to the range from fairly inaccurate contact lenses and glasses to very high precision lenses for the projection of nanometer features on integrated circuits. The final desired shape of each of those lenses is obtained by four steps: sawing, drilling, grinding and polishing (accurate production would not be possible without measuring which is needed as feed-back). After an overview of the subjects that will be treated in this chapter the concepts of grinding and polishing will be explained in this introduction.

In Section 2.1 some existing grinding (Subsection 2.1.1 - Subsection 2.1.4) and polishing techniques (Subsection 2.1.5 - Subsection 2.1.8) will be discussed. Many more techniques exist, like computer controlled grinding [jon82], ultrasonic flow polishing [jon98], and laser polishing [veg98], but we restrict ourselves to the above mentioned techniques.

The new technique that is the subject of this thesis: Fluid Jet Polishing (FJP), is a shape correcting and roughness reducing technique. It will be described in Section 2.2. The origin and the setup will be described, a comparison will be made to classical grinding and some of the advantages of Fluid Jet Polishing will be listed.

It is important to know the difference between grinding and polishing. Therefore, the two concepts will be explained in more detail here. Grinding is a process that generates the desired shape of a surface. It has a high material removal rate, because the stress induced by the grinding particles on the surface is high enough to cause fracture. When fracture occurs the process is in 'brittle mode'. Unfortunately, grinding causes sub-surface damage: cracks are present just below the surface. This is an unwanted phenomenon because it causes light to scatter. Typically, surface roughness values are reduced from an initial value of $\sim 150 \mu\text{m}$ to a final value of $5 \mu\text{m}$ peak to valley (PV) by loose abrasive grinding. Fine grinding can reduce the roughness to 300 nm , and precision grinding can reduce the roughness to values as low as 10 nm PV . As a rule of thumb the amount of sub surface damage on a surface is approximately equal to the peak-to-valley roughness for loose abrasive grinding, it is always smaller than two times the peak-to-valley roughness [lam99]. This result is valid for a broad range of glasses and abrasives. The surface roughness is measured with a white light interferometry.

Polishing is a process used for the finishing of a component. The component is shaped to its final shape, the sub surface damage layer is removed and the roughness is reduced to less than 2 nm PV . The polishing process is a ductile one, i.e. it causes no fracture. Both chemical and mechanical effects are important in the polishing process. The polishing process consists of the following steps: water penetrates the glass surface, ions are

exchanged between modifier ions in the glass and hydrogen ions in the water, thus forming a hydrated layer. This layer is softer than the bulk of the glass. The polisher particles remove this softer layer by scraping or shearing off the glass surface [coo91]. Typically, average surface roughness values after polishing are less than 2 nm. Typical surface accuracies are better than $\lambda/5$ (100 nm). This is clearly a more severe demand than the standard specifications for mechanical surfaces.

The existing grinding and polishing techniques can be categorised according to their functioning principle [fah99a]. The principle that is best suited depends on the required shape of the specific optical surface. With respect to shape, surfaces can be divided in flats, spheres, rotationally symmetric aspheres, and non-symmetric aspheres which are also called 'free forms'. The shape generation can be done by a tool shape copying process or the surface evolution calculation principle can be used. In the case of tool shape copying the shape of the tool is transferred onto the shape to be produced, like for example in the case of a curve generator. In the case of a surface evolution calculation the shape of the tool or the processing time is computed and controlled as a function of the position, like it is done in computer numerically controlled (CNC) production or in the case of segmented lap polishing. The shaping tool can have a point contact, a line contact or an area contact with the surface to be produced. The contact can be a solid body one (two or three body), a fluid one or a gaseous one. Two body contact occurs when a tool and a sample are in contact, three body contact occurs when a hard tool, abrasive particles and a sample are in contact. The process can be load controlled or feed controlled. This has been summarized in Table 2.1.

Table 2.1 Tool contact methods and some examples

Tool	Processing area	Control	Abrasive	Example
solid body: three body	area	load	loose abrasives	loose abrasive grinding
solid body: two body	area	load feed	fixed abrasives	fixed abrasive grinding
fluid (solid particle erosion)	area point line	wear	solid particles	FJP
gaseous	area point line	wear	atoms / molecules	ion beam assisted etching

2.1 Existing grinding and polishing techniques

In this section some existing grinding and polishing techniques will be described. Classical grinding and polishing will be treated, because of their historical value and because they are still widely used owing to their accuracy. Some more recent techniques will be described if they have a connection to FJP.

2.1.1 Classical grinding and Preston's equation

The aim of grinding is to produce a surface as close to the desired shape as possible and to make the surface as smooth as possible in order to minimize the subsequent polishing time. The material removal rate is high as compared to polishing, because fracture is allowed to occur. To ensure that a smooth surface can result from an initially rough or wavy surface, more material should be removed from the higher parts of the surface than from the lower parts. This means that a rigid tool is needed.

In classical grinding a rigid iron or brass tool (the lap) is moved under pressure over a glass surface, or vice versa, with abrasive particles suspended in water between them, see Figure 2.1. The abrasives usually are silicon carbide or aluminum oxide particles (loose abrasive grinding). Typical material removal rates are 3 $\mu\text{m}/\text{min}$ for 5 μm particles to 90 $\mu\text{m}/\text{min}$ for 100 μm particles [lam99]. In stead of using loose abrasives in a slurry, diamond impregnated tools can also be used (fixed abrasive grinding). The water is used to cool the glass and the tool, to remove debris and to help circulate the particles between the glass and the tool. Classical grinding is a load controlled process, which means that the load on the lap is the parameter that is controlled, and not the in-feed rate. Because the load is only transferred to the glass where the abrasives make contact between the tool and the glass, and because the tool is a rigid one, high stresses are applied to the glass causing fracturing to occur [kir94]. When the tool and the sample are in contact over the entire surface the removal will occur over the entire surface. When contact only occurs at one small part of the surface the removal will be more rapid there, because locally much higher pressures can be obtained.

To predict the amount of removed material Preston's equation is widely used [pre27]. His equation predicts the wear W to be

$$W = \int Kpv dt, \quad (2.1)$$

in which K equals Preston's coefficient [$\text{m}^3\text{s}^2/\text{kg}$], which is a process dependent constant, p is the pressure applied to the tool [Pa], v is the velocity of the lap relative to the glass [m/s] and the integral is taken over the processing time t . Preston's coefficient incorporates all material properties and process parameters except the nominal pressure and the relative velocity [lam97].

Depending on the abrasives used and the removal speed, grinding can be a ductile or a brittle process. If chips of glass are removed by fracture as suggested above the process is clearly brittle. Classical grinding is by default a brittle process. If the grinding process is ductile, it should be stated explicitly to avoid confusion. Classical grinding is well suited for flat and spherical shapes. When sub-aperture tools are used or stressed laps, aspherical shapes can also be ground. Sub-aperture tools are tools that are much smaller than the

sample. Aspherical shapes can now be produced by controlling the position of the tool. Stressed laps are laps whose shape is controlled by actuators. During the entire grinding process the shape should be controlled as a function of the position of the lap with respect to the surface, in order to apply the required pressure to each position.

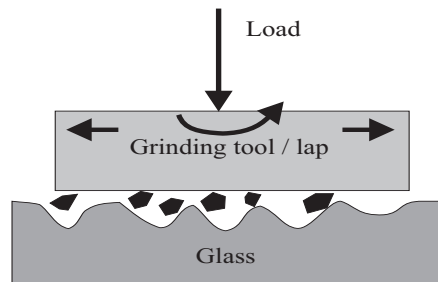


Fig. 2.1 Schematic picture of the grinding process (size of the abrasives exaggerated). The tool is rigid and does not deform.

2.1.2 Abrasive jet cutting

In abrasive jet cutting abrasives are mixed with water forming a slurry. The abrasives and the carrier fluid are accelerated to very high speeds (a few hundred meters per second). This high speed slurry reaches the sample and can cut or drill away material. Depending among others on the material that is being processed and the cutting velocity, the removal can be in the brittle or in the ductile regime. Brittle materials such as glass, ceramics or rock will usually show material removal by crack growth and intersection and most material will be removed for an angle of impact perpendicular to the surface. Ductile materials such as most metals will show a material removal in a regime where the material is either cut or caused to deform plastically under impact, in this case more material is removed when the abrasives impact at a more oblique angle. Models for both processes can be found in literature [pau98].

In order to transform the slow jet into a high speed one (a few hundred m/s), the nozzle should have a very narrow opening (some tenths to tens of mm). It should also be resistant to abrasive wear, therefore it has to be made from e.g. sapphire. The abrasives can be pre-mixed, mixed in the nozzle (see Figure 2.2) or two separate beams can come out of the nozzle and be combined in the air behind the nozzle. A result of the slurry being mixed in the nozzle is that the concentration of particles in the outer parts of the beam is higher than that in the center. The slurry can be re-used or can be used only once. The abrasive jet cutting process is mainly used for drilling and cutting of materials, not for the generation of (a)spherical surfaces, although it should be possible to do so.

2.1.3 Water-jet cutting

Water-jet cutting is a process that is related to abrasive slurry jet cutting. The main difference is that in water-jet cutting pure water is used at a high pressure, and no abrasives are added. The nozzle should be wear resistant again, because pure water at high pressure erodes the nozzle material.

In several textbooks extensive descriptions can be found about the fundamentals of water jetting, explanations of terms like nozzle, water-jet, orifice, descriptions of high pressure systems, cleaning applications, several applications of high pressure water-jets, theoretical considerations, safety, health etc. [sum95] [hoo00]. When cutting through a 1 mm thick ceramic plate (Al_2O_3) with water at 3000 bar typical cutting speeds of 24 mm/min. can be obtained. The roughness of the cut face is very high, and depends on many parameters, like the type of material that is being cut, the water pressure, and the cutting speed. Care has to be taken when using this method, because the water-jet can easily penetrate the skin at pressures above 160 bar. A pulsed jet can already damage the skin at pressures as low as 3.5 to 5 bar.

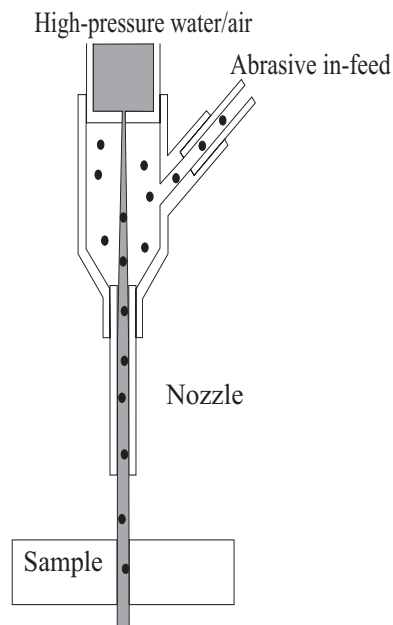


Fig. 2.2 Schematic drawing of a high speed abrasive jet cutting nozzle, where the in-feed of abrasives is separate from the high speed water flow. If the water is replaced by air an abrasive blasting nozzle results. If there is no abrasive in-feed a water jet cutting device results.

2.1.4 Abrasive blasting

An alternative to erosion with abrasives in a fluid is to use the abrasives and accelerate them in air [she66a] [she66b]. This can be done at various velocities, from a few meters per second to a few hundred meters per second. At low velocities this technique is used for cleaning of surfaces, at high velocities cutting and drilling is possible. Slurry erosion proceeds at a rate several times faster than that of air-borne particle erosion according to Zu [zu91]. This is due to the fact that particles are embedded in the surface in air-borne erosion, and are thereby hindering other particles in their attempt to erode the surface. The fluid that is present during slurry erosion ensures that this does not happen. Since the velocity of the slurry and the velocity of the particles are in the same order, enough water

particles will be present to remove the abrasive particles from the surface. The obtainable surface roughness is not as good as that obtained with traditional polishing. Two large disadvantages of using air as a carrier medium instead of water are that the beam is less well confined and the particles are sped up less effectively.

2.1.5 Classical polishing

Classical polishing is a chemo-mechanical process. The purpose of polishing is to shape within $\lambda/5$ or better, to remove all sub surface damage (SSD), and to reduce the peak to valley (PV) surface roughness to less than 5 nm. By definition surface fracture does not occur in the polishing process [cum95]. During classical polishing small abrasive particles ($< \sim 3 \mu\text{m}$) are moved over a glass surface. The particles are embedded in a visco-elastic (like pitch) or elastic (like felt or rubber) material, which is mounted on a lap, which has the inverse shape of the shape that is generated. This polishing lap is pressed against the surface and is forced to move over it, but it can rotate freely. In between the lap and the surface water is present [coo90].

A pitch lap will start off with particles on the pitch surface, but as a function of time more and more particles will be pressed into the pitch, until all particles are in contact with the surface, see Figure 2.3. During the polishing process fresh polishing particles are supplied continuously (hence the name ‘fresh feed’ polishing). Because the lap is deformable it will take on the shape of the surface. The lap shape can be changed by changing the process parameters such as e.g. the tool path, the workpiece-tool orientation and the rotary speed. Typical material removal rates for classical polishing are $0.5 \mu\text{m}/\text{min}$ [lam99]. Since the polishing process is ductile a low surface roughness can be obtained, just under 1 nm rms.

In the polishing process the material removal is much slower than during grinding. This is a direct consequence of the fact that the material removal is in the ductile regime. The same amount of material should be removed over the entire surface to increase the surface smoothness and to remove the subsurface defects. Because the polishing tool is in contact with the glass over a substantial part of the surface, and because they move with respect to each other, only flat and spherical surfaces can be polished using this technique. In principle aspheres could be polished classically when sub-aperture pads or specially shaped pads are used.

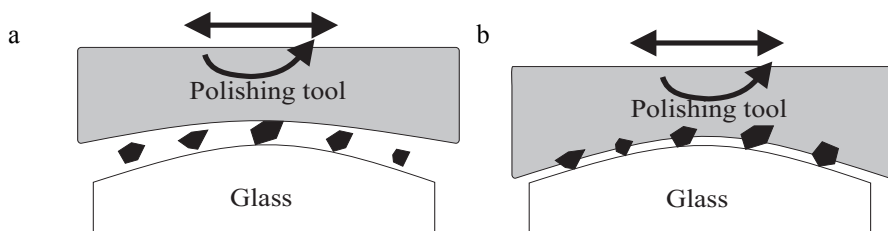


Fig. 2.3 Schematic drawing of the polishing process. a) At the beginning of the process. b) The process after some time. The polishing tool (lap) deforms to take on the shape of the glass and the abrasive particles are embedded in the lap. Water is present between the tool and the glass.

2.1.6 Bowl feed polishing

Bowl feed polishing is a polishing process usually applied to obtain a very low roughness (down to 0.1 nm rms) on flat glass or silicon surfaces. Like in classical polishing the process uses a deformable tool and abrasive particles in water. The difference is that the sample and the tool are immersed in the slurry, and that no slurry is added once the process has started. Due to the rotary speed of the tool with respect to the workpiece the abrasive particles slowly move towards the edge, and fall over the edge. The concentration of abrasives diminishes continuously resulting in the low final roughness [win92]. The material removal rate is much lower than in the case of classical polishing.

2.1.7 Magneto Rheological Finishing

Magneto Rheological Finishing (MRF) is a finishing technique in which a locally solidified fluid is used as a tool to process a surface. The fluid consists of magnetic particles (typically carbonyl iron), nonmagnetic abrasive particles, water and stabilising agents. The fluid flows from a nozzle to a collector over a rotating wheel, as can be seen in Figure 2.4. At the location of the sample a strong magnetic field hardens the fluid. This hardened fluid is the effective tool that removes material from the sample [jac99]. The process can be used on various optical materials. On optical glasses a typical removal rate of 10 $\mu\text{m}/\text{min}$ is observed and smoothing can be achieved up to ~ 1 nm rms. Form errors can be reduced from a few λ to $\lambda/5$ PV. MRF is a sub-aperture technique, which means that the removal spot is smaller than the total area that is being processed. Therefore care has to be taken when large amounts of material are removed over the entire surface. The generation of mid-spatial frequencies should be avoided.

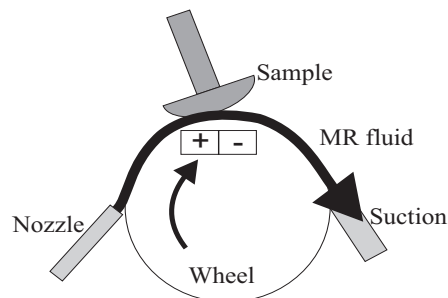


Fig. 2.4 Schematic view of the MRF setup. The magneto rheological (MR) fluid consists of magnetic particles, nonmagnetic abrasive particles, water and stabilising agents. The fluid flows from the nozzle to the suction device over the rotating wheel. At the location of the sample a magnetic field stiffens the fluid.

2.1.8 Ion beam assisted etching

Ion beam assisted etching is a very high precision shaping technique. A high energy beam of particles of atomic size (inert gas ions) impinges on a surface in high vacuum, knocking atoms out of the lattice. The beam can be smaller or larger than the sample. Ion beam assisted etching can be used for final figure and roughness corrections on metals, ceramics and semiconductor surfaces. In the fine correction step typical removal rates are 25-

200 nm/min., typical focused beam diameters are 50-200 μm [sha00]. Roughness reductions are possible to well below 0.5 nm peak to valley [whi94]. The ion beam assisted etching technique can also be used in a more coarse regime, where material removal rates are typically 10 mm^3/min , the shape errors are 1-2 μm , the micro roughness is 50-100 nm rms and no sub surface damage occurs [sch01]. The main disadvantage of this technique is that a high vacuum is needed. Advantageous is that it is possible to generate aspherical surfaces and that local corrections can be made.

2.2 Fluid Jet Polishing

Now that some existing techniques for grinding and polishing have been described, the origin and setup of the new technique that is the subject of this thesis (Fluid Jet Polishing) will be explained. In Subsection 2.2.1 the origin of FJP will be described, in Subsection 2.2.2 various options will be described for the components of which the FJP setup could be built. And the final choices that were made for the setup components will be clarified in Subsection 2.2.3. Then FJP will be compared to classical grinding in terms of the force between the particles and the surface in Subsection 2.2.4. Finally, in Subsection 2.2.5 the advantages of the FJP method will be listed.

2.2.1 The origin of FJP

A few years ago a new shaping and finishing technique was developed [fah98], [fah98b] called Fluid Jet Polishing (FJP). The principle of operation originates from two completely different techniques: abrasive slurry jet machining (see Subsection 2.1.2) and bowl feed polishing (Subsection 2.1.6). In slurry jet machining both ductile and brittle materials can be cut, owing to the very high pressures that are used. The surface quality of the resulting cut surface is not very good. The advantage of the second technique: bowl feed polishing is that an excellent surface quality can be obtained because the force that presses the abrasive particles against the lap is much smaller.

Fluid Jet Polishing is an intermediate method that can both shape and polish. It uses a slurry jet for shaping, but at a low pressure. Due to the fact that the particles move relatively slowly over the surface (compared to the velocities in abrasive jet cutting), the resulting surface quality is much better than in the case of abrasive jet cutting.

2.2.2 Possible setup components

The first requirement to produce an abrasive jet is to compose an abrasive slurry, either in the entire setup or in the last part of the nozzle only. The basis of the slurry can be e.g. water, oil or octanol, all of these liquids are used frequently in the optical fabrication industry. The abrasive particles in the slurry can be any grinding or polishing compound. Various sizes and concentrations of silicon carbide, aluminum oxide, diamond, glass beads, or steel shot could be used. The slurry has to be sprayed onto the surface material to be processed. This can be done by forcing it to go through a nozzle, by means of a pump of any kind, or by forcing the water out of its storage vessel by means of air pressure or a height difference. The nozzle can be an arbitrarily shaped tool that directs the water in a specific direction. The nozzle can be made from any material, like plastic,

wood, stainless steel, ceramics or sapphire. The advantage of the latter two materials is that they show much less wear than the other materials. The wear of these nozzles is not an issue since FJP uses a low pressure (up to 15 bar) while these nozzles are designed to withstand the high pressures used in water- or abrasive-jet cutting (a few hundred bar). The slurry could be re-used or it could be used only once. In the case of re-use of the slurry it is important to verify that the slurry is not contaminated by dust, dirt, glass particles or parts of the setup that have been worn.

2.2.3 The experimental setup

The FJP setup that was built consists of a few elements only. An overview of the setup can be found in Figure 2.5. In a tank, water and a grinding and/or polishing compound are mixed by mechanically stirring. The water with the homogeneously mixed particles in it is referred to as the slurry. This slurry is pumped from the tank by means of a low-pressure pump (0 to 15 bar) and guided through a nozzle. The nozzle is positioned above the surface being processed where the stand-off distance and the angle with respect to the surface normal can be chosen freely. The sample or workpiece can be rotated and translated in one direction with respect to the nozzle. After processing the surface, the slurry is collected and guided back to the tank for re-use. The slurry is not filtered in this setup.

In the setup used, a plastic food storage container is used as a tank. The stirrer is a rotation device with a cement stirrer, and two different pumps are available for use, a peristaltic and a membrane one. The workpiece is placed on a metal holder using wax, this holder is placed in a unit that can rotate. This unit is fixed on an aluminum tray, which can translate in one direction with respect to the nozzle that is fixed. The space between the nozzle and the workpiece is shielded by a plastic cover, which prevents the slurry from spraying through the surrounding area. Various kinds of nozzles can be used. The types that have been used most (and are described in this thesis) are metal and plastic nozzles that are designed for gluing applications and stainless steel nozzles that are designed for cleaning purposes. Various slurries have been used, including various sizes of silicon carbide, aluminum oxide, and opaline (cerium oxide).

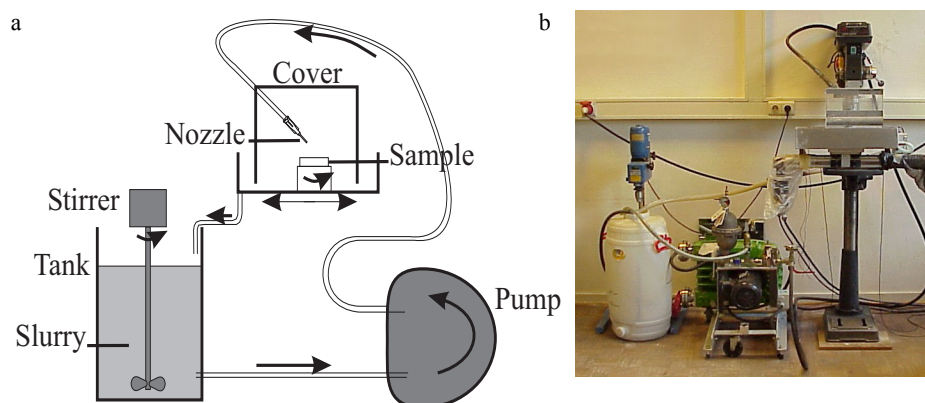


Fig. 2.5 Overview of the FJP setup, both schematic (a) and a picture of the real setup (b).

Table 2.2 Summary of the elements of the experimental FJP setup

element	description
pump	verderflex peristaltic pump model nr. 120.0158 and hydra-cell membrane pump max. 15 bar, less than 10 l/min.
hoses	standard hydraulic hoses, reinforced with steel wire ITR SAIAG 1SN DIN 20022 NW10 ITALY, working pressure 130 bar, inner diameter approx. 6 mm, total length approx. 3 m
nozzles	amongst others Lechler cleaning nozzles (hollow cone, full cone, solid stream) [www2] and EFD dispensing components (little gluing 'needles' for applying glue to small surfaces) [www8]
stirrer	IKA Werke RW16 basic laboratory stirrer
tank	50 liter plastic food containers and 5 liter steel containers
cover	plexiglas
slurry	amongst others aluminum oxide (5 - 15 μm), silicon carbide (8 - 63 μm), cerium oxide (1 μm) typically 5 or 10 weight% are added to the water

Another setup that has been realised is one in which the main frame that holds the nozzle and the workpiece is a bench lathe, see Figure 2.6. The pump, tank, stirrer and recycling system are identical to the system described above. The workpiece is mounted in the head shown on the left. This head can rotate at 250 to 1700 rotations per minute. The nozzle is located on the right hand side of the workpiece pointing towards the surface in the horizontal plane. Both the nozzle and the workpiece are shielded by one plastic cover that keeps the slurry inside the recycling loop. The nozzle is mounted in a holder that can be translated in two directions (to and from the workpiece and in and out of the paper) and it can be rotated in this plane. These movements are carried out by three step engines (the three cylindrical units at the right-hand side of the figure). The white wires at the right-hand side go to the unit that controls the movement of the step engines.

Yet another setup that has been realised (at FISBA-Optik, a cooperating company in Switzerland) is a computer numerically controlled (CNC) one. On an existing LOH machine some alterations have been made to make it possible to implement FJP on the machine. A pump has been connected externally, the upper spindle has been changed, so the FJP fluid could flow through it, and the fluid is forced to return to the tank after hav-

ing processed the glass. The main advantages of the FJP setup on this type of machine are the fact that the translation of the workpiece (mounted on the lower spindle) is very accurate, the fact that the upper and lower spindle can rotate rapidly and accurately, and the fact that the angle and height of the nozzle can be set accurately.



Fig. 2.6 The bench lathe based FJP setup with the sample mounted on the left-hand side, the nozzle pointing towards the sample, in the horizontal plane, and the step engines that control the nozzle movement shown on the right.

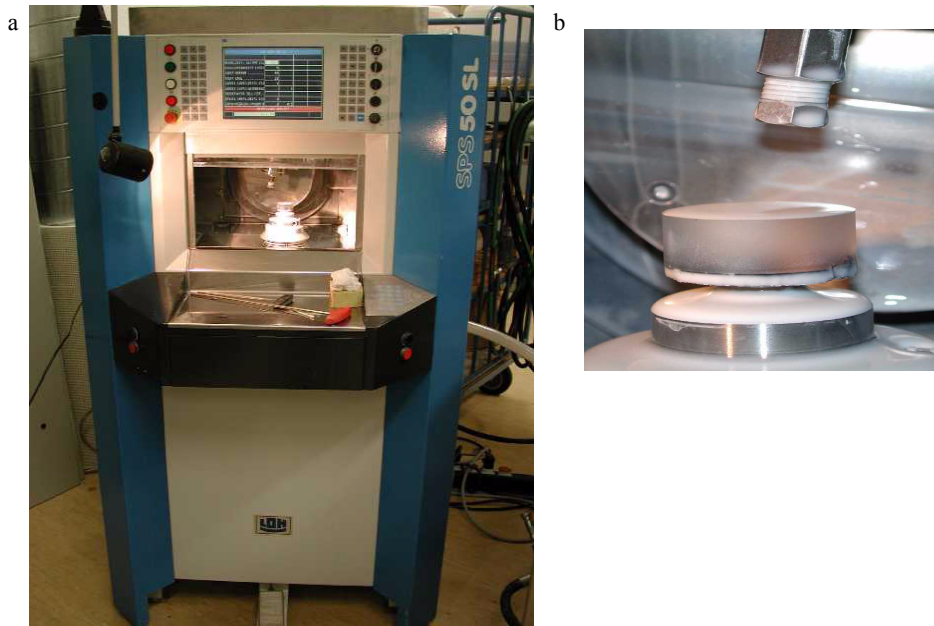


Fig. 2.7 a) Picture of the CNC based experimental FJP setup located at FISBA-Optik, Switzerland, with a detailed picture of the nozzle and the workpiece (b).

2.2.4 Comparison between FJP and classical grinding or polishing

There are some differences between classical polishing and FJP. The first one is that classical polishing is a three-body process, which will cause errors to average out. If the pressure on the pad accidentally increases, it will be distributed over all of the abrasives. If the velocity of one of the grains in the case of FJP increases, this will locally cause more material removal. This does not average out, since the particles operate individually. Another difference is that the classical process polishes the top part of the surface only. If a deep depression is present somewhere in the surface it will not be smoothed by the classical process, but the FJP process is able to remove material from deeper lying parts of the surface. A third difference is that the size of the abrasives that can still remove material in a ductile way is much larger in the case of FJP than in the classical case. A similarity between FJP and classical polishing is that the material removal rate has the same order of magnitude. FJP can be operated at material removal rates between 0.2 nm/min and 2 $\mu\text{m}/\text{min}$. Classical polishing typically has a removal rate of 0.5 $\mu\text{m}/\text{min}$ [lam99].

A coarse estimation can be made of the local pressure that is involved in the case of classical grinding or polishing. If we assume that this will be the same order of magnitude as in FJP we can deduce the interaction time that occurs in the case of FJP. Assume that in the classical case a load F of 2 kilograms is applied to a pad with a surface area of 10 cm^2 . We will further assume that 10% of the pad is covered with abrasive particles that actually make contact with the glass surface. The local pressure, p , equals

$$p = \frac{F \cdot g}{A} = \frac{2 \cdot 9.81}{1 \cdot 10^{-4}} = 196 \cdot 10^3 [\text{Pa}], \quad (2.2)$$

where A is the effective area of contact [m^2], and g is the gravitational acceleration [m/s^2].

In the case of FJP we will assume a slurry velocity of 20 m/s , a cross section of the slurry jet of 1 mm^2 , a density of the abrasives ρ of 3000 kg/m^3 , and a 10% weight concentration of abrasives is added to the slurry. In one second a volume of $20 \cdot 10^{-6} \text{ m}^3$ will pass by. Of this volume, 10% consists of abrasives. The mass of these abrasives, m , will equal their density ρ times their volume V

$$m = \rho \cdot V = 0.006 [\text{kg}]. \quad (2.3)$$

The following relation should also be valid

$$F_t \cdot \Delta t = m \cdot \Delta v, \quad (2.4)$$

where F_t is the force the particles transfer during time Δt , m is their mass, and Δv their change in velocity. The maximal velocity change will occur when the particles come to a complete stop, from their initial velocity of 20 m/s . The exerted pressure p equals the force that the particles transfer per unit time, divided by the surface area over which they do so, A

$$p = \frac{F_t}{A} = \frac{m \Delta v}{A \Delta t} \approx 200 \cdot 10^3 [\text{Pa}]. \quad (2.5)$$

From this equation we find for the average interaction time

$$\Delta t = \frac{m\Delta v}{Ap} = \frac{0.006 \cdot 20}{(1 \cdot 10^{-3})^2 \cdot 2 \cdot 10^5} = 0.6[s]. \quad (2.6)$$

This estimation is an upper limit since we have assumed that all particles make contact with the surface, and that they transfer all of their kinetic energy to the surface. This is an over-estimation, as will be shown in Chapter 4.

2.2.5 Advantages and risks of the FJP method

FJP is a shaping and polishing method that can be very useful for shape corrections and roughness reduction, especially of difficult to reach parts of a surface. The advantages of the FJP method are:

- The ‘work tool’ does not erode, so the machining spot shape is very constant (the work tool being the effective area of the impacting particles, not the nozzle).
- Both roughness reduction and shape corrections are possible with one method.
- Even complicated aspheres can be polished with FJP, because there is no direct contact between a pad and the workpiece. If the dwell time is correctly adjusted for every point on the surface, the same amount of material can be removed everywhere. This results in a surface that is polished, without introducing shape alterations.
- The setup is not expensive in its most basic form. Accurately controllable translation and rotation stages and computer software will increase the price.
- The slurry is recycled, so the method is environmentally friendly.
- The process is cooling and removing the debris during the process owing to the water that is used.
- The slurry can be changed to an optimal pH value [kal91], viscosity [gol90], concentration etc. (high and low material removal rates can thus be obtained).
- The stationary removal profile can be optimised by choosing a specific nozzle and impact angle (very small and very large removal spot profiles are possible).
- The processing can be sped up by using several nozzles simultaneously.

There are also some risks that have to be overcome in order to build a satisfactorily working setup, these risks include:

- The pump pressure should be stabilised until an acceptable fluctuation is reached.
- The setup will wear due to the abrasives. The wear can be minimised by building a setup in which the slurry is mixed at a stage as late as possible, or part of the setup will have to be repaired or replaced on a regular basis.
- FJP is a sub-aperture technique, which means that care should be taken when controlling the movement of the nozzle over the surface, to avoid mid spatial frequencies. It is possible to increase the size of the abrasive jet until it is larger than the optics to be treated.

3 Measurements

Research into material removal critically depends on the measuring possibilities. There is no way of knowing how much material was removed if it can not be measured. The accuracy with which the material removal can be measured limits the accuracy with which the processing can be carried out. In Section 3.1 some parameters will be defined to quantify the roughness of a surface. Section 3.2 then describes some existing techniques for measuring the shape and the roughness of an optical component. The described techniques include interferometric comparison to a reference surface, scanning a well defined tip over a surface while keeping track of its position (profilometer or AFM), and qualitative inspection of a surface through a microscope. All of these existing techniques are used after the processing has been done. The most ideal case would be if the measurements were done during the processing. This would make it possible to stop the process at the exact moment in time when the desired surface shape and roughness are reached, saving time and money. One possible way to monitor the surface state (roughness, sub surface damage, scratches) is by using iTIRM (intensity-detecting Total Internal Reflection Microscopy), which is well suited for in-process monitoring of flat surfaces [bij99] [fah02b]. This technique will be described in Section 3.3 together with an example of its application.

In order to monitor the local material removal during the FJP process a different method has been used. An interferometric measurement method has been designed for this purpose and a prototype has been built [bru02]. This will be described in Section 3.4. The measurement system will be discussed in Subsection 3.4.1. The measurements make use of temporal phase unwrapping (TPU) allowing for a large working range. The principle of TPU will be discussed in Subsection 3.4.2. An experimental result will be shown and the capabilities of the system will be discussed in Subsection 3.4.3. Finally, some conclusions will be drawn concerning this setup in Subsection 3.4.4.

3.1 Surface characterisation parameters

When a surface is produced it should be measured to see if it meets the specifications. Thereto both the shape and the roughness of the surface should be measured. The transition between those two is not as clear as it seems. The irregularities can be split up in regimes of scale lengths between certain values, as can be seen in Figure 3.1. One possible division is [bjo98]:

- i. short scale, or ‘micro roughness’ or ‘high spatial roughness’ having scale lengths smaller than 1 μm ,

- ii. mid-spatial scale, with scale lengths from 1 μm to 1 mm and
- iii. long scale, corresponding to optical figure / curvature having scale lengths > 1 mm

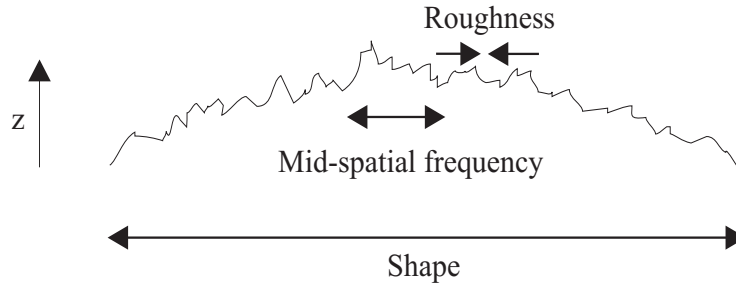


Fig. 3.1 Schematical picture of the difference between roughness, mid-spatial frequencies and shape.

This division suggests that samples with a diameter below 1 mm do not have a shape, but only mid-spatial frequencies. The exact cutoff between figure and mid-spatial frequencies has to vary with the optics size. Surface shape can be defined as a flat surface, as a sphere with a certain radius, as a cylinder with a certain radius, as an asphere (e.g. hyperboloids or ellipsoids) or any combination thereof. The difference between the ideal surface and the actual surface should be specified e.g. by comparing the surface to a reference surface.

The definition of roughness is: 'A measure of the closely-spaced irregularities or texture of a surface'.

To define the roughness of a surface a number of parameters is used. The additional information that is needed, apart from the value of a roughness parameter is the area over which the roughness has been measured, which frequency components have been included, whether or not filtering has taken place, where on the surface the measurements were carried out, if the measurements have been averaged, and in the case of a contact-measurement what the size of the scanning tip was. The definition of four of the most commonly used parameters is as follows [ben89] [din01] [wyk95].

R_a : The average roughness as calculated over the entire measured array. In the case of N discrete measurement points of a height z_i , and an average height \bar{z} this can be represented as

$$R_a = \frac{1}{N} \sum_{i=1}^N |z_i - \bar{z}| \quad (3.1)$$

R_q (or rms): The root-mean-squared roughness calculated over the entire measured array. In the case of N measurement points of the height z_i , with an average height \bar{z} this can be computed as

$$R_q = \sqrt{\frac{1}{N} \sum_{i=1}^N (z_i - \bar{z})^2}. \quad (3.2)$$

R_t : The peak-to-valley difference calculated over the entire measured array. With H_1 the highest measured point and L_1 the lowest measured point

$$R_t = H_1 - L_1. \quad (3.3)$$

R_z : The average of the five greatest peak-to-valley separations. With H_1 through H_5 the five highest measured points and L_1 through L_5 the five lowest measured points

$$R_z = \frac{1}{5} \sum_{i=1}^5 (H_i - L_i). \quad (3.4)$$

These roughness values should be computed after the shape-components of the surface have been removed. If the R_a value of the roughness as measured with the Wyko profilometer is compared to that measured with the alpha-step line scanning device we get two different values. This is due to the fact that the alpha-step only scans over one line on the surface, with a fixed length, and the needle tip has a certain radius. The Wyko calculates the R_a based on information from a two-dimensional area. With the appropriate software it is possible to apply low or high pass filters based on the frequencies of interest, and masks can be applied to change the size of the area of interest.

As an example 100 equally spaced values for the height of a surface have been selected, see Figure 3.2. The average surface height is 9.6 nm, the five highest points are 15, 15, 15, 14, 14 nm, the five lowest points are 4, 4, 5, 5, 5 nm. The roughness values can now be calculated from the heights of the 100 points, and they are $R_a = 2.15$ nm, $R_q = 2.59$ nm, $R_z = 10$ nm, $R_t = 11$ nm.

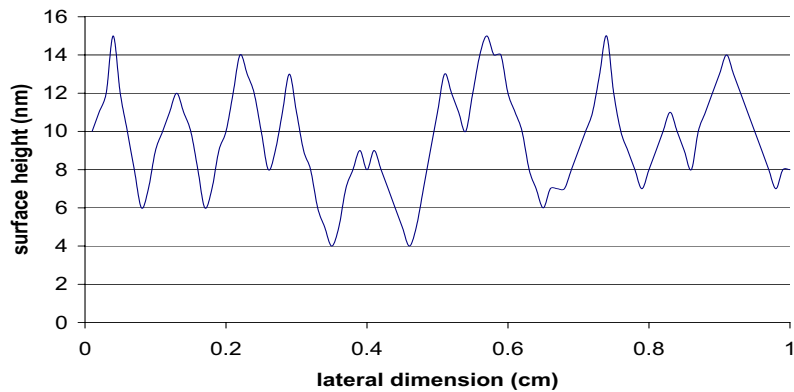


Fig. 3.2 Example of a surface that consists of 100 points, which is used to illustrate the computation of the roughness parameters.

3.2 Existing measurement techniques

In this section some surface shape and roughness measurement techniques will be described. The techniques can be divided into contact and non-contact methods. The obvious advantage of non-contact methods being that the surface is not damaged by the measurement. The simplest contact technique, that renders information on the shape of the entire surface, is placing a test glass on the surface to be measured, see Subsection 3.2.1. Another contact method used for shape and roughness measurements is making a one-dimensional scan over the surface with a sharp object (a line-scanning device), see Subsection 3.2.2. Of the non-contact methods the Nomarski microscope will be described in Subsection 3.2.3. Very small surface defects can be visualised with this type of microscope. In Subsection 3.2.4 the use of an interferometer will be described, both for shape and roughness measurements. Finally, the operating principle of a scanning electron microscope (SEM) will be treated in Subsection 3.2.5. This type of microscope can be used to visualise very small details of a surface.

3.2.1 Test plate

A test plate is a polished glass plate with a well defined shape (flat or spherical). The test plate is placed on the surface to be inspected. White light or sodium light shines on the combination of the test plate and the surface to be inspected. If the two surfaces have exactly the same shape, light reflecting from the bottom of the test plate and from the top of the surface to be measured have a constant phase-difference of π , due to the fact that one of the beams reflects from a transition to a denser medium. This means that the beam amplitudes cancel each other, and a ‘black’ surface is observed. If the two surfaces slightly deviate from each other in shape, an air-gap will be present between them, see Figure 3.3. The incident beam partly reflects at the lower surface of the test plate, resulting in the beam R_1 , and the other part of the beam reflects from the top of the surface to be measured, R_2 . The width of the air-gap is $h(x)$. For angles of incidence close to normal incidence on the surfaces, the phase difference between R_1 and R_2 is

$$\Delta\Phi = \frac{2\pi}{\lambda}(2 \cdot h(x)) - \pi. \quad (3.5)$$

So two beams will destructively interfere if $2h(x)$ equals 0 or any whole number of wavelengths. A wedge-shaped air gap between the two surfaces will produce a regular pattern of straight fringes. These fringes are called Newton fringes (or Newton rings in the case of circular fringes) [twy42].

What can be measured with a test plate is the deviation from a reference surface. If a shift of 1/8 th of a fringe can be seen and sodium light ($\lambda = 590$ nm) is used, shape deviations of up to 40 nm in height can be detected. A disadvantage of using test plates is that they can only be used if the surface is smooth enough; moreover the reference surface has to be virtually in contact with the surface to be tested, which could result in scratches on the surface.

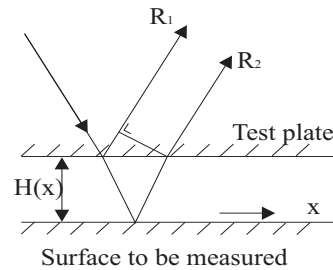


Fig. 3.3 Illustration of the interference of two beams, reflecting from the bottom of the test plate (R_1) and from the top of the surface to be measured (R_2). The surfaces are separated by an air gap of width h .

3.2.2 Line-scanning method

The principle of operation of a one-dimensional line-scanning method is that a hard, pointy object (needle or tip) is moved over the surface at a controlled velocity and with a controlled force. The vertical movement of the needle is amplified and plotted as a function of its horizontal movement. This renders information on the shape (if the needle is scanned over a large distance) or on the roughness (if the scan is performed over a short distance). Typical scan distances are tens of micrometers to tens of millimeters. The vertical range is usually in the order of tens of nanometers to tens of micrometers. The output of these devices can be a printout on paper, or the measured data can be stored in the computer. Some types of these scanning devices are the alpha-step made by Tencor [www4], the Mitutoyo, Dektak [www3], Talysurf made by Taylor Hobson [www5], and many more exist. The computation of all of the roughness parameters is theoretically possible if the surface profile is known. With the alpha-step average roughness values between 5 nm and some tens of micrometers can be measured. The length of the scan is of influence on the roughness value, because longer scans contain lower frequency components that are not filtered out.

3.2.3 Nomarski microscope

A Nomarski microscope can be used for qualitative inspection of surfaces. Very small variations in the surface height can be made visible. This microscope uses the shearing principle. The principle of operation is as follows: light from a light source in the Nomarski microscope is linearly polarized, it travels via a beam splitter to the Nomarski wedge, see Figure 3.4. This wedge transforms the beam in two orthogonally linearly polarized beams that are shifted slightly with respect to each other. The two beams are reflected back from the sample's surface and are combined by the analyser. The resulting interference pattern shows the difference in height of the sample and a slightly shifted version of the sample. Surface height variations of 0.05 nm can be made visible with this technique in the direction of the shift induced by the wedge, but no information can be obtained in the direction perpendicular to it.

Variations on the Nomarski principle also exist, like the Nomarski system with processing software that can give quantitative results on surface roughness and shape [toe00], and two-dimensional surface characterisation can be obtained by scanning the Nomarski wedge in two directions [cog94]. The maximum height difference that can be detected between two points at a certain lateral distance is limited by the resolution of the system.

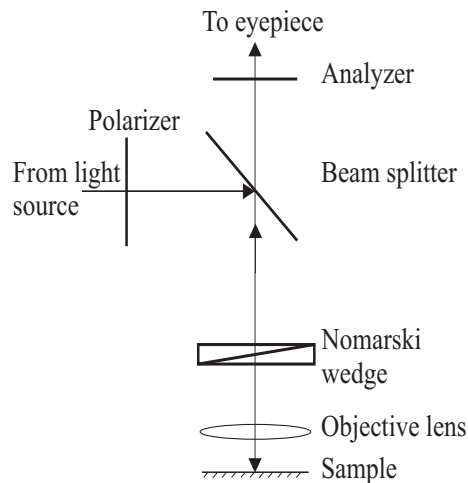


Fig. 3.4 Schematic view of a Nomarski microscope.

3.2.4 Profilometer and interferometer

For the measurement of shapes an interferometer can be used. Many companies sell them, like for example Wyko [www6], Zygo [www15], and Fisba [www16]. We have used a Wyko Vision interferometer. It uses a laser as light source, the interferometer is of the Fizeau type, and phase stepping is incorporated in the system. The fringes cannot be resolved any more if the surface is steeper than 200 nm / mm. Newer models of the Wyko are available that can resolve up to 4 times as much [www6].

For the measurement of roughness over a small area (max. 200 x 300 μm), again many types of interferometers can be used. We used the Wyko RST 500. It uses a white light source in combination with a red filter, it is based on a Mireau interferometer (see Figure 3.5), and it also uses phase stepping. The interferometer scans its focus through a calibrated optical distance and records the position at which interference fringes appear on the (x,y) positions of the surface. Thus the height information is known at the (x,y) coordinates. Surface irregularities of less than 1 nm can be detected with this interferometer. The maximum depth difference that can be detected between two points that are 5 μm apart is approximately 200 nm. It is not possible to measure steeper slopes, because the

fringe density becomes too large to measure with the available number of pixels in the CCD-camera.

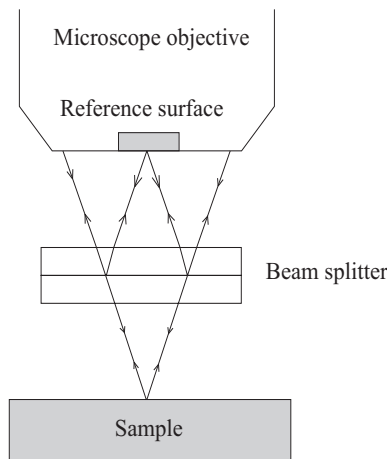


Fig. 3.5 Principle of a Mireau interferometer.

3.2.5 Scanning electron microscope

A scanning electron microscope (SEM) [www10] can be used, for example, to visualise the shape of various abrasive particles (Appendix II) and the structure of glass surfaces (Subsection 4.5.2). A short description of the operation principle of the SEM will be given (Figure 3.6). A SEM is built in a way analogous to a reflecting light microscope. Because it uses electrons to image instead of light, magnification factors of 5 to 300 000 can be obtained. It is possible to depict the surface structure in reflection (SEM) or in transmission mode (TEM) if the sample is thin enough. The composition of the sample can also be determined in the same microscope.

The first prerequisite on the samples is that they have to be conductive. If they are not conductive by nature they can be coated with a thin layer of gold by e.g. sputter deposition. This allows for the electrons that are used for imaging to be transported away from the sample. The second demand is that the samples have to be able to withstand vacuum. The inside of the microscope including the sample is in vacuum, to make electron beam formation and transmission through the electro-optical column possible and to prevent dirt from settling on the sample.

The operation principle of the SEM can be explained by following the path of the electrons through the microscope, starting with their generation. The electron gun creates a high energy beam of monochromatic electrons. This gun consists of a tungsten filament as cathode, from which electrons are originating. They accelerate towards the anode by a large voltage difference (typically 100 kV). Then magnetic lenses focus the electrons to a very fine spot. Deflection coils are used to scan the focused beam over the sample row by row, like in a television. The incident electrons can be back-scattered by the sample, secondary electrons (usually K-shell) can be emitted by the specimen, as well as Auger electrons (emitted when an electron falls back to the K-shell), or x-rays can be emitted (they

are used for compositional analysis). The origin of the back-scattered or secondary electrons can be determined and this renders information on the shape of the sample under investigation. The position of the detector depends on the operation mode of the microscope (transmission or reflection).

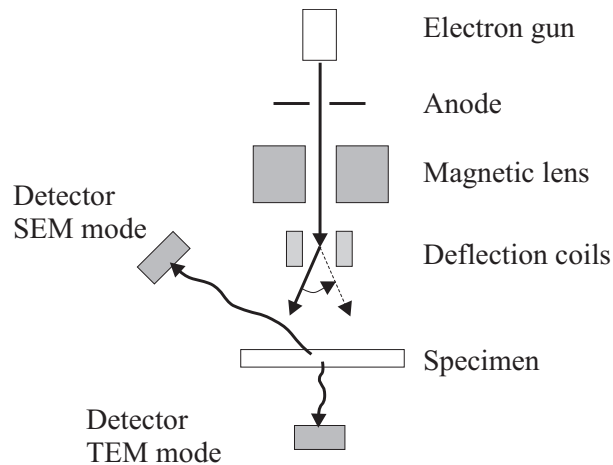


Fig. 3.6 Schematic view of a scanning electron microscope (SEM). In reflection mode the upper detector is used. For measurements in transmission (TEM) the sample should be thin enough. In that case the lower detector is used.

3.3 In-process roughness measurements using iTIRM

iTIRM (intensity-detecting Total Internal Reflection Microscopy) is a method for in-process monitoring of the surface state. At this moment it is well suited for laboratory use for flat surfaces. The principle is similar to the existing TIRM technique [tem81] in some ways. In the TIRM technique laser light shines onto the surface of interest from the inside of the sample, under an angle larger than the critical angle of total reflection. In the case of an ideally smooth surface, all the light will be reflected from the surface of interest, and no light is detected above the surface, see Figure 3.7. The difference between TIRM and iTIRM is that in iTIRM the reflected light is measured instead of the transmitted light. As a reference the intensity of the original laser light is also measured to correct for possible fluctuations in the output power. The advantage of measuring the reflected light is that the measurement can be done while the process continues, see Figure 3.7. Both TIRM and iTIRM are non-destructive measuring techniques. The main difference between the two techniques is that TIRM can be used to qualitatively inspect the quality of the surface, while iTIRM quantitatively measures the total quality of the surface (including sub surface damage). The amount of reflected light will be influenced by the total surface quality, which includes the surface roughness, sub surface damage, and scratches in the surface.

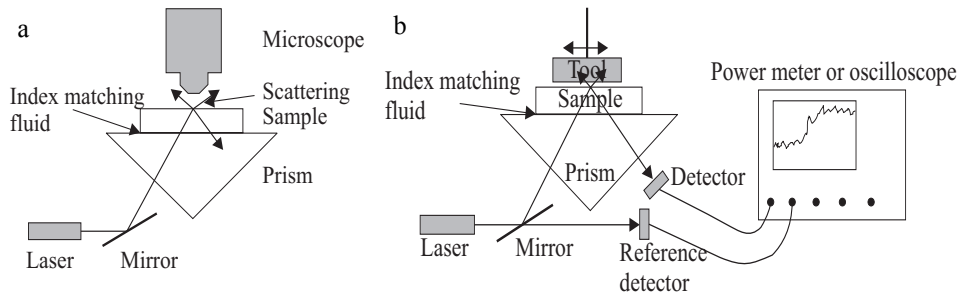


Fig. 3.7 Schematical drawing of the TIRM setup (a) and the iTIRM setup (b). Both systems can be used to monitor the surface quality. In the case of TIRM the scattered light is observed with a microscope and in the case of iTIRM the amount of reflected light is detected with an oscilloscope.

The iTIRM setup has been tested initially by moving the measurement spot from a polished part of the sample's surface ($R_a = 2$ nm) to the ground part ($R_a = 180$ nm), and back. This shows a decrease in the measured output voltage of the detector from a value of 330 mV to 260 mV and back to 330 mV [bij99]. Another experiment has been conducted to determine the working range and accuracy of the iTIRM technique. A flat #800 SiC ground BK7 surface (300 nm rms) was polished classically for two hours. Every ten minutes the process was stopped, the samples were cleaned and their roughness was measured with three different techniques: an alpha-step line scanning device, a Wyko interferometer, and the iTIRM technique. When the surface was very rough the interferometer could not measure the roughness, when the surface had a low roughness the alpha step could not accurately measure the roughness. Measurements have also been done on rougher initial surfaces. The iTIRM technique could measure the surface quality throughout the entire roughness range of some μm to 0.8 nm. Measurements on samples with rms roughness values between 1 and 3 nm, not in-situ, have shown that a distinction could be made between samples with a roughness difference of 0.1 nm rms [bij01].

A big advantage of an in-process monitoring technique for the surface state is that the process can be stopped whenever the desired final surface state has been reached such that no time is wasted. The process can also be monitored and warnings can be issued when the process runs dry for example. During a classical polishing process the roughness is expected to decrease, reach a certain value and maintain that roughness. This means that the iTIRM signal will increase and reach a certain value. If the iTIRM signal suddenly decreases this means that the roughness of the surface increases and that something has gone wrong in the process (e.g. the process is running dry).

As an example of a typical in-process iTIRM signal two classical polishing processes have been compared to each other as can be seen in Figure 3.8. In one process a load of 1 kg was applied to the pitch tool, in the other case a load of 4 kg was used. The slurry that was used was CeO_2 . The glass that was used was BK7, with an initial roughness of 300 nm. The two signals of the iTIRM process are shown in the figure as a function of time, along with some Nomarski images of the surface at three moments in time. One can see that both processes started with an identical surface roughness. The processes end with an

identical roughness as well (1 nm), when they reach the top plateau level. The roughness in the process with a 4 kg load improved faster than in the case of the 1 kg load. The reason for the vertical width of the signals is because of water droplets blocking part of the beam occasionally. This decreases the amount of light that is detected, so the highest value of the signal at any moment in time should be taken into account only.

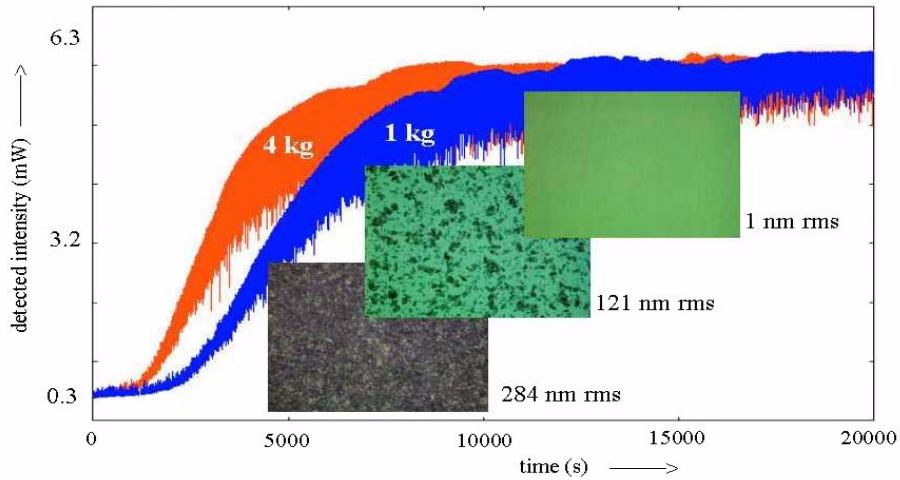


Fig. 3.8 Comparison of two classical polishing processes with different loads as a function of time. The two signals indicated by 1 kg and 4 kg are the iTIRM signals. The three rectangular shaped areas show Nomarski images of the roughness of the surface at three moments in time.

3.4 In-process shape measurements

In order to monitor the shape of a flat surface that is being processed with FJP as a function of time, an interferometric measurement setup has been designed and a prototype has been built. The setup will be described in this section, as well as the principle of temporal phase unwrapping. Then a description of the experimental verification of the measurement method will be given. This section will conclude with some conclusions concerning the measurement setup.

3.4.1 Measurement setup

A measurement system to be used in combination with FJP has to be rigid and suited for use in a wet and vibrating environment. The principle of the designed system is drawn schematically in Figures 3.9 and 3.10. As can be seen in the latter figure, helium-neon light is used and a collimated beam is made. The beam travels through a polarizing beam splitting cube (PBC) which splits the beams into two beams: one beam goes to the sample as a reference beam (this beam is s-polarised) and the other beam passes through the cube as the p-polarised object beam. Both light beams enter the surface to be measured from beneath. The light is reflected under total internal reflection conditions, in this way

the surface shape is measured without being influenced by the slurry on top of the surface. For the transition from BK7 to air the critical angle equals 41° , for the transition from BK7 to water it is 61° . In the setup the angle was chosen to be larger than the critical angle for the BK7 to water transition, namely 62.6° .

The object spot and the reference spot are combined by a beam splitter cube and imaged onto the two CCD cameras in the system. The beam passes through a polarization plate before it interferes and reaches the cameras. In one of the paths to the CCD cameras a quarter wave plate (qw-plate) is inserted to provide an additional $\pi/2$ phase step. Both interference images from the CCD cameras are required to compute the amount of material that has been removed. This is computed using the 2-bucket temporal phase unwrapping (TPU) algorithm that will be described in the next subsection. The indicated cover plate prevents the systems optics from getting wet by the slurry. From Figure 3.9 and Figure 3.10 it can be seen that the sample on which the spot is being made is placed on a special anvil-shaped holder. The gap between sample and holder is filled by an index matching fluid. The capillary action of the index matching fluid is the only force that keeps the sample and the holder together. The facets of the holder are slanted to obtain perpendicular incidence on the entrance and exit planes. Within the material the beams propagate under an angle exceeding the angle of total internal reflection with respect to the surface being processed.

The whole measurement system was designed to fit into the existing FJP setup, as shown in Figure 2.5. The laser used for this setup was a 5 mW HeNe laser ($\lambda = 632.8$ nm) and the output of this laser is guided to the setup via an optical single mode fiber. The light intensity inside the system was lowered to levels acceptable to the CCD cameras by changing the coupling efficiency of the laser beam into the fiber.

3.4.2 Temporal Phase Unwrapping

In temporal phase unwrapping (TPU), the idea is to follow the phase difference evolution between the reference and the object beam, and add all phase increments. As long as the phase change between two successive recordings (in our case typically 5 sec.) is between $-\pi$ and π , the phase obtained by accumulation of all these phase changes will be added up correctly. This means that the maximum removal rate that can be monitored at our recording rate equals $5.4 \mu\text{m}/\text{min}$. (this follows from Equation (3.12), with an index of refraction of BK7 of 1.52, a λ of 632.8 nm and an α of 62.6°). The weak point in the TPU approach is that it can not be used for static phase measurements. The strong point is that it can be used to measure phase changes, and since only the changes are recorded the actual phase distribution is of no importance. This allows for the use of low quality optics.

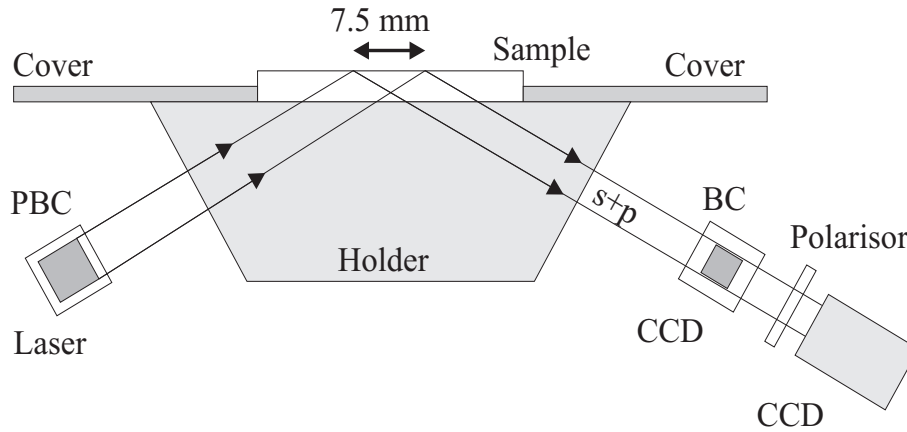


Fig. 3.9 Side view of the measurement setup. Light enters from the left hand side (the laser), passes through the polarising beam splitting cube (PBC), through the holder, into the sample, and ends up via a non-polarising beam splitter cube (BC) in the two CCD cameras at the right hand side.

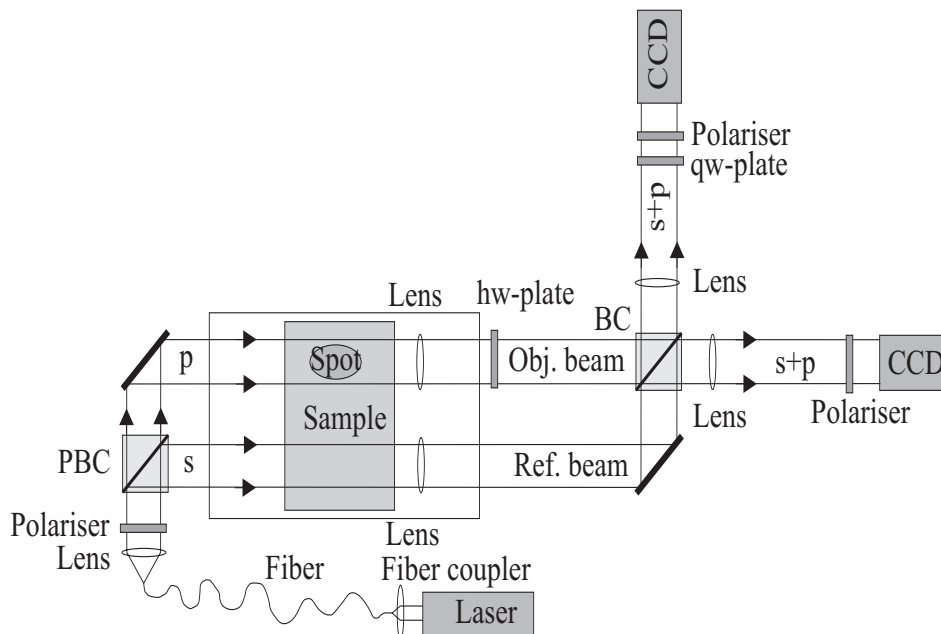


Fig. 3.10 Top view of the measurement setup. Light leaves the He-Ne laser, is sent into a single-mode fiber, leaves the fiber via a lens as a collimated beam, reaches the polarising beam splitting cube (PBC) which splits the light into a p-polarised object beam and an s-polarised reference beam. A non-polarising beam splitter cube (BC) combines both beams and sends two beams to the two CCD cameras. The lenses in the setup take care of the imaging of the spot on the CCD cameras. hw-plate is a half wave plate, qw-plate is a quarter wave plate.

In order to be able to calculate the phase change a number of approaches can be followed. A commonly used method is to record enough phase-stepped images to calculate the phase at each time, followed by a subtraction of two phase distributions for two successive recordings. This requires a minimum of three phase-stepped images per recording. We have chosen for a different approach where the actual phase is never calculated but where only the phase difference is obtained. In our approach two phase-stepped images per time suffice. For each time t two images are recorded that differ in phase by $\pi/2$. The intensities of the two recordings are a function of the position (x,y) in the image.

$$I_0(x, y) = I_B \{1 + M_d \cos[\varphi_{ref}(x, y) - \varphi_{obj}(x, y)]\}, \quad (3.6)$$

$$I_{\pi/2}(x, y) = I_B \{1 - M_d \sin[\varphi_{ref}(x, y) - \varphi_{obj}(x, y)]\}, \quad (3.7)$$

where I_B is the background intensity and M_d the modulation depth. The quantity $\varphi(x,y)$ denotes the phase distribution of the reference and the object beam, dependent on the subscript. The object beam is the beam that reflected on the part of the surface being machined while the reference beam reflected on a part of the surface that is not machined. The phase change between two successive recordings, say recordings at time t and at time $t + T$ can be obtained via [bru98]

$$\Delta\varphi(t, t + T) = -\frac{\pi}{2} - 2 \operatorname{atan}\left(\frac{I_0(t) - I_{\pi/2}(t + T)}{I_{\pi/2}(t) - I_0(t + T)}\right), \quad (3.8)$$

where the subscript 0 and $\pi/2$ indicate the phase step between the two interfering beams, the object and the reference beam. To obtain the total phase change between two moments in time ($\Delta\Phi(t, t + NT)$) all of the phase changes between the recordings in between those times have to be added.

$$\Delta\Phi(t, t + NT) = \sum_{i=0}^{N-1} \Delta\varphi(t + iT, t + T + iT). \quad (3.9)$$

From Equations (3.8) and (3.9) it follows that to calculate the first phase change four interferograms have to be recorded. For each successive phase change only two new interferograms are required, they can be combined with two previous recordings to obtain the phase change information.

3.4.3 Experimental verification

To test the presented measurement method an experiment was carried out in which a cylindrical nozzle was used at an angle of 45° with a 10% #800 SiC slurry. The processing was carried out for ten minutes which resulted in a spot with a maximum depth of $3 \mu\text{m}$ (removal rate of $0.3 \mu\text{m}/\text{min}$). During the material removal interferograms were recorded every 10 seconds, two for each time t . One with a zero phase step ($I_0(t)$), the other with a $\pi/2$ phase step ($I_{\pi/2}(t)$). The images of the zero phase step are shown in Figure 3.11. The first image is shown in the top left hand corner, from there the images are ordered from left to right with time of recording, and then from top to bottom. Only every fourth image is shown in order to reduce the number of images. The routine used for image capturing and data analysis was written in LabView. Although this is a versa-

tile programming environment the resulting programs are relatively slow. The system can capture one set of two phase-stepped images per five seconds. For this experiment an interval time of 10 seconds was set. Because the FJP setup with the settings of slurry type, concentration and velocity in this experiment, has a low removal rate, the phase changes were never outside the allowed range pointed out before. The first image is recorded prior to the processing. On this image the influence of a water droplet can be seen. The fact that this effect can only be seen on the first image shows that a wet layer causes no problem. The reason that we can see the droplet on the surface, even though the angle of reflection is larger than the angle of total internal reflection, can be explained by assuming that the droplet is thin enough to get reflection from the top interface. The light that is present within the droplet is the evanescent tail of the incident light. If the droplet, or layer, is thin enough for this tail to be twice the thickness then the effect of the top surface can be seen in the reflected light beam. In the first image the fringes that are present are not straight. This is caused by the fact that the initial surface is not perfectly flat. The material removal in the generated spot is symmetric, but appears distorted by the initial curvature of the fringes.

The number of fringes increases as a function of time until a clear ‘smiley’ is formed. Since the light that is used is from a Helium Neon laser the wavelength is $\lambda = 632.8$ nm. As check on the fidelity of the obtained interferograms an image obtained by a simple test glass setup (Newton fringes) is also shown with a sodium lamp ($\lambda = 589$ nm), see Figure 3.12. The horse shoe, or ‘smiley’ shaped spot in Figure 3.12 is elongated with respect to the spots in Figure 3.11. This is due to the fact that the in-process measurement is performed under a large angle while the Newton fringes were recorded perpendicular to the surface. The depth obtained from a simple fringe counting approach of the Newton fringes is ≈ 3 μm while the depth calculated from the TPU data results in 2.8 ± 0.1 μm . The error margin in this value originates from the noise level in the measured data. Although the system was designed to be as rigid as possible it was found that the fringes outside the machined area shifted as a function of time. This indicates that the sample was not rigidly fixed to the holder. Since the sample was only ‘glued’ with an index matching fluid it could be pushed away by the force of the slurry jet impinging on it. The shift in fringe positions can be seen in the interferograms of Figure 3.11.

To convert the phase change to an amount of material removal the angle of incidence has to be taken into account, as well as the wavelength used and the refractive index of the glass being processed. The phase change shows a dependence on the spot depth with a factor of 2, due to fact that the measurement is done in reflection. The change in path length l for the beam reflected on the spot, with respect to the reference beam equals

$$l = 2h \cos(\alpha), \quad (3.10)$$

where h is the change in spot depth, and α is the angle of incidence of the light beam with respect to the surface normal. The phase difference between object and reference beams, due to this path length change l in a material with refractive index n , is

$$\Delta\phi = \frac{2\pi n(\lambda)}{\lambda} l, \quad (3.11)$$

in which λ is the wavelength of the light used.

The depth h of the area of removed material is obtained via a combination of Equation (3.10) and Equation (3.11)

$$h = \frac{\Delta\phi\lambda}{4\pi n(\lambda)\cos(\alpha)}, \quad (3.12)$$

where $\Delta\phi$ is the measured change in phase difference between object and reference beam. From Equation (3.12) it follows directly that for accurate measurements the refractive index of the material being worked upon has to be known precisely, as well as the angle of incidence α inside the material. The value of $h = 3 \mu\text{m}$ corresponds to a phase change between object and reference beam of about 14π (this follows directly from Equation (3.12)), which equals seven fringes. In the bottom right hand image of Figure 3.11 this is the number of fringes that has been added with respect to the image shown in the top left hand corner. This visual approach yields the correct depth. The automatic system is less accurate due to a shift of the fringes with time. The final limiting factor in terms of maximum height that can be measured by this monitoring setup is the fringe density. The interferograms that are recorded should contain fringes that can be resolved by the cameras. The minimum number of CCD pixels per fringe should be two. For more accurate measurements a larger number, say about ten, should be used.

3.4.4 Conclusions

From this section we have seen that the experimental issues when building a measurement setup to monitor the changes in the surface shape during the FJP process were slurry on the surface and vibrations. These were tackled by measuring from within the sample under total internal reflection conditions and by reflecting both the object and the reference beam on the sample being processed. From the interferograms shown it follows that the created setup works satisfactory. The way in which the sample is fixed inside the setup needs to be improved. It is believed that the sample moved due to the forces of the slurry jet. The alignment of the measured spot with respect to the machined spot will have to be made more flexible.

The presented results prove that the temporal phase unwrapping method can be used to in-process monitor the spot formation as encountered in fluid jet polishing. The high number of fringes in the last image could be unwrapped since this is done in sixty intermediate steps that only monitor the difference in the number of fringes between the two successive images. Although the sample was not rigidly connected to its holder we were still able to accurately measure a footprint. The difference between the real depth of the spot and the outcome of the new measurement system is assumed to be due to the drift of the sample caused by the forces induced on it by the slurry jet.

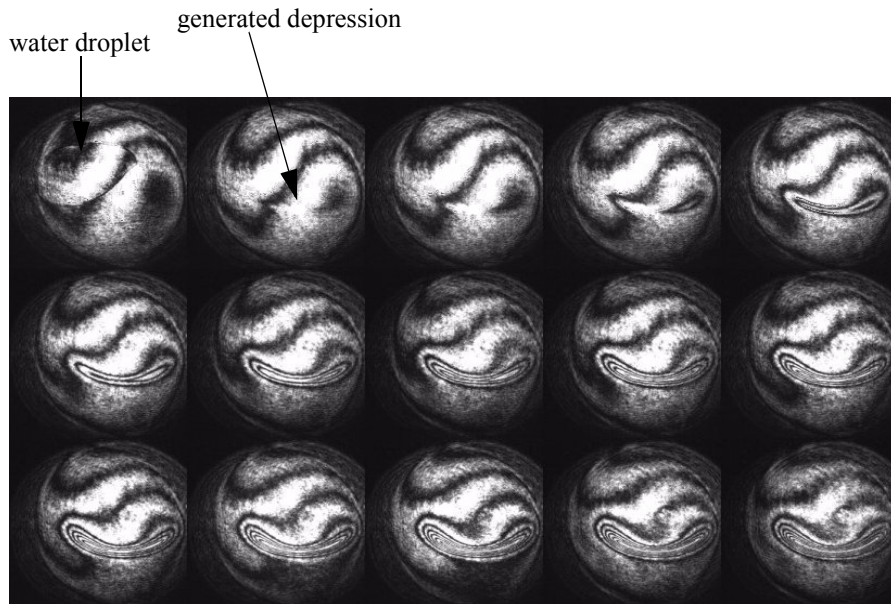


Fig. 3.11 Some of the interferograms obtained with the new measurement setup described in this section. A $\sim 3 \mu\text{m}$ deep spot is generated in 10 minutes. Two subsequent images shown here are 40 seconds apart. The real width of the spot is approximately 3 mm. The interferograms are compressed in the vertical direction by a factor of approximately 1.5.



Fig. 3.12 Newton fringe visualisation of the final spot from Figure 3.11. The spot has a width of approximately 3 mm.

4 Models for FJP

In order to gain a better understanding of the FJP process, the principle behind various aspects of this material removal technique has been investigated. In this chapter a description is given of the various process models, some models originate from existing literature and can be applied to FJP, other models have been developed especially for FJP. In the first section some definitions will be given, to unambiguously define parameters that are used in the models that will follow. In Section 4.2, the material removal model as described by Lawn [law75] will be presented for brittle mode removal as well as a modification that we have developed for ductile mode removal. In the third section the theoretical pressure distribution in the slurry jet will be derived. In Section 4.4, a model is presented with which the position of particles in a streaming fluid can be described. Thereto the boundaries of the flow itself are computed first, then the flow is computed in the entire area where liquid is present, and finally single particles are released in the flow and their trajectories are calculated.

The subject of Section 4.5 is the prediction of the amount of removed material by one particle. In Section 4.6, using the material removal profile of a stationary spot, we deduce the resulting material removal profile in the case of a nozzle and a work piece that are moving with respect to each other. In the last section, a model is derived for the finally resulting surface roughness, which is based on randomly impacting particles. The effects of the pressure, the number of impacts, the initial surface roughness and the diameter of the abrasive particles are analysed.

4.1 Definitions

To avoid confusion it is important to clearly define some parameters that characterise the exact settings of an experiment. In the case of positioning a nozzle with respect to the surface to be processed three important parameters play a role: the angle of impact (α), which is defined as the angle between the nozzle and the surface to be treated in degrees, the stand-off distance (h), which is the shortest distance between the end of the nozzle and the surface in meters, and the nozzle radius a in meters. A schematic representation of these parameters can be found in Figure 4.1.

The slurry itself can be characterised by the type of particles (e.g. aluminum oxide, silicon carbide, cerium oxide), their concentration c , the slurry carrier (usually water), and the average particle diameter d in meters. The type of abrasives determines the density and the particles shape (flat, round, irregularly shaped, elongated etc.). In Appendix IV an overview can be found of some commonly used abrasives.

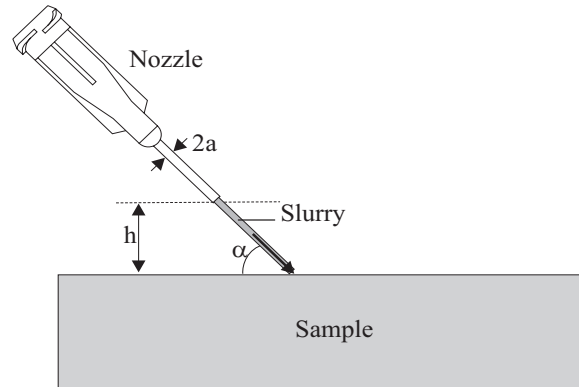


Fig. 4.1 The impact of the jet on the sample and the parameters that are related to the flow from the nozzle, the nozzle radius a , the stand-off distance h , and the angle of impact α .

4.2 Crack formation

Ductile and brittle material removal processes are essentially different. In order for a process to be in the ductile regime, only a limited amount of material can be removed per second. Brittle processes have no limited material removal rate, since the removal occurs via the occurrence of cracks. Bifano [bif91] shows that the transition between ductile mode and brittle mode material removal depends on the depth of removal. The energy required to plastically deform material depends on the volume to be deformed. The energy required to initiate cracks depends on the area of the crack. The ratio of energy required for ductile and brittle material removal thus depends on the volume divided by the area of removal, which is proportional to the depth of cut. For small machining depths, ductile regime removal will be energetically more favorable.

Lawn [law75] has described a model for the brittle mode material removal as seen from a microscopic point of view. In the case of brittle material removal a load is applied to the surface (the down-pointing arrows in Figure 4.2), which causes a permanent impression on the surface and a plastically deformed zone, indicated by the grey area in Figure 4.2. The load is increased further, which causes the plastically deformed area to grow and it causes a lateral crack to open below the applied load. Increasing the load further causes the crack to grow even further. When the load is decreased (indicated by arrows pointing up in Figure 4.2) the crack closes, but does not disappear. This is the origin of sub surface damage. Next median cracks will appear just below the plastically deformed zone. These median cracks will continue to grow until they intersect with other cracks, or with the upper surface of the material. The entire area enclosed by the median cracks is thus removed from the surface.

Analogous to the brittle mode material removal model by Lawn, a model can be described for the microscopic process that occurs in the case of ductile material removal.

In this case a small load is applied to a surface, indicated by the arrow pointing downwards in Figure 4.3. A small permanent impression results in the surface, surrounded by a plastically deformed zone, indicated by the grey area. When the load is removed again, indicated by the arrow pointing upwards, the permanent depression remains and some material remains plastically deformed. The removal will only be in the ductile regime if the applied load is small enough. For even smaller loads the material will be elastically deformed only, and when the load is removed, the surface will return to its original shape.

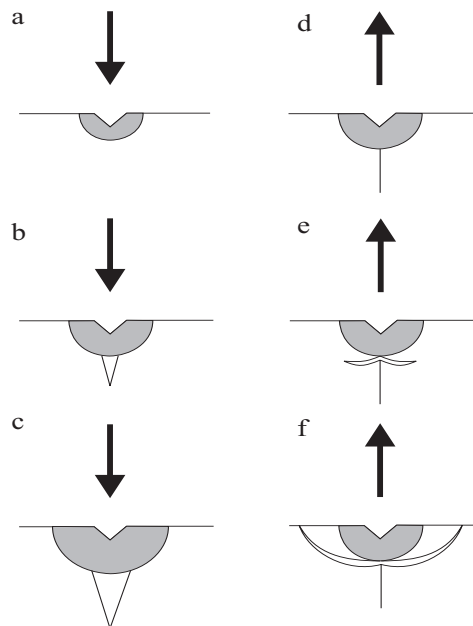


Fig. 4.2 Model of the material removal process in the brittle case according to Lawn [law75]. The process of cracking is illustrated by the six figures that show consecutive moments in time. The arrow indicates an increasing load (a, b, c) or a decreasing load (d, e, f). The grey areas are plastically deformed. An area of permanent deformation is visible in the top of the surface, and cracks appear at the bottom of the plastically deformed zone.

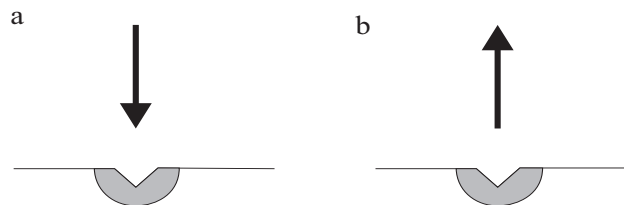


Fig. 4.3 Model of the material removal process in the ductile case. a) An increasing load causes a permanent impression in the surface, surrounded by a plastically deformed area (colored grey). b) Cracks do not occur when the load is removed.

4.3 Theoretical pressure distribution in the slurry jet

The slurry jet that is used in the FJP process has water as a ‘carrier’. It contains abrasive particles (grinding or polishing ones) with a diameter of tenths of μm to tens of μm . The concentration of these particles can vary between some hundredths of a percent to some tens of percents. The typical diameter of the jet is some millimeters, and its typical velocity is some tens of m/s. The velocity of the abrasive particles will be approximately equal to that of the carrier-fluid, because they are so small. This is proven by a balance of forces calculation in Appendix I. The particle velocity has also been measured using a Laser Doppler Anemometer (LDA), see Subsection 5.1.4.

In order to get an idea of the type of flow that occurs in our setup it is interesting to calculate the Reynolds number of the flow. Flows with a Reynolds number smaller than 2000 are laminar, for Reynolds numbers between 2000 and 4000 the flow is in a transitional mode, and if the Reynolds number is larger than 4000 the flow is turbulent [www12] [www13]. In our setup the flow is definitely in the turbulent regime, as can be seen from the Reynolds number Re :

$$Re = \frac{\rho v d}{\eta} = 1.99 \cdot 10^4, \quad (4.1)$$

where ρ is the density of the fluid (998.23 kg/m³ for water at 20° and atmospheric pressure), v the average fluid velocity (20 m/s), d the diameter of the fluid stream (1 mm), and η the dynamic viscosity of the fluid (1.002 10^{-3} Pa·s for water at 20° and atmospheric pressure) [jan87].

How the slurry flows out of the nozzle depends heavily on the shape of the nozzle and on the medium through which the slurry flows. The surrounding medium plays a very important role in the eventual break up of the jet [hoy77]. Van Dyke [dyk82] has collected pictures of various flows of water through water and of water through air. His visualisations give a good impression of the flow of the jet. Flows of water in air are not slowed down or dispersed much. Therefore we can assume that the velocity distribution in the jet will not change dramatically from one position in the jet to a position slightly further down-stream.

Now we come to the main subject of this section, namely the pressure distribution in the jet. The pressure distribution of water on a surface on which it impacts at perpendicular incidence has been calculated e.g. by Leach and Walker [lea66] and by Reh binder [reh76] in the case of high speed water cutting. They both studied the case of water cutting through stone at pressures of approximately 600 to 5000 bar and velocities of 340 to 1000 m/s. Even though the FJP process operates at a much lower pressure and velocity, it is interesting to look at the description given for higher pressures because of the similar results that are obtained in both cases.

Leach and Walker calculate the total force on the surface due to the velocity of the jet and assume that this force is equal to the radial symmetrical pressure distribution multiplied by the area over which the pressure is applied

$$\pi a^2 \rho u^2 = \int_0^R (p(r) - p_0) 2\pi r dr, \quad (4.2)$$

where a is the jet radius, ρ the density of the fluid, u the average fluid velocity, $p(r)$ the pressure of the fluid on the sample, p_0 the ambient pressure, r the radial coordinate, and R that radial distance where the pressure is approximately equal to the ambient pressure. After the assumption that the pressure distribution will be a function of the normalised radial coordinate (r/R)

$$p' = \frac{p - p_0}{\frac{1}{2}\rho u^2} = f\left(\frac{r}{R}\right) = f(r') \quad (4.3)$$

and the boundary conditions that the normalised pressure should be 1 and its slope 0 at a radial distance 0, and the pressure should be zero and its derivative should be 0 at $r = R$, Leach and Walker [lea66] arrive at a pressure distribution of

$$p = p_0 + \frac{1}{2}\rho u^2 \left\{ 1 - 3\left(\frac{r}{R}\right)^2 + 2\left(\frac{r}{R}\right)^3 \right\}. \quad (4.4)$$

Rehbinder [reh76] refers to Leach and Walker but then states that it is convenient to describe the pressure distribution as

$$\frac{p}{p_0} = e^{-\frac{1}{2}\left(\frac{r}{R}\right)^2}. \quad (4.5)$$

The relation of the pressure as a function of the normalised radius (r/R) according to Equation (4.4) and Equation (4.5) is shown in Figure 4.4.

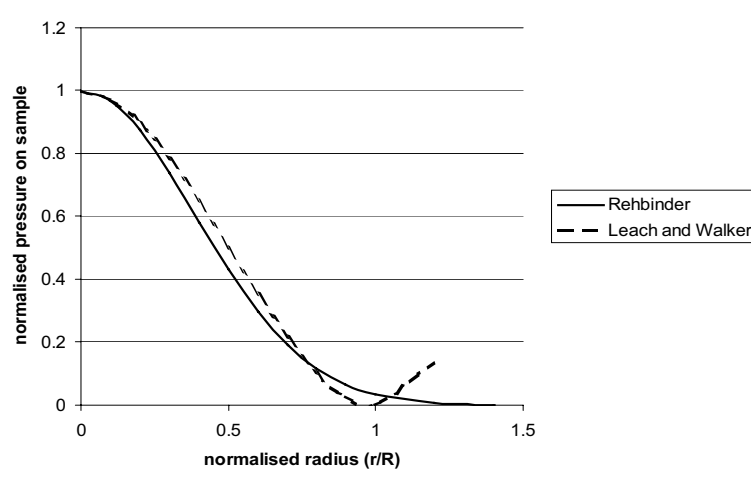


Fig. 4.4 The normalised pressure on the sample versus the dimensionless radius, according to Rehbinder's theory and according to Leach and Walker.

When comparing the predicted pressure according to the models by Rehbinder and Leach and Walker the one by Rehbinder seems more realistic, because the pressure continues to decrease for increasing radial distance.

In order to understand the observed footprints that result in the case of a cylindrical nozzle a model has been constructed. Thereto a number of assumptions have been made about the flow. First of all, we assume that the pressure distribution has a constant maximum value for points close to the axis, up to a certain radius, and that it falls off according to a Gaussian profile outside of this area, which is Rehbinder's [reh76] assumption. Secondly, we assume that the slurry propagates through a homogeneous medium (air). Thirdly, we assume that the amount of material that is removed depends on the pressure gradient, because the movement of the particles in the slurry away from the point of impact is determined by this quantity. And finally, we assume that the material removal in the experiments is very small, so the angle between the abrasives and the glass surface is constant and independent of the machining time.

Even though our slurry does not diverge, its direction of propagation will be changed upon impact on the surface. We will assume that this change of direction can be simulated by a diverging Gaussian profile. The slurry propagates in the z direction, from the nozzle opening where $z = 0$. The plane perpendicular to the z -axis is the (w,y) plane. The surface of interest is the (x,y) plane. The x -axis makes an angle α with the w -axis, see Figure 4.5. The pressure distribution in the Gaussian beam is computed first, then the tilt angle between the direction of propagation of the slurry and the (x,y) plane of interest is taken into account. The pressure distribution in the x,y plane is computed from the pressure in the Gaussian beam and the tilt angle. The material removal is assumed to be proportional to the absolute value of the derivative of the pressure in a certain point. In Figure 4.5 the computed material removal spots have been plotted for perpendicular incidence as well as for an angle of incidence of 45° . The results show a good resemblance with the experimental data. By changing the nozzle shape, or the angle of incidence, the removed profile can be altered in order to optimise it for the shaping process.

4.4 Computation of the position of impacting particles in a flow

To compute the material removal as seen from the single particle impact point of view the following approach can be followed. First one should compute where the water flows (by determining the boundaries of the stream also called the free-streamlines), then these free streamlines can be used as boundary conditions for a finite difference calculation that determines the position of all the streamlines. The definition of a streamline is that it is a contour on the surface of the stream function. Streamlines are continuous lines on which the tangent of any point is parallel to the velocity at that point. The difference in height or value of two streamlines is related to the mass flux between the streamlines. From the position of all the streamlines the fluid velocity can be computed as a function of the position. As a final step the trajectory of particles in this stream has to be computed. These steps will be treated in the following subsections.

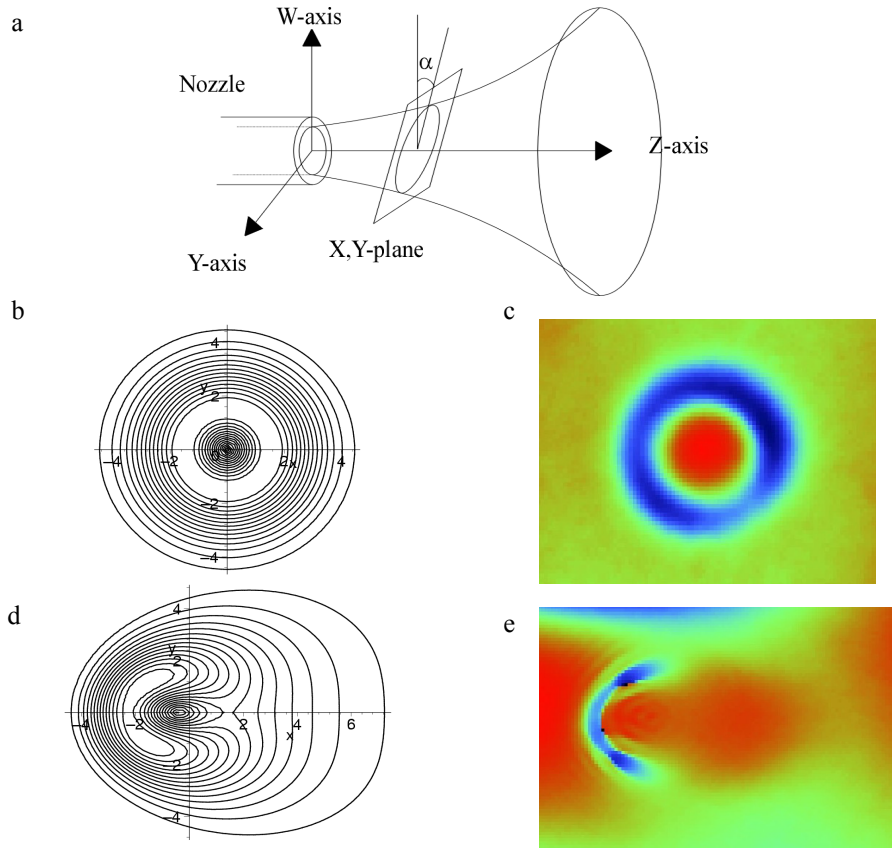


Fig. 4.5 a) Definition of axes for the computation of the material removal. b) The computed profile of the depression for an angle of incidence of 90° , c) its corresponding experimental result. The diameter of the spot is approximately 3 mm. d) The computed profile for an angle of incidence of 45° and e) the corresponding experimental result, with a width of approximately 3 mm.

4.4.1 Computation of free streamlines under an angle

Milne-Thomson (p. 295 - 306) [mil77] describes an analytical approach to compute the free streamlines of two impinging jets in two dimensions, under an arbitrary angle. Free streamlines are streamlines that separate fluid in motion from fluid at rest. This fluid at rest can also be absent (like in our case where we have a fluid in air). Along a free streamline the stream function, the velocity and the pressure are constant.

Two uniform streams A_1 and A_2 have the same speed at infinity. They meet and branch off into two other streams B_1 and B_2 , see Figure 4.6. The stagnation point is taken as the origin, the x -axis is in the direction of the A_1 stream. The asymptotic direction of the streams A_2 , B_1 , and B_2 make an angle of respectively α , β , and γ with the x -axis. The widths at infinity of the streams A_1 , A_2 , B_1 , and B_2 are h_1 , h_2 , k_1 , and k_2 .

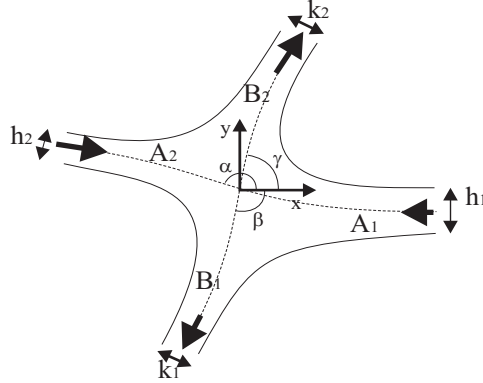


Fig. 4.6 Overview of two impinging streams (A_1 and A_2) and the two streams flowing away (B_1 and B_2), the width of the beams is indicated by h_1 , h_2 , k_1 , and k_2 so are the x and y axes. The stagnation point is that point where the x and y axes originate.

The assumption has been made that no energy is lost e.g. to heat the system. Assuming that no chemical reactions occur, mass should be conserved and the following relation should hold in the two dimensional case

$$h_1 + h_2 = k_1 + k_2. \quad (4.6)$$

Because momentum should also be conserved in both the x - and the y -direction the following relations should also hold

$$h_1 + h_2 \cos(\alpha) - k_1 \cos(\beta) - k_2 \cos(\gamma) = 0, \quad (4.7)$$

$$h_2 \sin(\alpha) - k_1 \sin(\beta) - k_2 \sin(\gamma) = 0. \quad (4.8)$$

If only the parameters of the incoming beams are known, this leaves us with four unknown parameters (β , γ , k_1 , k_2) and three equations. Therefore a general solution can not be found. If the setup is symmetrical one extra constraint is applied, and a solution can be found.

To compute the effect of a jet impacting a plane at an angle, a symmetrical situation is constructed and only one part of the situation is considered to be of interest, the other part is considered to be virtual. The directions of all flows is reversed. The following case is therefore studied: two jets, B_1 and B_2 , impinge onto each other, under angles β , and γ where

$$\gamma = 2\pi - \beta = -\beta. \quad (4.9)$$

The horizontal axis is the symmetry axis and can be taken as the impacted plane, see Figure 4.7. The direction of A_2 will be the opposite of A_1 , therefore

$$\alpha = \pi. \quad (4.10)$$

The width of the two incoming streams (one real and one virtual) have to be the same,

$$k_1 = k_2. \quad (4.11)$$

With the general equations (4.6) - (4.8) and the special conditions of equations (4.9) - (4.11) we can find that

$$h_1 = k_1(1 - \cos(\beta)), \quad (4.12)$$

$$h_2 = k_1(1 + \cos(\beta)). \quad (4.13)$$

This tells us how much water will flow to the left hand side, and how much will flow to the right hand side as a function of the angle of impact β .

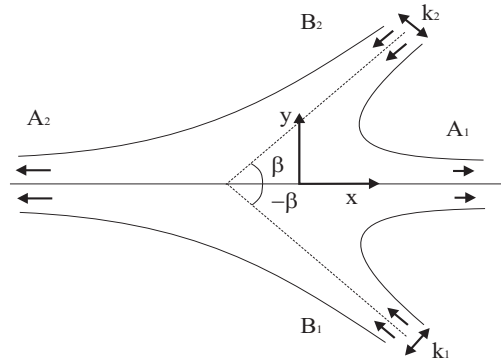


Fig. 4.7 The special case where the impacting streams make an angle β and $-\beta$ with the x axis, and the out-flowing streams are in one plane.

Milne-Thomson derives an equation for the free streamlines in Sections 11.34 and 11.35 of his book [mil77] as a function of the parameter θ , which is defined as the direction of the velocity. The final result is Equation (4.14), in which $z = x+iy$. When all the parameters are entered correctly (with the aid of Equations (4.11) - (4.13)) the x and y coordinates of a free streamline can be found as a function of the parameter θ by respectively setting the real and imaginary parts of the equation to zero.

$$\begin{aligned} \pi z = & \frac{i}{2}(-h_2 \alpha e^{-i\alpha} + k_1 \beta e^{-i\beta} + k_2 \gamma e^{-i\gamma}) + \\ & h_1 \log\left(\sin\left(\frac{\theta}{2}\right)\right) + h_2 e^{-i\alpha} \log\left(\sin\left(\frac{\theta + \alpha}{2}\right)\right) \\ & - k_1 e^{-i\beta} \log\left(\sin\left(\frac{\theta + \beta}{2}\right)\right) - k_2 e^{-i\gamma} \log\left(\sin\left(\frac{\theta + \gamma}{2}\right)\right) \end{aligned} \quad (4.14)$$

If an angle of impact of 45° is chosen and $k_1 = 0.25$, we find for $h_1 = 0.42$ and for $h_2 = 0.072$ from Equation (4.12) and Equation (4.13). This results in the free streamlines as shown in Figure 4.8. This has been computed using a Matlab program. Note the small amount of liquid that flows to the right hand side. In practical situations exactly these boundary conditions will only occur in the first part of the process when the surface still has its initially flat shape. Once some material has been removed the surface is no longer flat. This will cause the flow profile to deviate from the one shown here.

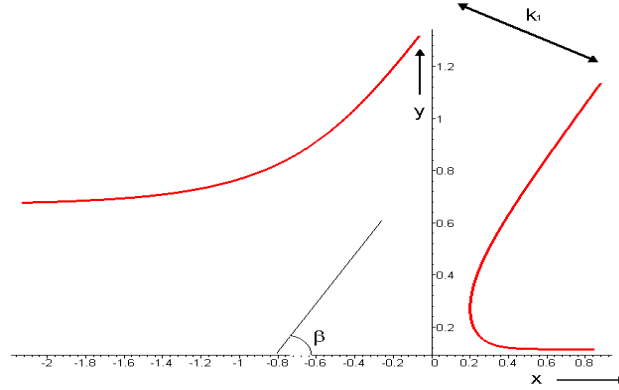


Fig. 4.8 The free streamlines as calculated from Equation (4.14) with an angle of incidence β of 45° and a width of the incoming beam $k_1 (= k_2) = 0.25$ (arb. units).

4.4.2 Computing intermediate streamlines

The position of the free streamlines is now known. To compute the position of the intermediate streamlines a finite-difference program is used. The entire area of interest is divided into discrete rectangular elements. The value of the streamlines along the boundaries is fixed, and the values of the intermediate points are determined by the following procedure by White [whi99].

The stream function ψ is by definition an integral solution of the streamline equation. The two characteristic properties of the stream function are that its value is constant on each stream line and that the mass flow between two streamlines is equal to the difference in streamline value of the two streamlines. The stream function has to conform to Laplace's equation, which equals

$$\frac{\partial^2 \psi}{\partial x^2} + \frac{\partial^2 \psi}{\partial y^2} = 0. \quad (4.15)$$

The function ψ will be defined at discrete positions (i,j) only, and will be denoted as $\psi_{i,j}$, see Figure 4.9. The algebraic approximations of the first and second derivatives of ψ in the x and y directions are

$$\frac{\partial \psi}{\partial x} \approx \frac{1}{\Delta x} (\psi_{i+1,j} - \psi_{i,j}) \quad (4.16)$$

$$\frac{\partial \psi}{\partial y} \approx \frac{1}{\Delta y} (\psi_{i,j+1} - \psi_{i,j})$$

$$\frac{\partial^2 \psi}{\partial x^2} \approx \frac{1}{\Delta x^2} (\psi_{i+1,j} - 2\psi_{i,j} + \psi_{i-1,j})$$

$$\frac{\partial^2 \psi}{\partial y^2} \approx \frac{1}{\Delta y^2} (\psi_{i,j+1} - 2\psi_{i,j} + \psi_{i,j-1})$$

When these approximations are combined with Laplace's equation the following equation can be obtained:

$$\Psi_{i,j} \approx \frac{1}{4}(\Psi_{i,j+1} + \Psi_{i,j-1} + \Psi_{i+1,j} + \Psi_{i-1,j}). \quad (4.17)$$

The stream function in the central point thus equals the average of the four neighboring stream function values. The numerical error of the discretised equation as compared to the exact solution of Laplace's equation is proportional to the square of the mesh size Δx and Δy [whi99].

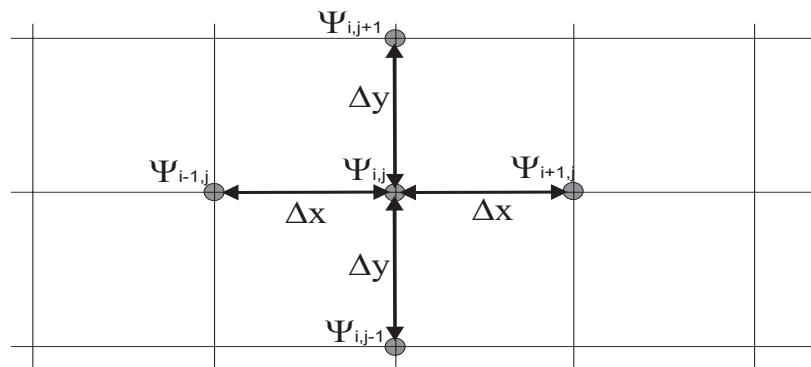


Fig. 4.9 Overview of the stream function at a point (i,j) and at its four neighboring points.

A routine has been written in Matlab that computes the intermediate values according to Equation (4.17). As input the boundary conditions and the grid are given. The value of the stream function represent the amount of mass flow between that streamline and the streamline that was chosen to be zero. Since the x and y -axes are in arbitrary units and the velocity of the flow is not specified an arbitrary value of the stream function can be chosen here. As boundary conditions the value of the stream function of the sample that is being impacted has a value 0 (arbitrarily chosen). Since the stream function is per definition constant along a solid object it is arbitrarily chosen to have a value of 10 for the upper streamline (left side), and the value of the stream function of the lower (right hand side) boundary is -0.67 as shown in Figure 4.8. The value -0.67 is derived from the amount and direction of the two flows streaming away to the left and right hand side. The amount of water that is streaming to the right hand side is 15 times as small as that flowing to the left hand side. Therefore if we choose a value of the streamline of 10 at the left hand side we should take a value of -0.67 for the streamline at the right hand side. The stream function at the two out-flowing streams (left and right) varies linearly from 0 to their extreme value at the free streamline to ensure a uniform, constant outflow velocity. The stream function of the incoming stream changes linearly from the value of the left hand side boundary to that of the right hand side boundary, because the inflow is assumed to have a constant velocity over the entire opening. After a few hundred (in this case 250) iterations the stream function is known in all intermediate points as well. This is shown in Figure 4.10.

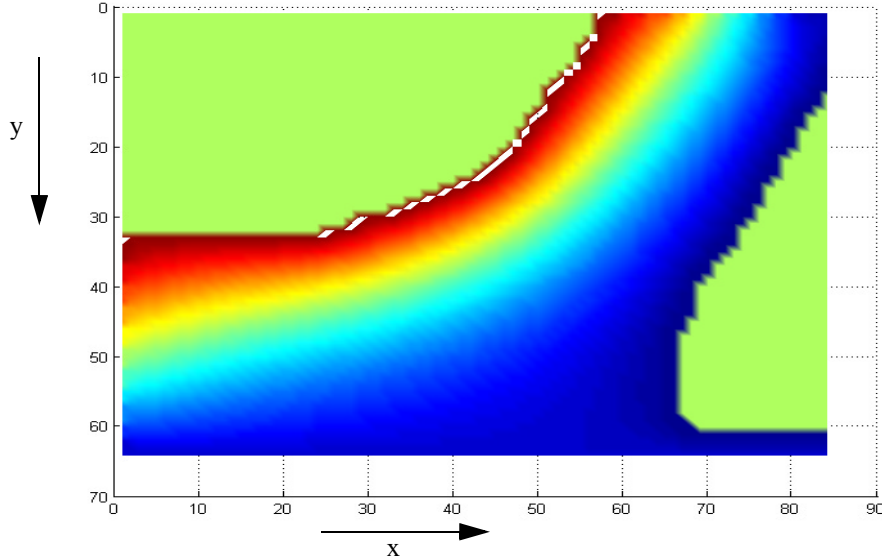


Fig. 4.10 Stream function in the 64×84 points in the x,y plane as calculated with the Matlab routine that uses Equation (4.16) and the boundary conditions that the streamline should be 10 for the left hand boundary and it should be -0.67 for the right hand boundary (x and y in arbitrary units).

4.4.3 Computing the velocity from the stream function

The velocity can be computed at any point of the flow from the stream function, according to White [whi99] by using

$$\begin{aligned} v_x(i,j) &= \frac{\Psi_{i,j+1} - \Psi_{i,j}}{\Delta y} \\ v_y(i,j) &= - \frac{\Psi_{i+1,j} - \Psi_{i,j}}{\Delta x} \end{aligned} \quad (4.18)$$

This corresponds to the definition of the streamlines which states that they are continuous line on which the tangent of any point is parallel to the velocity at that point. The resulting velocity distribution at some discrete points can be seen in Figure 4.11.

4.4.4 Computing particle trajectories in the slurry

The flow has now been characterised by the velocity distribution that is described in Equation (4.18). The final step is to compute where, under which angle and with which velocity particles impact the surface depending on where the particles are released in this flow. In practical situations the distribution of particles in the flow can be homogeneous, but it is also possible that more particles are in the outer parts of the flow. In our flows we will assume that particles are homogeneously mixed in the tank and that they are therefore also homogeneously distributed in the stream coming out of the nozzle.

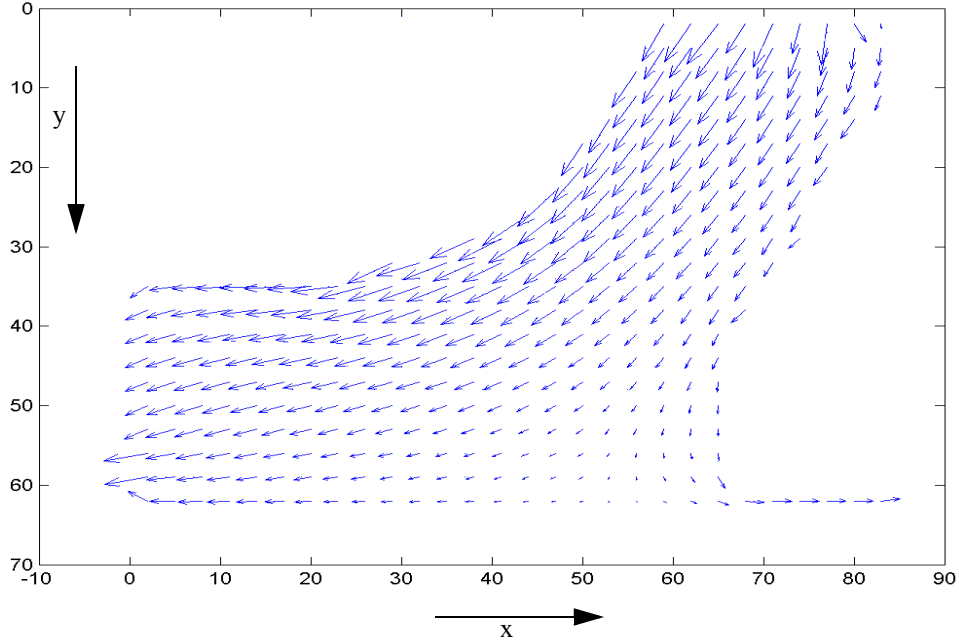


Fig. 4.11 Velocity distribution of the fluid with the stream function as shown in Figure 4.10 (x and y in arbitrary units).

Van Haarlem [haa00] describes the force law that particles have to obey to in his PhD thesis, for the case where the density of the particles is much larger than that of the fluid. The force on a single particle, F_p , depends on the mass of the particle, m_p , the velocity of the fluid, v_f , and that of the particle, v_p , the gravitational acceleration g , and the particle response time τ_p according to

$$F_p = \frac{m_p}{\tau_p}(v_f - v_p) + m_p g. \quad (4.19)$$

This response time can be seen as a time scale over which the particles respond to changes in the flow conditions. The particle response time is defined as

$$\tau_p = \frac{2\rho_f \left(\frac{d}{2}\right)^2}{9\rho_p \eta_f}. \quad (4.20)$$

where ρ_f is the density of the fluid (kg/m^3), ρ_p the density of the particle (kg/m^3), d the abrasive particle diameter, and η_f the kinematic viscosity of the fluid. The kinematic viscosity is equal to the dynamic viscosity divided by the density.

As initial condition the particle can be assumed to have the same velocity as the fluid. The force on the particle is computed, the resulting displacement of the particle in the fluid is computed, and at the new position of the particle this process is repeated. After many iterations the total trajectory of the particle is known. From Equations (4.19) and (4.20) one can see that small particles or particles in a viscous fluid will follow the veloc-

ity distribution of the fluid very closely. Larger or heavier particles or particles in a less viscous flow will deviate more from the equi-velocity lines in the fluid, as indicated in Figure 4.12. A Matlab program has been written to compute the particle trajectories.

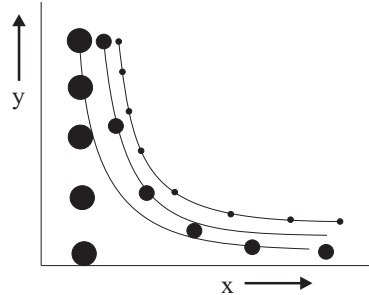
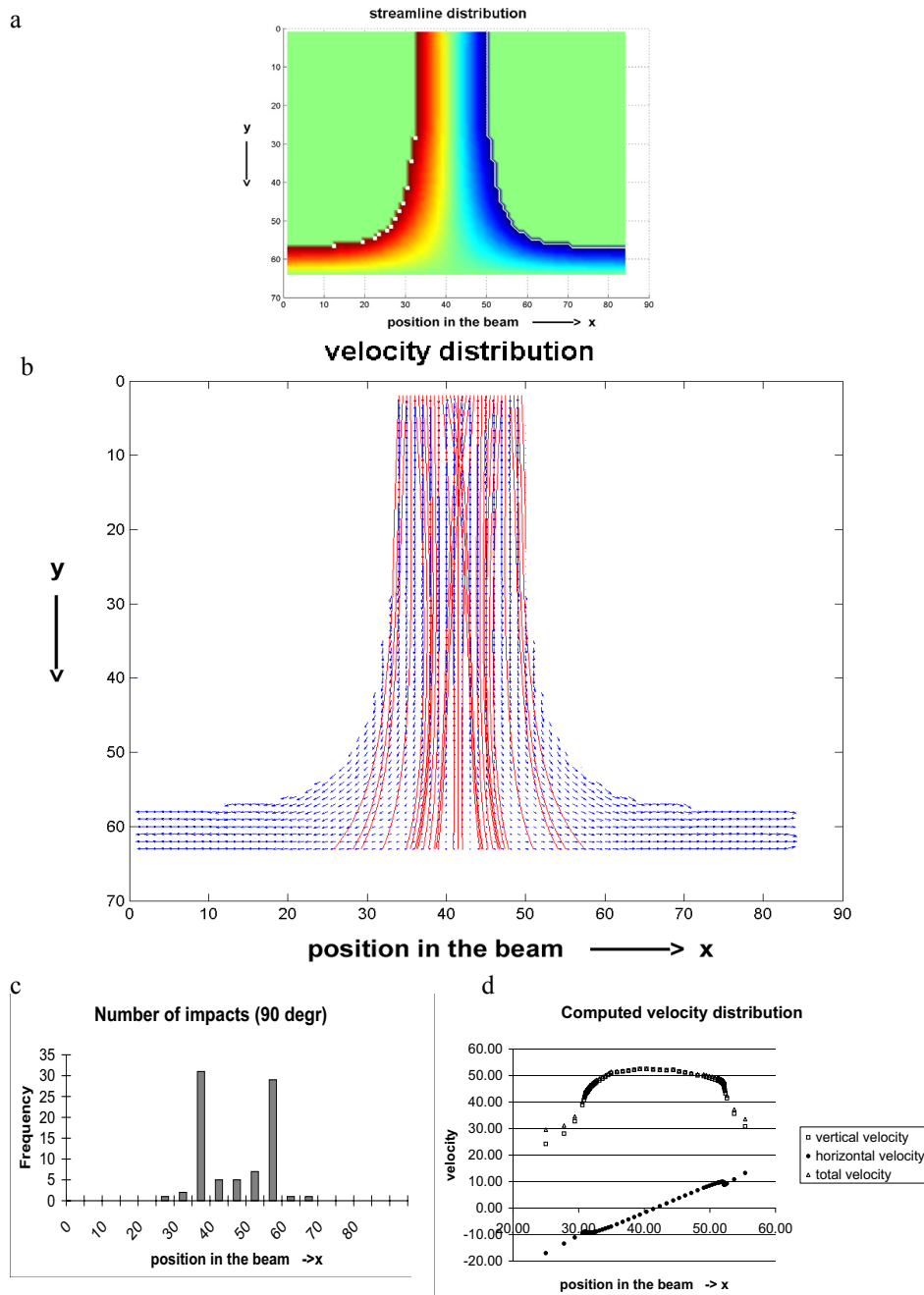


Fig. 4.12 Illustration of various particles in a flow. The solid lines represent equi-velocity lines in the fluid, the solid circles are particles in the fluid. Larger, heavier particles and particles in a less viscous fluid deviate more from the fluid velocity lines.

As an example the case of a jet impacting at 90° (perpendicular) on a surface will be shown here. In Figure 4.13 a) the potential lines in the fluid are shown, in Figure 4.13 b) the velocity of the fluid is shown as small arrows and the trajectories of the 85 particles with identical mass of which the trajectories were computed can be seen as solid lines. The particles were released equally spaced throughout the fluid at the top of the in-flow. The number of impacting particles on a certain part of the surface is depicted in the histogram in Figure 4.13 c). In Figure 4.13 d) the horizontal and vertical velocity component of the particles at the moment of their impact is shown.

So, even without taking their individual velocities and angle of impact into consideration, the typical experimentally observed w-shaped profile (see Subsection 5.1.4 for the typical removal profiles for various angles of impact) already emerges from this very simple calculation of the number of impacts as a function of the position of impact.

This model has a number of limitations. The first limitation is that it is a two dimensional model only. Another limitation of the model is the fact that the particles do not play a role any more once they have reached the surface. In reality the particles will have to flow away over the surface. They will be in the way of other particles approaching the surface. They can also be hit by other particles. The concentration of the particles in the slurry is an important factor that determines the magnitude of this effect. And the impact of the turbulent jet will disturb the flow. This model only takes a flat surface into account, as it appeared in the beginning of the experiment. The removal that the impacting particles cause is not taken into account for the shape of the surface for the subsequently impacting particles.



4.5 Microscopic model of material removal by one single slurry particle

Now that the location, direction of incidence, and velocity of the impacting particles are known, the effect of one impact should be known in order to compute the final removal profile by super-positioning of the removal of all the individual impacts. In these calculations one should not forget to take the relative velocity of the particles with respect to the surface into account. When the sample is rotating or translating, this extra velocity component can not always be ignored. When the sample velocity comes in the range or exceeds that of the slurry, it should be included in the calculations.

It is possible to compute the effect of the impact of one single particle in a number of different ways. Three different methods will be highlighted here. In Subsection 4.5.1 a finite element approach will be described; in Subsection 4.5.2 a very simple estimation of the material removal will be given, based on SEM observations of a surface after processing. And finally, in Subsection 4.5.3 the estimation of the amount of removed material as given by Finnie [fin58] will be described.

4.5.1 Finite element approach

The material removal according to a finite element approach has been carried out e.g. by Woytowicz and co-workers [woy99] in Dyna3D, a software package for non-linear finite-element analysis developed in the Lawrence Livermore National Laboratory [www9]. Woytowicz and co-workers describe the solid-particle erosion by constructing a finite element model of elastic spheres impacting on the surface of a material that can deform both elastically and plastically. The exact material removal depends on the damage mechanism that is assumed to apply, and the exact material properties. Several important phenomena in the case of multiple impacts are not considered, like particle-particle interactions, uncertainties in the particle velocities, imperfections in the particles or the substrate etc. The computations Woytowicz et al. carried out are very time consuming. Simulating two hundred impacts took more than a day on a standard desktop computer. The obtained results heavily depend on the assumed values of the material properties and damage mechanisms. In a real experiment the number of impacts is approximately $3 \cdot 10^9$ per second over the entire footprint of approximately 8 mm^2 (we take 1 liter per minute, which contains 100 grams of #800 SiC, with a density of 3100 kg/m^3 and a diameter of $7 \text{ }\mu\text{m}$). This means that every part of the surface with an area equal to the cross-section of a particle is impacted 30000 times per second. To compute the effect all these particles have on a larger area and with a processing time of a few minutes would take much too long. Therefore, we will not follow this approach. We will investigate a simple estimation and we will look at the solution presented by Finnie.

4.5.2 Simple estimation

In order to obtain a simple estimation of the total amount of removed material we will assume that the material removal is caused by the total effect of all the individual spherical particles, each removing a chip of material, with a volume depending on the particles velocity and approach angle. From scanning electron microscope images the approximate width and length of a single impact can be obtained, see Figure 4.14. For particles with an average diameter of $7 \text{ }\mu\text{m}$ the width of the impacts (w) was approximately $1/50$ th

of the impacting particles diameter (d), and the length of the impacts (l) was maximally 1/10 th of the diameter. The particle velocity (v) can be split up in a component perpendicular to the surface that is responsible for the depth of the impact (h), and a component parallel to the surface that is responsible for the length of the impact (l). The width of the impact then follows from the depth and the length and the impacting particles geometry. This results in

$$l = C_1 d v \cos(\alpha), \quad (4.21)$$

$$h = C_2 d v \sin(\alpha). \quad (4.22)$$

$$w = C_3 \sqrt{8dh - 4h^2}, \quad (4.23)$$

in which α is the angle of impact, which should be between 0 and 90°, and C_1 , C_2 , and C_3 are constants, see Figure 4.14. As an estimation of the total volume that has been removed W the product of length, height and width of the impact is taken

$$W = lhw. \quad (4.24)$$

In Figure 4.15 the material removal W has been plotted as a function of the angle of impact α .

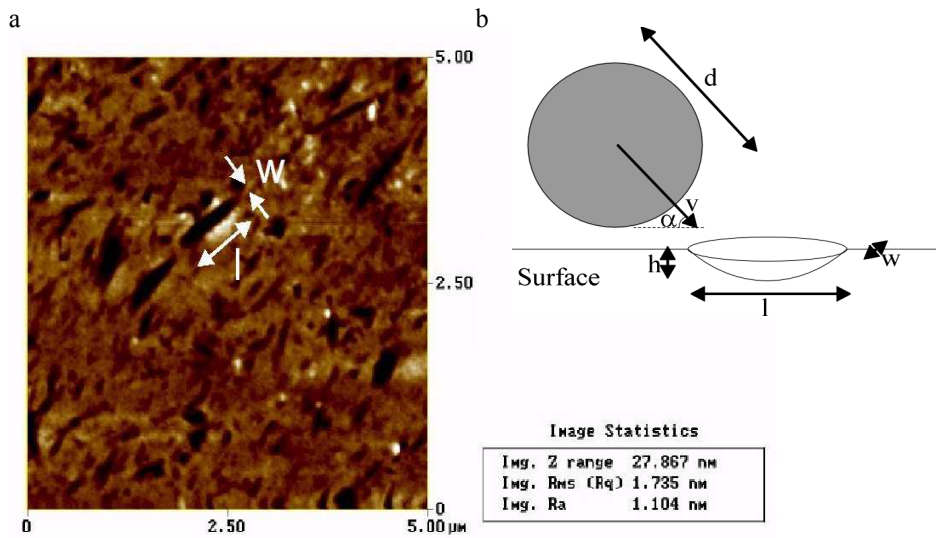


Fig. 4.14 a) A SEM picture giving an indication of the amount of removed material per impacting particle. b) The definition of the length l , the width w , and the height h of removed material by an impacting spherical particle with a diameter d , a velocity v , and an impact angle α (picture is not to scale).

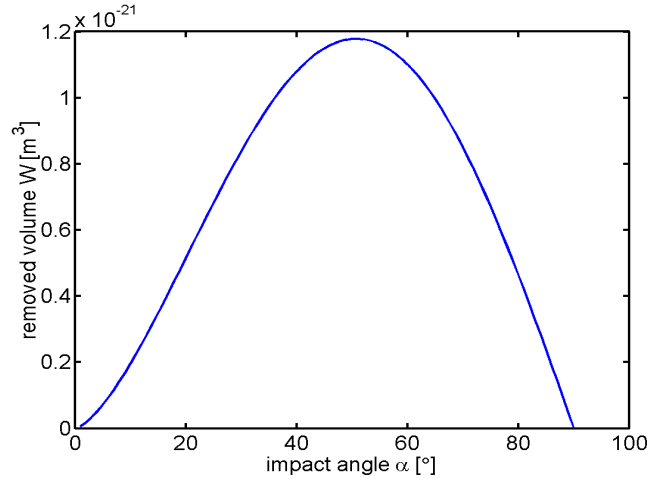


Fig. 4.15 The predicted amount of removed material W , in cubic meters, as a function of the impact angle α , in degrees, according to our simple model.

The maximum length of a single impact occurs for particles approaching the surface parallel to the surface. The removed volume will be zero there, because the depth of the impact will be zero. The maximum depth of one impact is reached for perpendicular impact, but the volume removed is zero again, because the length of the impact is zero. Another model could have been chosen here in which the length and the depth of the single impacts have a constant added to them, but we have chosen to use this simple model because we assume that the material is scraped away from the surface. If the velocity component in the horizontal or vertical direction is zero, the particle can not scrape away material. We assume that the particles do not have sufficient energy to initiate cracks, so brittle mode removal does not occur.

As an indication of the constants C_1 , C_2 , and C_3 we can look at the SEM picture in Figure 4.14. The surface was generated with particles with a diameter of $1 \mu m$, and a velocity of 20 m/s . The maximum depth is approximately 28 nm , the maximum length of a single impact that can be seen is $0.7 \mu m$ and the width of the impacts is maximally $0.14 \mu m$. In our approximate model the value of C_1 should therefore be 0.035 s/m , C_2 should be 0.007 s/m , and C_3 should then be 0.3 . The maximum height range of 28 nm indicates that the material removal is ductile in this case, as will be shown in Section 6.5.

4.5.3 Finnie's estimation

Finnie has investigated the erosion of ductile metals by studying the impact of irregularly shaped solid particles at various angles [fin58]. Thereto the equations of motion are written down of a single abrasive grain interacting with the surface. From the equations of motion the particle trajectory is computed. The volume of removed material is then estimated based on the calculated trajectory. In these calculations the rotation of the particle is neglected. A remark about this neglect can be found at the end of this subsection.

Finnie states that his approach is only allowed for ductile materials, and not for brittle ones. When brittle materials are processed in the ductile regime his approach is valid though. Finnie has studied the effect of particles in air, not in water, but the effect particles have upon impact are similar. The trajectory of the particle before it reaches the surface is very different, but this is not taken into account in his analysis. Finnie has deduced an angle dependence by making an assumption about the cutting time of the particles as a function of the angle of impact. For small angles of impact particles will cut out part of the surface and leave again. The cutting stops when the particle leaves the surface. At larger angles of impact the cutting stops before the particle has left the surface, because the particles velocity has become zero, see Figure 4.16. From these assumptions Finnie has deduced that the volume removal W depends on the angle of impact α according to

$$\begin{aligned}
 W &= C \left[\sin 2\alpha - \frac{6}{K_f} \sin^2 \alpha \right] & \text{if } \tan \alpha \leq \frac{K_f}{6} \\
 W &= C \left[\frac{K_f}{6} \cos^2 \alpha \right] & \text{if } \tan \alpha \geq \frac{K_f}{6}, \\
 C &= \frac{\rho y_t M v^2}{p_c l K_f}
 \end{aligned} \tag{4.25}$$

where M is the mass of the total amount of impacting particles, v is the velocity of the particles, ρ is their density, p_c is the constant horizontal component of the contact stress, K_f is the ratio of the vertical and the horizontal force component which is constant and assumed to be equal to 2, l is the length of the contact area between the abrasive and the surface, and y_t is the maximum depth the abrasive penetrates into the surface.

The complete derivation can be found in Appendix IV. The angle dependent wear according to Finnie's model is shown in Figure 4.17 for the normalised case. We can compute that the predicted weight loss is the same in both parts of Equation (4.25) at the limiting angle: $\tan \alpha = \frac{1}{3}$, and equals $W = \frac{3}{20} \frac{l \rho M v^2}{p_c y_t}$ there. The first derivatives of both functions are also identical at this angle. The maximum erosion occurs at a slightly lower angle where $\tan(2\alpha) = \frac{2}{3}$.

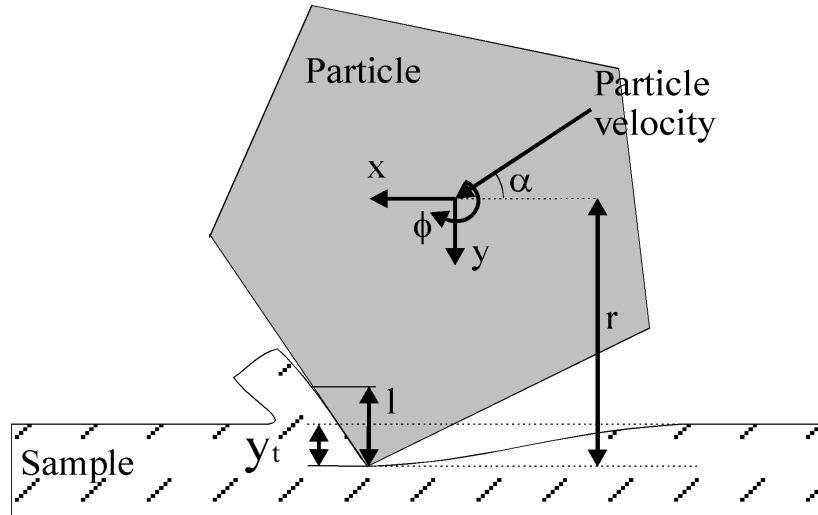


Fig. 4.16 Schematic view of the impact of a particle on a surface and the amount of material that is being removed, according to Finnie's model. The coordinate axes are x and y , the rotation of the particle is given by ϕ , the angle of impact of the particle is α , the distance from the particles center of mass to the point where the particle cuts is r , y_t is the depth of cut and l is the length over which the particle and the sample are in contact.

In Figure 4.17 Finnie's data points have been plotted for measurements he has carried out of the relative weight loss of low carbon steel, copper and aluminum, when eroded by silicon carbide grains. When the results from his model are compared to his experimental data the agreement at low angles of impact is good, but at 90° the erosion is greatly underestimated. This is caused by the fact that at normal incidence the particle has no tangential velocity. The model assumes that material removal is caused by the tangential velocity of the particle, so the model can not represent the impact at a perpendicular angle of incidence. In situations of perpendicular incidence material can also be removed due to brittle processes, which is also not covered by Finnie's model.

Finnie's model does not take the rotation, shape, hardness or strength of the abrasive into account [fin03]. Some extensions to Finnie's model have been described in later articles [fin60]. In these articles Finnie concludes that sharp particles will cause more erosion than perfect spheres, which he has confirmed by experiments. In the model, particles that are closer to the spherical shape will have a higher value of K_f . If the abrasives are harder than the surface, their hardness has no effect on the removal. If they are softer than the surface, the material removal will decrease greatly with decreasing hardness. The strength of the particle is also important. If it has a high strength it will cut as one unit. If the strength is too low it will fracture. This will reduce the removal rate, because the diameter of the particles has decreased. In 1995 Finnie states [fin95] that neglecting the rotation of the particle is not correct, and that taking rotation into account reduces the angle where maximum erosion occurs. In the same article he states that the material removal depends on the velocity to a power slightly larger than 2, typically 2.3 to 2.4.

And finally a remark has to be made about the difference between the angle dependence of the material removal caused by single particle impacts, as covered by Finnie's model described in this section and the angle dependence of the material removal as described in Section 5.5. The material removal that has been measured in Section 5.5 is described as a function of the angle between the jet and the surface. This is not the same as the angle of incidence of the individual particles, as should be clear from Section 4.4.

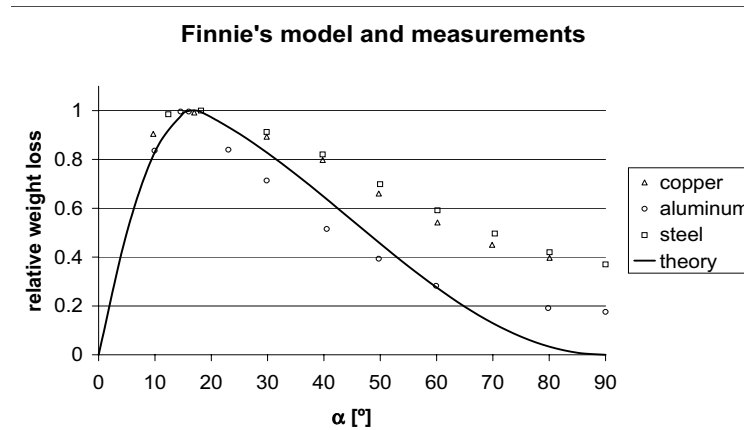


Fig. 4.17 Normalised relative weight loss as a function of the angle of impact of the particle (not of the jet), according to Finnie's model, and some measurement data according to Finnie of SiC grains on copper, aluminum and steel [fin58].

4.6 Removal profile over an area larger than the footprint

In this section the theoretical effect of either translating or rotating a sample underneath a fixed nozzle with a known footprint will be discussed first. Then the surface deviations that occur in the center will be treated.

4.6.1 Theoretical influence of translation or rotation

To compute the removal profile over an area larger than the footprint the first requirement is that the footprint itself is known, either by accurate measurement of a produced footprint, or by computation of the expected footprint. This computation can be done according to the method described in Sections 4.3 or 4.5, but then in three dimensions.

Once the stationary spot shape is known, the effect of translation and rotation can be studied. If the speed of the slurry is large compared to that of the work piece, the total effect that a nozzle has on a translating or rotating work piece can be shown to be the sum of the effects of the stationary spot at all the scanned locations. The final surface removal is denoted by $q(x,y)$ which represents the removed material as a function of the location on the surface (x, y) . This final shape can be computed as the integral over the processing

time (from t_0 to t_1) of the surface shape of the stationary footprint $f(x,y)$ at the positions over which it moves during the processing time.

$$q(x, y) = \int_{t_0}^{t_1} f\{x - x_0(t), y - y_0(t)\} dt \quad (4.26)$$

Where $x_0(t)$ and $y_0(t)$ describe the trajectory of the spot over the surface in time. As a simple example the footprint is chosen to be a delta function, the spot is moving in the x direction following a trajectory described by the function $v \cdot t$, and the spot has no velocity in the y -direction. When the spot moves over the surface from $t=t_1$ to $t=t_2$ the resulting material removal $q(x,y)$ will be

$$q(x, y) = \int_{t_0}^{t_1} \delta(x - vt, y) dt = -[\varepsilon(x - vt, 0)]_{t_0}^{t_1} = \text{rect} \left[\frac{x - v \frac{(t_1 - t_0)}{2}}{t_1 - t_0} \right] \quad (4.27)$$

where ε is the step-function and $\text{rect}[x]$ is the rectangular function with unit value for $|x| < 1/2$. This corresponds to a removal of unit height on the y -axis from $x=v \cdot t_0$ to $x=v \cdot t_1$.

This material removal principle has been implemented in Maple and an example of the effect of translation and rotation is shown in Figure 4.18. For this example a stationary spot is defined (a), the spot is scanned in the horizontal direction only (b), it is scanned in the vertical direction only (c) and the work piece is rotated with respect to the nozzle while no translation took place (d). The sample that is being processed is limited to a rectangular area in this simulation, which is the reason for the sudden ending of the profile. The experimental validation of this approach can be found in Section 6.6.

If the relative speed of the work piece comes closer to that of the slurry, the work piece speed will have to be taken into account. One way of implementing this effect would be by changing the velocity as a function of the position of the spot, another possibility would be to change the spot shape according to the location on the sample. This could for example be done by using an expanding nozzle and changing the distance between the nozzle and the surface.

If the footprint is scanned over the surface while the sample is rotating it is possible to obtain sufficient overlap between two adjacent passes over the surface. The necessary overlap depends on the tolerable height fluctuations on the surface. Assume that the stationary footprint is Gaussian shaped, and has a full width at half maximum of approximately 3, see Figure 4.19 a). The resulting surfaces can be seen for spots that are added after a shift of 1 and 2 units in figures b and c respectively. When the spots are added with a shift of 2 the resulting surface shows a wavy character. For an overlap that results when the spot is shifted 1 unit the waviness of the final surface is not perceptible anymore. In practical situations it is easy to reach this overlap. Assume that the spot diameter is 3 mm and we want to overlap the spot in such a way that the shift equals 0.5 mm, which is even smaller than the shift of one unit in Figure 4.19 b). Assuming that the nozzle is scanning with a velocity of 10 mm/s, we need a rotational velocity of 20 revolutions per second.

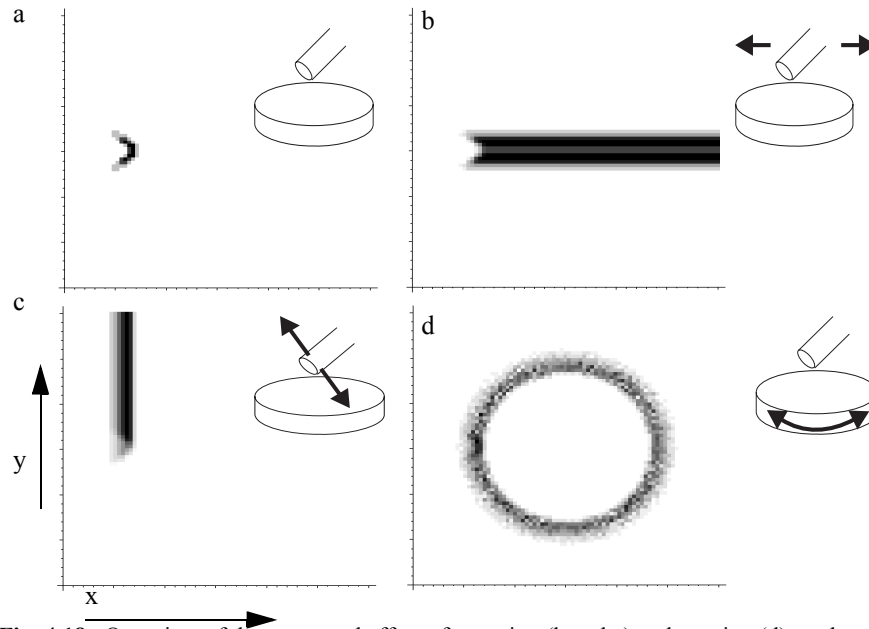


Fig. 4.18 Overview of the computed effect of scanning (b and c) and rotating (d) on the total material removal, when the stationary footprint in a) is used. Darker areas indicate more material removal (a larger value of $q(x,y)$). The size of the sample is limited to the visible square area.

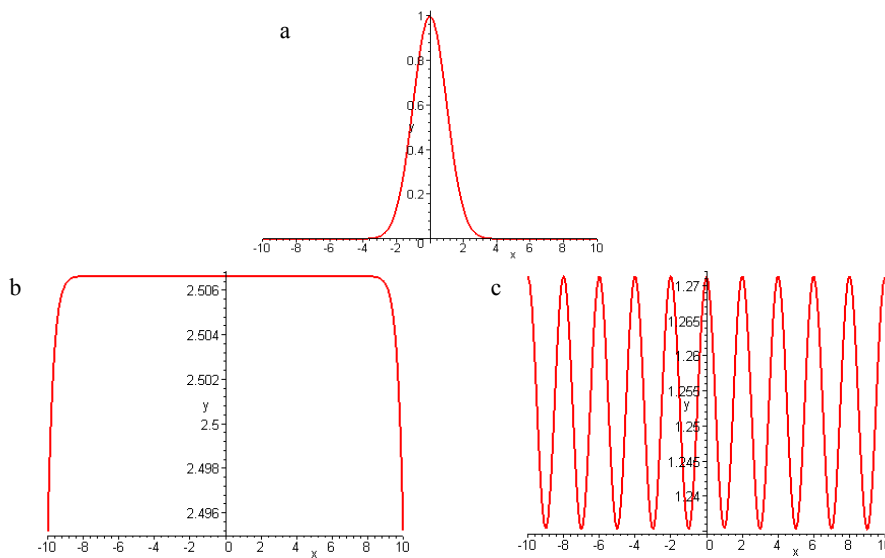


Fig. 4.19 a) The initial Gaussian spot shape with a full width at half maximum of approximately 3 units. b) The resulting surface when several spot traces like the one in a) are added after a shift of one unit. c) The resulting surface when several spots like the one in a) are added after a shift of two units.

4.6.2 Surface errors in the center of the work piece

The removal of the right amount of material from a rotating work piece is complicated in practical cases, especially in the center, due to the fact that the removal spot will overlap itself there because of its finite size. Both the velocity of the work piece and the surface area to be treated are zero in the center and increase towards the edge of the sample (proportional to the radius of the sample). To remove the correct amount of material over the entire surface the speed of rotation and/or the dwell time should be controlled as a function of the position of the nozzle. The dwell time is the amount of time that the nozzle stays at one position.

We will now take a look at the theoretically resulting surface shapes that occur when a small nozzle scans over a surface that is rotating, while the velocity of the nozzle is controlled as a function of its position. The nozzle is assumed to scan from outside the sample on one side to just outside the surface on the other side of the sample. This condition is relevant to prevent edge effects from occurring. The surface area of a ring with width dr at a distance r from the center of rotation equals $2 \cdot \pi \cdot r \cdot dr$ so it increases linearly with the distance r . Therefore the removal at a point of the surface $q(x,y)$ will be inversely proportional to the distance r . The material removal at a location will also be inversely proportional to the velocity at that position $v(r)$. These two factors determine the amount of time that the material removal can occur at a certain point on the surface. The material removal can be computed as

$$q(x, y) \propto \frac{1}{rv(r)}. \quad (4.28)$$

A routine has been written in Matlab to visualise the generated surface shapes depending on the removal per second and the velocity of the nozzle with respect to the work-piece. The nozzle is one x one element large. Four cases will be presented. In the first situation the velocity was chosen to be constant and independent of the position on the surface. As a consequence of Equation (4.28) the surface shape will be inversely proportional to r , this can be seen in Figure 4.20 a). The surface under consideration is 50 x 50 elements large, and the removal spot is one element in size. The removal took place over the entire surface. If the area of interest would have one element in the center (in the case of an odd number of elements in any direction) the distance to the center becomes zero there, and the removal would be infinitely large. Since this is not a physically realistic situation the removal at the central element is then computed based on the average removal of the neighboring elements. In the second situation the material removal is uniform over the entire area. This is a result of choosing a velocity that is inversely proportional to r . The resulting surface can be found in Figure 4.20 b). The third situation is the production of a spherical surface with a radius of curvature R . The amount of material that should be removed as a function of r can be shown to be equal to

$$q(r) = R - R \cos\left(\arcsin\left(\frac{r}{R}\right)\right). \quad (4.29)$$

From Equations (4.28) and (4.29) the velocity that is needed to generate a spherical shape can be seen to be

$$v = \frac{1}{Rr \left(1 - \sqrt{\frac{R^2 - r^2}{R^2}} \right)} \quad (4.30)$$

In Figure 4.20 c) an example is given of a convex sphere with a radius of curvature of $R = 50$. To obtain a concave spherical surface a velocity of

$$v = \frac{1}{Rr \left(\sqrt{\frac{R^2 - r^2}{R^2}} - \sqrt{\frac{R^2 - r_m^2}{R^2}} \right)} \quad (4.31)$$

should be chosen, where r_m represents the maximal value of r that can be reached. The concave surface with a radius of curvature of $R = 50$ is shown in Figure 4.20 d).

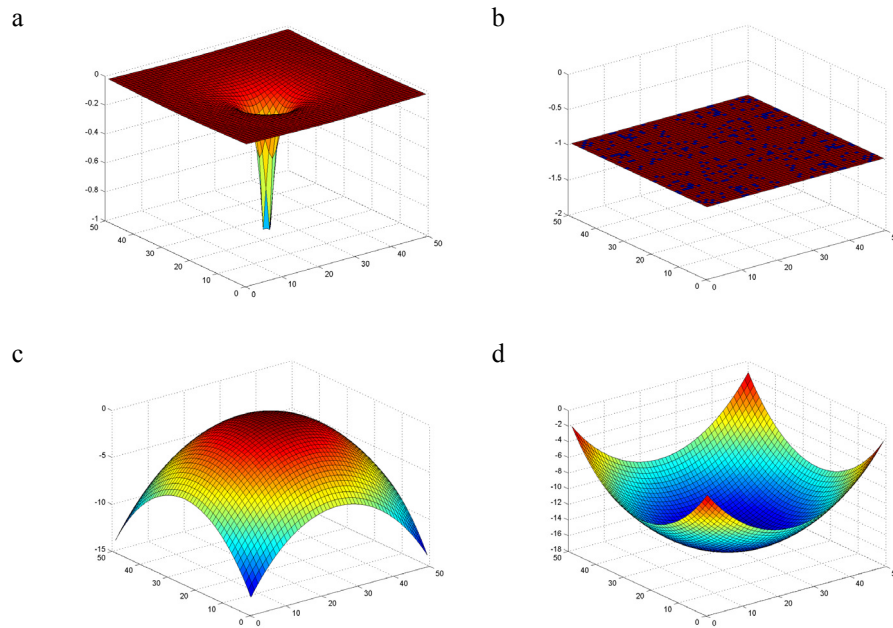


Fig. 4.20 Resulting surface shapes after material removal for four different cases (computed values). The velocity of the nozzle with respect to the surface over the rotating sample was a) constant, b) inversely proportional to the radial distance r , c) dependent on r according to Equation (4.30) d) dependent on r according to Equation (4.31).

When processing in the center of a rotating surface is carried out too long or not long enough a typical surface shape results. As an example we will show some of the possible surface shapes that can occur in Figure 4.21. In this schematical figure some cross-

tions are shown of resulting surfaces for an increasing amount of processing time in the center of the work piece. For very short times spent in the center, a peak will remain visible (a). For very long times spent in the center a depression will result (e). Two examples of experimentally obtained surfaces that show these defects can be found in Figure 4.22. An example of a correctly produced flat sample can be found in Subsection 6.6.2.

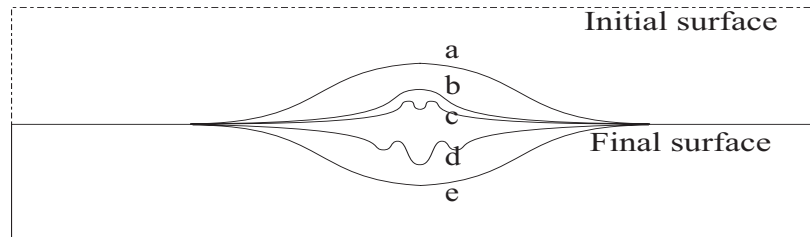


Fig. 4.21 Rough sketch of an axial section through a work piece. The strongly exaggerated profiles that can occur in the center of a work piece are shown for an increasing processing time in the center as compared to the rest of the surface when going from a) to e).

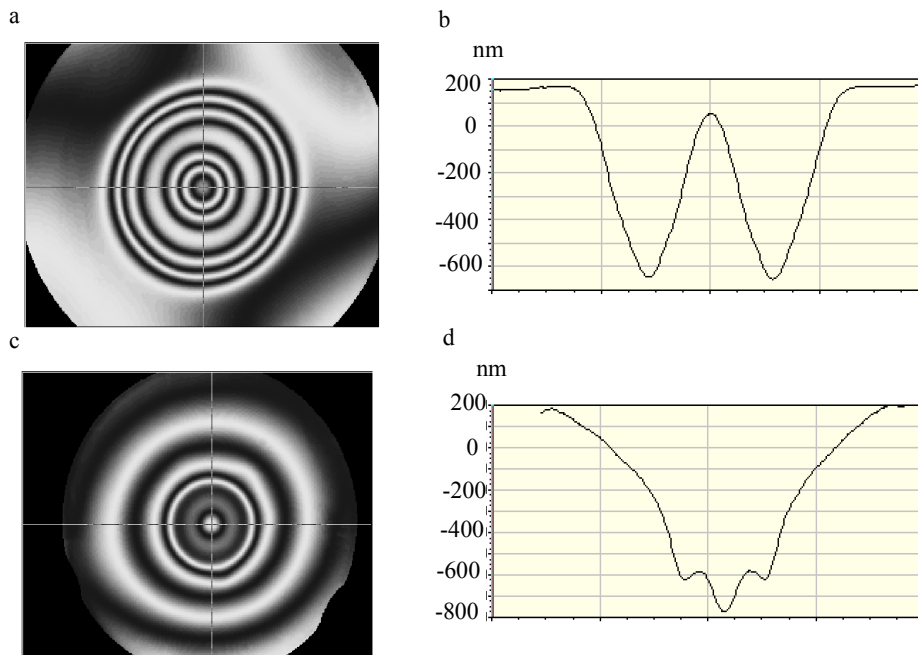


Fig. 4.22 Two measured surface profiles and the corresponding cross-section through the surfaces that occur when the processing time in the center is too short (a) and (b) or too long (c) and (d). These cases correspond to the predicted situations b and d in Figure 4.21.

4.6.3 Application - nozzle design

When shape corrections should be carried out on part of a surface, while other parts of the surface should not be changed, certain stationary footprints are preferred over others. As an example of an application of the model described by Equation (4.26) the design of a new type of nozzle with a preferred footprint will be described here. The stationary footprint of a cylindrical nozzle has the property that most material is removed in a ring shaped area around the center, and hardly any material is removed in the center, see Figure 4.23 a). To perform shape corrections on a surface, without damaging the surrounding area it would be easier to have a stationary footprint that shows the largest removal in the center. When the profile in Figure 4.23 a) is rotated around the position marked with an o, the profile in b) results. This computed result has the required property of a deepest depression in the center. To obtain such a footprint a rotation of the nozzle could be carried out around a point inside the nozzle. From a mechanical point of view this is not attractive. The same result is obtained by inserting a stationary helix into the cylindrical nozzle. A helical structure (when the diameter and other characteristics are chosen correctly) makes the water move in a spiralling way, as if the nozzle were rotating around the o. In the case of a perfectly stationary pressure the slurry will leave the nozzle following the same trajectory as inside the nozzle. A cross section through the jet at a fixed distance from the nozzle would reveal that the slurry is always in one fixed part of its spiralling motion. Small variations in the pressure will change the precise motion of the slurry. The average of all the slurry motions results in the average profile that has its deepest part in the center.

A prototype has been built and its stationary footprint was taken, and it turned out to be as expected: deep in the center and less deep towards the edges, as can be seen in part d) of Figure 4.23. The outer diameter of the nozzle is 2.5 mm, the inner diameter of the helical structure is 1.5 mm.

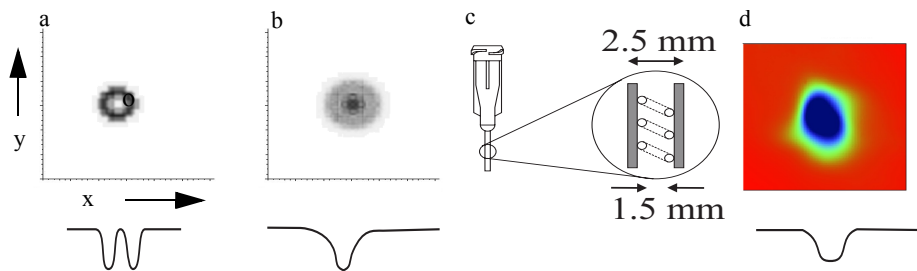


Fig. 4.23 a) The stationary footprint of a cylindrical nozzle with a circle (o) indicating the position around which the rotation was carried out. Darker areas represent deeper parts of the surface. b) The resulting profile after rotating the profile in a) around the circle (o). c) The modified cylindrical nozzle with a helical structure inside. d) The experimentally obtained footprint from the nozzle in c). A schematical representation of the cross sections of the spots is given below the corresponding spots.

4.7 Final surface state (micro roughness)

The roughness that results during processing is an important issue. When removing material from a polished surface the processing should not increase the roughness, and when the initial surface roughness is high, the rms roughness should be decreased to a few nanometers for low quality optics and to less than 1 nm for higher quality optics. In this section the influence of the FJP process on the roughness of the processed surface will be studied. To investigate which parameters determine the final roughness a three dimensional model has been developed. The roughness data resulting from simulations will be presented here. The experimentally obtained roughness results are described in Section 6.7.

Surface roughness parameters can be calculated from the height distribution of the surface. In our model, particles are assumed to impact at random locations on the surface. They each have a fixed amount of energy, which they use to remove a fixed volume of material. When it is not possible for the particle to impact the random location due to protruding areas around this location, we suppose that the material removal that should occur in the center is distributed evenly over all points of contact between the particle and the surface. In Figure 4.24 an example is given of a particle impacting on a surface. The grey area will be removed by the particle. The figure only shows a two-dimensional case which is symmetric as well. This is not a limitation of the model but it is for the ease of understanding only.

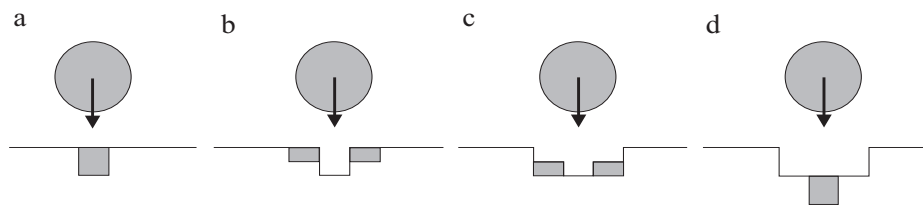


Fig. 4.24 Basic features of the model for particles impacting on a surface. If there are no surface protrusions the particle will remove a fixed volume from the center of the impact location (a and d). In the case of protruding parts of the surface, these will be removed first (b and c). For simplicity this drawing depicts a symmetrical two-dimensional case.

Furthermore, the assumptions have been made that all impacting particles have identical mass, velocity, and angle of impact, and that they each remove the same amount of material when impacting. The effects of the shape of the particles, their hardness, and their strength are not taken into account.

The lateral dimensions over which one particle is assumed to remove material from the surface are taken as unit length, and the depth of the material removal per impact is also taken as unit length initially. In a later stage the effect of a change in kinetic energy of the particles can be incorporated in the depth of the material removal per impact, and the effect of the angle of impact can be described by making the particle remove material over an area larger than 1 x 1 element.

As an example, the surface upon which particles can impact is chosen to have a size of 10×10 elements of unit length. In Figure 4.25 a) the roughness of an initially perfectly smooth surface has been plotted as a function of the number of impacts (from 0 to 10000). In Figure 4.25 b) the same number of impacts occurred on a surface that initially had a random height distribution between 0 and 100. In Figure 4.25 c) the initial surface has a random distribution between 0 and 1000. The roughness of the smooth surface first increases to a certain value. The roughness then fluctuates around the equilibrium value. The roughness of the initially rougher surface decreases to a certain value and then remains stable at this value. The roughness of the very rough surface decreases, but does not reach the same low roughness as the other surfaces within the first 10000 impacts. The final roughness is not yet reached, because the average number of impacts per element is only 100, and the initial roughness was chosen to be 1000. When the impacts continue (up to approximately 50000 impacts) almost the same final roughness is reached as for the surface, that was smoother initially. The small dependence on the initial surface roughness is caused by the fact that relatively deep pits are present in a surface with a certain initial roughness distribution. To remove each of these pits a relatively large amount of material should be removed over the entire surface.

Apart from the initial surface roughness, other parameters that can be varied within this model are the effect of the impact of a single particle and the diameter of the impacting particle. When the effect of one particle is increased (which can be compared to increasing the pressure of the jet or the kinetic energy of the particle) the roughness of relatively rough surfaces decreases more rapidly, but the finally obtained roughness is also higher than it would be for lower pressures. This is a logic consequence since each particle has a larger effect, so on a smooth surface the impact of one particle will increase the roughness more than for a particle at lower pressures. For relatively smooth surfaces the final roughness will also be higher when the effect of one particle is larger.

When the diameter of the impacting particle is increased (without increasing its impacting energy) the roughness decrease proceeds at the same rate as with small particles, but the final surface roughness is better for larger particles, because these particles have an effect over an area that is larger, so the removal will be more uniform. Some simulation results have been summarized in Table 4.1, and Figure 4.26 to show the effect of the various parameters on the final roughness and the rate at which roughness reduction is obtained. These simulations show that the most rapid way of reaching a certain final roughness is by using a number of different settings after each other, see Figure 4.27. The first setting should cause a rapid roughness reduction, but it will not reach a low final roughness, the second setting then reduces the roughness further, but not as fast as the first step. And this can be continued in many different steps. The particle diameter could be used as a parameter for these steps, but it is more practical to change the velocity of the particles.

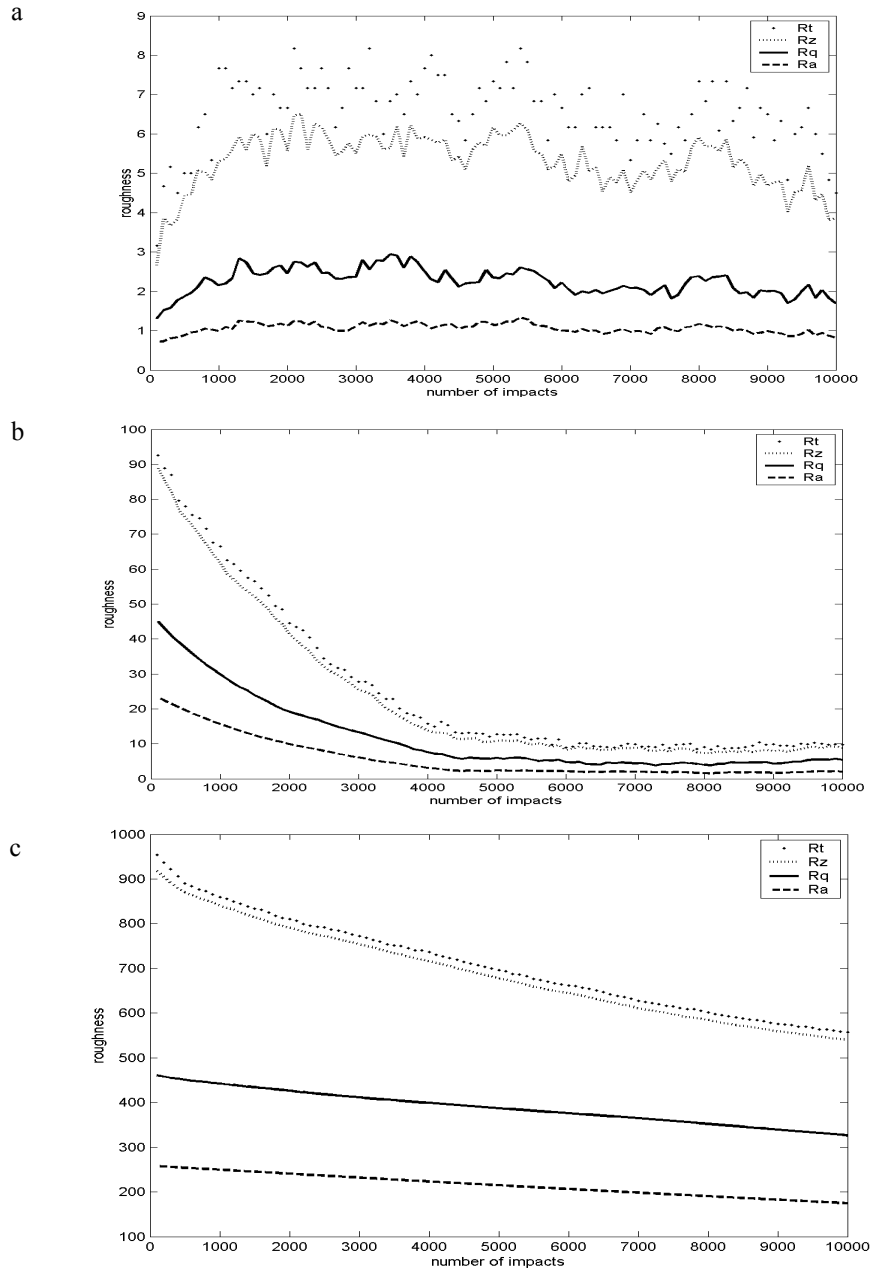


Fig. 4.25 Roughness values as a function of the number of impacts. Each figure shows the R_q , R_q , R_z and R_t value; these roughness parameters are defined in Section 3.1. a) shows the shape of an initially smooth surface, b) shows the effects on an initial surface with randomly distributed height values between 0 and 100, c) shows an initial surface with randomly distributed values between 0 and 1000.

Table 4.1 Effect of process parameters on the roughness reduction speed and on the final roughness, computed with the random impact model described in this section, all in arbitrary units. ‘-’ indicates that the aimed for roughness was not reached yet.

effect of one particle (arb. units)	abrasive diameter (arb. units)	initial surface roughness (arb. units)	number of impacts needed until $R_a < 10$	number of impacts needed until $R_t < 20$	Final roughness R_a (arb. units)	Final roughness R_t (arb. units)
1	7	1	-	-	1	6
1	7	10	-	-	1	6.5
1	7	100	1700	3400	1	7
0.2	7	1	-	-	0.8	5
0.2	7	10	-	-	1	6
0.2	7	100	5800	18000	1.5	7
5	7	1	-	-	2	13
5	7	10	-	-	2	13
5	7	100	400	700	2.5	13
1	1	1	-	-	1.8	10
1	1	10	-	-	1.9	11
1	1	100	1800	3600	2	10
0.2	1	1	-	-	1	6.5
0.2	1	10	-	-	1.2	8.5
0.2	1	100	9000	17000	3	14
5	1	1	-	-	2.5	16
5	1	10	-	-	2.5	17
5	1	100	400	1800	4	20

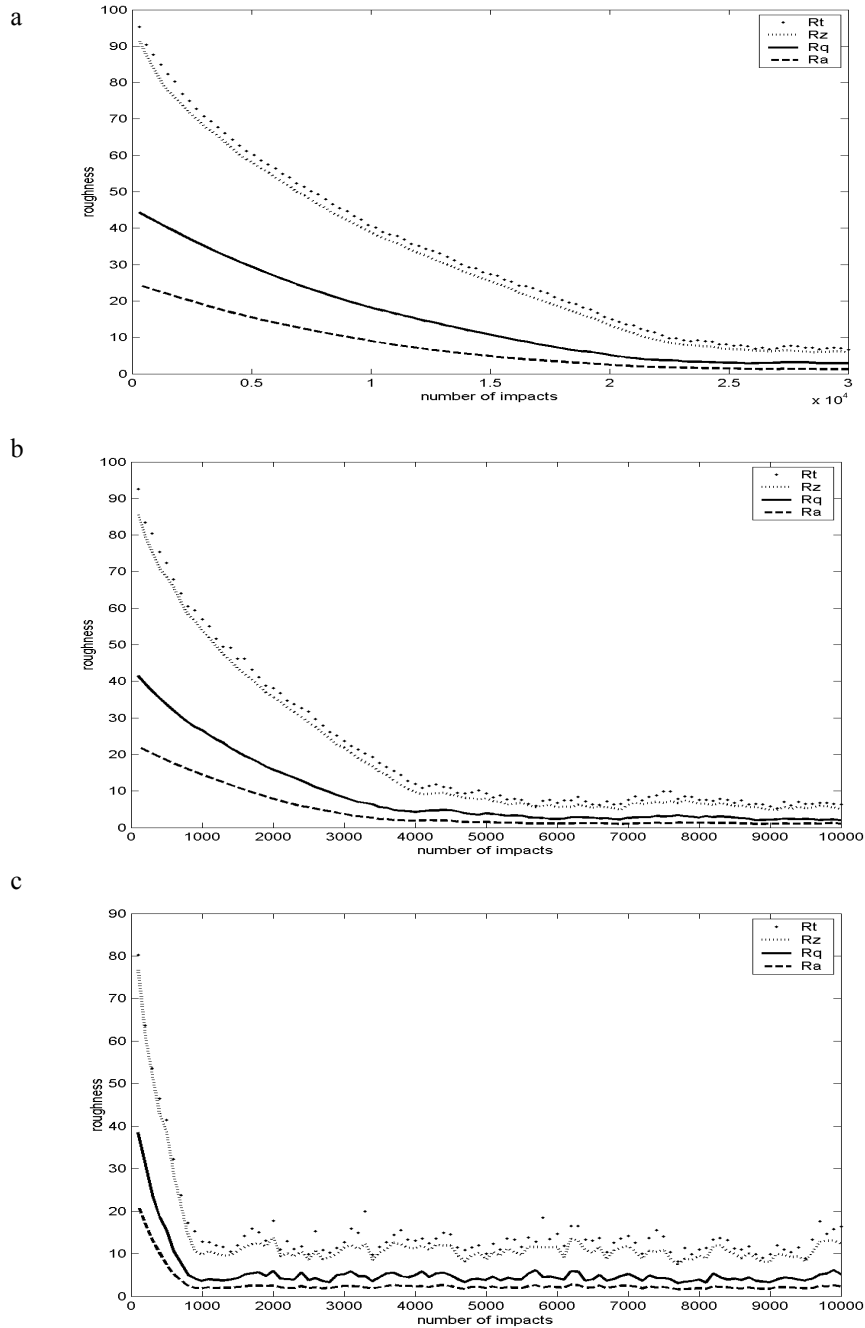


Fig. 4.26 Comparison of the roughness as a function of the number of impacts for three different values of the effect of one impacting particle. The effect of one particle is 0.2 in a), 1 in b), and 5 in c). The initial roughness is 100 in all cases, and the impacting particles diameter is 7.

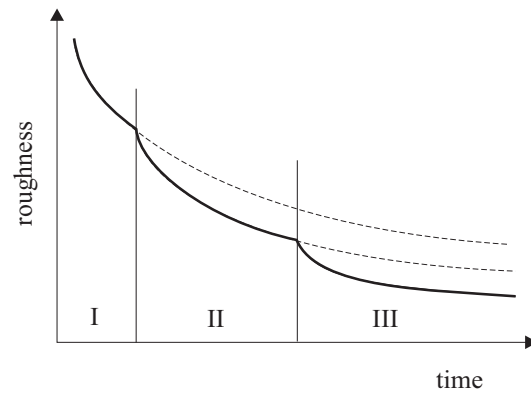


Fig. 4.27 Schematical representation of the reduction of roughness as a function of time by using three different process settings after each other.

5 FJP process parameters

In this chapter the theoretical and experimental relations will be described between the parameters that can be altered in the FJP setup and their influence on the material removal. In order to investigate the dependence of a certain parameter, this parameter is varied while the other parameters are kept constant. The value that is chosen for the fixed parameters is based on previous experiments and experience. Some typical values can be found in Appendix IV. All of the parameters like the pressure and the particle type and size are chosen in such a way that the process is in the ductile regime. Section 5.1 describes the dependence of the process on the various slurry parameters. This section is split into four subsections; Subsection 5.1.1 describes the effect of the particle concentration, Subsection 5.1.2 covers the type, size, and geometry of abrasive particles, Subsection 5.1.3 covers the effect of the slurry temperature, and Subsection 5.1.4 describes the effect of the particle velocity. Section 5.2 describes the effect of the stand-off distance. Section 5.3 treats the effect of the processing time, Section 5.4 discusses the effect of the material that is being processed, Section 5.5 shows the effect of the angle of impact, and Section 5.6 describes the influence of the nozzle shape.

5.1 Description of the slurry

The slurry that is used in the FJP process consists of a liquid carrier like e.g. water with homogeneously mixed abrasive particles in it. The slurry parameters that can be changed are the particle concentration (Subsection 5.1.1), the type of the abrasive particles and their size (Subsection 5.1.2), the temperature of the slurry (Subsection 5.1.3), and the particle velocity (Subsection 5.1.4). Various additives can be mixed into the slurry, like conservatives, particles that increase the homogeneity of the particle distribution, substances that change the pH value or the viscosity etc.

5.1.1 Particle concentration

A higher concentration of abrasive particles means that more particles will strike the same surface area per second. In principle this means that more erosion will take place, as long as the particles do not interfere with each other. Zu [zu91] has researched slurry erosion and he cites that a limiting concentration of 50 wt.% exists below which particle interference can be neglected in the case of slurry erosion. For higher concentrations the particles lose part of their kinetic energy due to these collisions, and the lost energy can not be used for material removal, but is converted into heat. Zu also compares some experiments in air-borne and water-borne abrasive particles. The investigated particles are

600-850 μm large. The abrasive velocity is very low: 4.5 m/s. He concludes that slurry erosion proceeds at a rate much larger than air-borne erosion and the ratio of the removal rates depends strongly on the angle of impact. The reason for the slower removal in the case of air borne erosion is the fact that particles get embedded in the surface and are not removed like in the slurry erosion case. The experimental conditions of Zu are different than in the case of FJP (larger particles and a lower velocity). We have not experienced non-linear effects for any of the concentrations we have used, so we can only say for sure that the limiting concentration is higher than 20%, which is the highest concentration we have used.

To investigate the concentration dependence an experiment was conducted with 6 μm aluminum oxide abrasives on flat BK7 samples. The concentration of abrasives was varied between 2 gram and 4000 gram per 20 liter (2 gram = 0.01 wt.% added to the water; 4000 gram = 20 wt.% added). The nozzle that was used was a 1.55 mm diameter cylindrical one. It was placed at 6 mm from the surface, at an angle of 70° with the surface. The pressure was 5 bar, the processing time 10 minutes. The depth of the generated profiles was measured as a function of the concentration. The results are depicted in Figure 5.1. The erosion indeed depends linearly on the concentration. Keep in mind that the concentration is not as high as the 50 wt.% that was mentioned earlier, so particle interactions are avoided. Using a slurry concentration of 50% or more is not advisable anyway since it can cause congestions in the system.

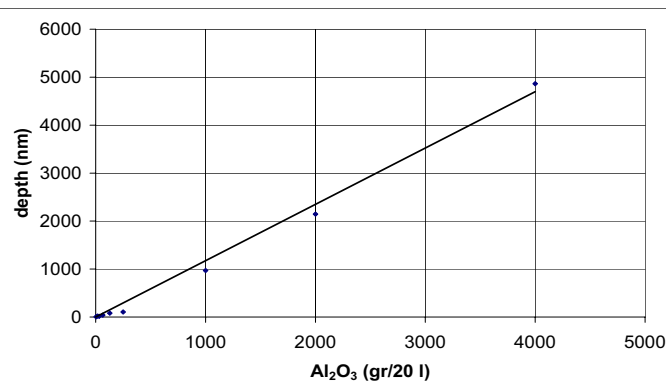


Fig. 5.1 Dependence of the erosion after 10 minutes on the abrasive concentration, for concentrations of 6 μm aluminum oxide ranging from 2 to 4000 gr / 20 liter.

5.1.2 Type and size of abrasive particles

Abrasive particles used in the FJP experiments are e.g. diamond, silicon carbide, cerium oxide, or aluminum oxide. In Appendix IV an overview can be found of some commonly used abrasives. Their diameter ranges from a fraction of a micrometer to 100 micrometer. They are not perfect spheres, but have a jagged shape. The exact particle shape depends on the type of abrasive. As an example, some SEM pictures of abrasive particles can be found in Appendix II. In the setup the particles will orient themselves in a certain

direction, in order to minimise the amount of friction they experience. The top angle of a particle is defined as $2\Psi_p$, see Figure 5.2.

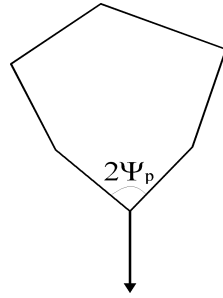


Fig. 5.2 Definition of the top-angle of an abrasive particle ($2\Psi_p$), when it is moving in the vertical direction, as indicated by the arrow.

The particle diameter that is specified for a certain batch of particles is an average value. As an example of the actual diameters that occur, a measurement of the diameter of an un-used #800 SiC batch was carried out, as can be seen in Figure 5.3. It is often said that #800 SiC has an average particle diameter of $7\ \mu\text{m}$. Here the diameter is measured with a Mastersizer by Malvern Instruments [www11]. This instrument uses the laser diffraction technique, which gives that diameter distribution that would occur for perfect spheres, so the irregular shape of the particles is not observed.

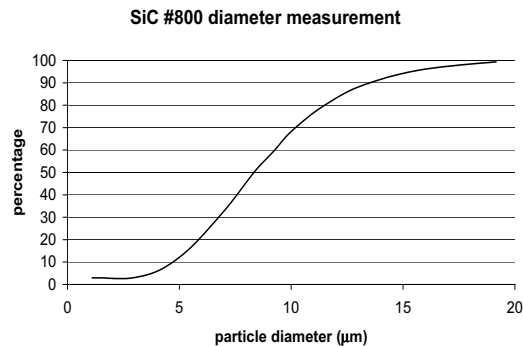


Fig. 5.3 Cumulative distribution of the particle diameters that are present in an un-used #800 SiC batch. Only 10% of the particles have a diameter smaller than $4.91\ \mu\text{m}$, 50% of the abrasives have a diameter smaller than $8.67\ \mu\text{m}$, and 90% of the abrasives have a diameter smaller than $14.08\ \mu\text{m}$.

The different diameters of the particles can be separated by sifting the particles through a series of sieves with successively finer mesh sizes. All the particles that can go through one sieve but not through the next end up in one batch. When a batch like this is sold it is common practise to specify the mesh size. Because of this separation method the diameter of the particles in one container will vary between certain values. The values between which the diameter varies depends on the type and geometry of the abrasive particles. Another method of particle size separation is by making water flow past them,

since then the particle weight can be used as discriminator between the different sizes. If a cascade of vertical tubes is built, and the water flows from the bottom to the top of each tube the particles will settle in a certain tube depending on their diameter [twy42].

Now that the diameter distribution of the particles has been discussed we will focus on the effect that the type and size of abrasives have on the material removal. The smaller the abrasive particles are, the less material they will remove, due to their smaller mass. Our experiments have shown that the material removal scales quadratically with the radius of the impacting particles. Notice that it is not the mass of the abrasives that is the important parameter (r^3). The contact area of the particles is apparently the important factor (r^2).

The material type and shape of the particles are also important, but they are less important than the radius of the particles. A reliable first estimate is to take into account the particle radius only, a more accurate estimation of the material removal can be found from an experiment with a specific slurry. In some papers a description of material removal as a function of abrasive shape can be found. Lambropoulos et al. [lam97] show that sharp particles result in a higher removal rate than blunt ones. They claim that the volume removal depends on $(\cot(\psi_p))^{7/6}$, in which ψ_p is half the top angle of the abrasives, see Figure 5.2. Finding the correct value for this parameter is not easy. The particles are irregularly shaped, which has to be accounted for by defining an average top angle. The actual top angle also depends on the abrasive process, since the particles will orient themselves differently in the case of classical grinding than in the case of FJP. In classical grinding the particles roll over the surface, so each of their sides will contact the surface, while in FJP the particles will orient themselves in the water-flow. Particles will orient the normal to their smallest surface area along the direction of the flow. Particles will prefer to hit the surface at a particular orientation. Finnie [fin60] states that round particles will remove less material than sharp ones. He also states that some particles are more effective than others, depending on their shape, but he does not quantify this statement.

The uncertainty in the removal can be large if the composition of the slurry is not known with sufficient precision, for example because the standard deviation of the particle diameter is larger than expected or specified, or because contaminating particles with very different properties are present in the slurry.

In order to investigate if the abrasive diameter plays a more important role than the shape of the abrasives, a number of experiments have been carried out. On BK7 samples various experiments were carried out under identical conditions, while only the slurry was changed. The slurries that were used were CeO₂ (1 μm), SiC #1200 (3 μm), SiC #800 (7 μm), Emery BM304 (5 μm), Al₂O₃ (15 μm), and Al₂O₃ (30 μm). In Figure 5.5 the amount of removed material has been plotted versus the abrasive diameter for every experiment. The erosion depth has been plotted, but since the area over which material was removed was the same for every experiment this is a scaled version of the removed volume. The area over which material is removed is ring-shaped with an outside diameter of approximately 3 mm. We show the quadratic line that fits best through the measured points. A quadratic line showed a better fit than a linear fit or a third power fit. As a first guess one would expect the material removal to depend on the mass of the impacting abrasives, so, in a first approximation, on the third power of their diameter, because

the energy of the impacting particles depends on their mass. This is apparently not true. The reason for this is that not all of the energy is used for material removal, some energy is used for the velocity of the slurry after impact, some energy is used for compression of the deeper lying layers of material (plastic deformation of the sub-surface damage layer), a part of the energy can be used to deform the abrasives, and a part of the energy is used to increase the temperature of the slurry. Exactly how much energy is used for each process is not clear, and when this distribution changes with the abrasive diameter this would also result in a diameter dependent erosion that does not obey a third power fit, see Figure 5.4.

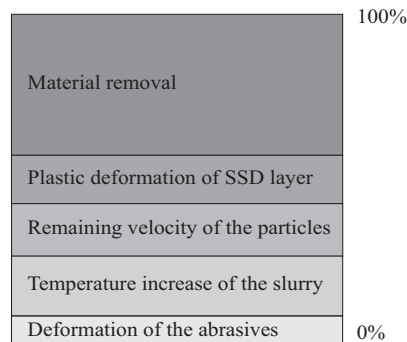


Fig. 5.4 Schematic view of the use of the kinetic energy of the abrasives. Only a part of the energy is used for the removal of material (SSD = sub surface damage).

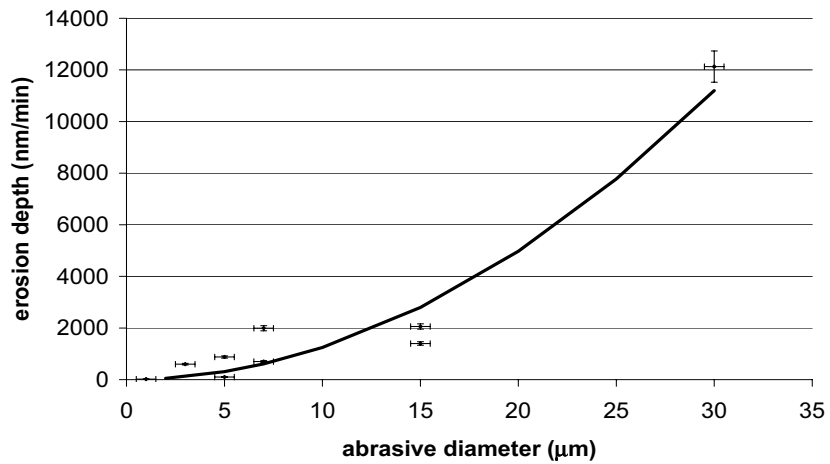


Fig. 5.5 Material removal as a function of the abrasive diameter.

5.1.3 Slurry temperature

Since the material removal in the case of FJP is based on the scraping effect of individual particles, and because no pitch is involved, and no temperature dependent slurries are used, we expect the process to be independent of the temperature of the slurry. In order to check this assumption experimentally a cylindrical nozzle was used at perpendicular incidence, a BK7 sample, a pressure of 5.5 bar, a stand-off distance of 2 cm, a 10% #800 SiC slurry, and the processing was carried out for 10 minutes. This experiment was done 8 times. The temperature of the slurry rose in those 80 minutes from 22°C to 30°. The maximum depth of the resulting profiles was, in chronological order: 8, 7.5, 7.7, 7.5, 8, 8, 8, 8 µm. Since the temperature increased continuously and with a factor of 6%, while the depth of the generated profiles shows a spreading of 30%, but not a continuous increase or decrease, we can conclude that the temperature does not effect the material removal rate.

5.1.4 Particle velocity measured with an LDA

The pressure that is built up by the pump to force the slurry through the nozzle, together with the area of the nozzle opening, results in the average velocity of the slurry. Therefore it is interesting to monitor the pressure. The dependence of the velocity on the pressure is described further on in this subsection. In the setups that were used a number of different pumps were applied. In the setup in Figure 2.5 a small membrane pump and a peristaltic pump were used. Both pumps show a pressure fluctuation of 10%. The pressure of the larger membrane pump of the setup at FISBA-Optik (as shown in Figure 2.7) showed a much larger fluctuation. The pressure in this setup has been monitored for 10 minutes using a pressure meter that was connected to the computer. The average pressure that was observed was 6.3 bar, the minimum pressure was 2.55 bar, and the maximum observed pressure was 8.85 bar (50% fluctuation). In Figure 5.6 the pressure can be seen to drift slowly. A different experiment showed an average pressure of 9.75 bar, a maximum of 14.85 bar and a minimum of 5.1 bar. The time between the lowest and highest pressure values was much shorter in this case. The pressure typically reached its lowest and highest value every minute in this case.

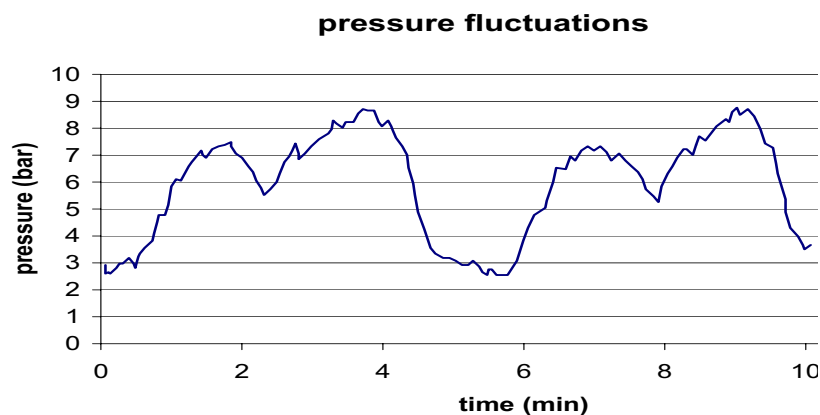


Fig. 5.6 The pressure as a function of time for the membrane pump in the setup at FISBA-Optik.

The abrasive particles are distributed through the entire jets cross-section and their velocity will depend on their position. The particle velocity distribution is an important parameter of the process. The exact shape of the nozzle will influence the flow profile. More information on different types of nozzles can be found in Section 5.6. In order to get an idea of the most commonly used flows a visualisation has been made of flows from a cylindrical nozzle and from a flat fan nozzle, see Figure 5.7. The direction of flow is vertical. The flow from the cylindrical nozzle starts as a solid cylinder of water with small disturbances at the outside. The magnitude of these disturbances grows and this causes the flow to obtain the irregular flow pattern that can be observed further away from the nozzle. The flow from the flat fan nozzle expands immediately, air is mixed into the jet, and the jet continues as separate water drops.

The velocity of the particles in the flow has been measured as a function of the radial position in the slurry flow using a Laser Doppler Anemometer (LDA) [www7]. An LDA can be used to determine particle velocities in two or three dimensions, depending on the setup. For the determination of the velocity component in the direction of the main flow of the slurry, one transmitter and one receiver are needed. Two laser beams from the transmitter intersect, forming the measurement volume. Within the overlapping area of the two beams the velocity of passing particles can be measured. The movement of the particles causes a Doppler shift in the light that is scattered by the particles and sent to the receiver. From this Doppler shift the velocity of the individual particles can be found. To measure two orthogonal velocity components, two pairs of laser beams will have to intersect in one measurement volume (e.g. one in the horizontal plane and one in the vertical plane). This can still be done using one transmitter and one receiver. For the measurement in three dimensions one transmitter and two receivers are necessary. In our case a two-dimensional measurement typically ran for ten seconds or stopped as soon as 10000 particles were detected. A picture of the LDA setup and a schematical picture of the measurement volume are shown in Figure 5.8.

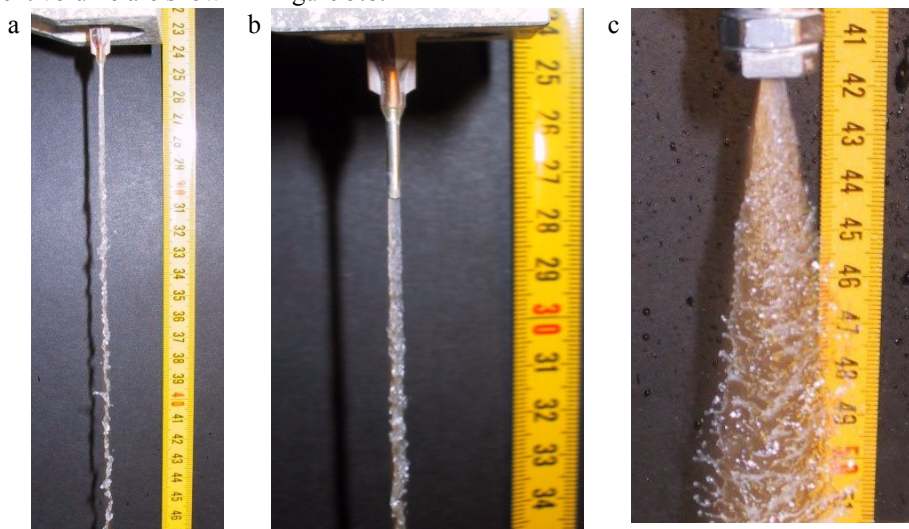


Fig. 5.7 Visualisation of the flow from a cylindrical nozzle (a and b) and from a flat fan nozzle (c).

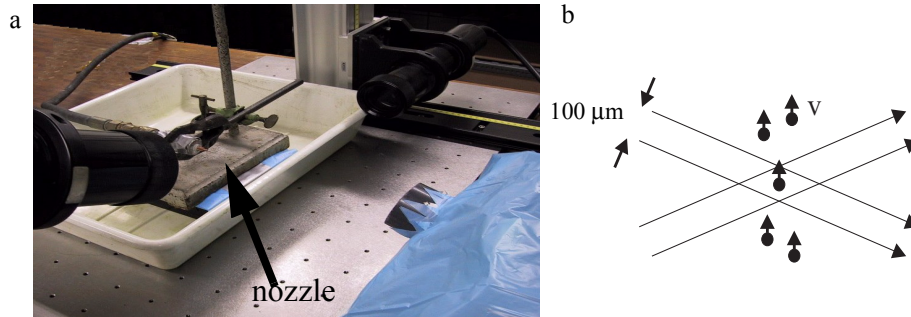


Fig. 5.8 a) The Laser Doppler Anemometer setup, consisting of the transmitter in the back and the receiver in the front, at an angle with the horizontal plane. The nozzle can be seen on the left hand side and the water drain pipe on the right hand side. b) A schematical view of the measurement volume. The two light beams (100 micrometer diameter) travel from the left to the right. The measurement volume is the overlapping part of the two beams. The horizontal velocity component of the particles that move through the measurement volume (v) can be determined.

The velocity measurement was carried out on a flow from a non-expanding cylindrical nozzle with a diameter of 1.36 mm at approximately 10 cm from the end of the nozzle. The measured velocity as a function of the position in the beam is shown in Figure 5.9. The fit through the points is the best fitting Gaussian curve

$$v = 12e^{-\frac{1}{18}(x-9)^2} \quad (5.1)$$

The lateral dimensions of the velocity profile seem much larger than one would expect. This is due to the fact that the water that flows from the nozzle is not a perfect beam. As can be seen in Figure 5.8 b) it is possible for parts of the water flow to end up some millimeters away from the symmetry axis. The measurement shown in Figure 5.9 is the summation of the velocity distribution over a time interval. When the entire beam has deviated in one direction first, and then in the other direction, the sum of the velocities observed in both cases is measured. Due to the fact that the diameter of the abrasive particles is very small (not more than a few tens of μm), the resulting velocity of the abrasive particles will be approximately equal to that of the surrounding water, see Appendix I.

In order to establish the relation between the pressure in the hoses and the velocity of the slurry that flows from a cylindrical nozzle, the pressure has been monitored, and the volume of slurry that flows through the nozzle in a certain time has been measured. From this volume the average velocity has been computed. The relation between the average velocity and the pressure is linear, see Figure 5.10.

We will now only consider the average velocity of the particles in the flow, and we will not take the lateral velocity distribution over the jet into account. To investigate how the amount of removed material will change with the average velocity, an experiment has been conducted in which the average particle velocity has been varied over a wide range. Every experiment was carried out for 10 minutes on float glass using a 20% 6 μm Al_2O_3 slurry. It is very likely that the material removal depth depends on the square of the aver-

age abrasive particle velocity, because the removal is caused by the energy of the impacting particles. The removal will show an offset value, because a minimum amount of energy required to remove material. If the energy is not high enough, the sample will only be elastically deformed, see Figure 5.11. The best fit of the depth as a function of the velocity is: $d = (0.207 \cdot v - 2.275)^2$, for $v > 11$ and $d = 0$, for $v < 11$.

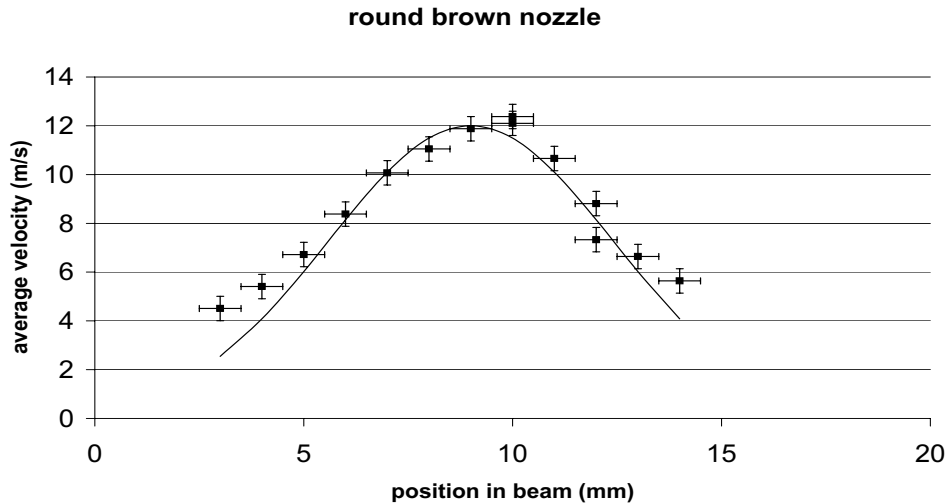


Fig. 5.9 The measured velocity as a function of the transverse position in the beam using the laser doppler anemometer. The points indicate measurements (with error bars), the solid line is the best fitting Gaussian curve through the data, see Equation (5.1).

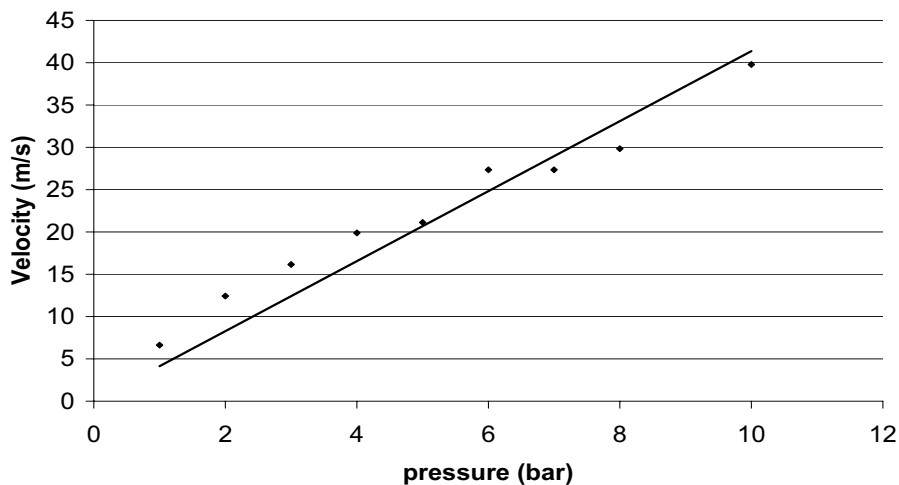


Fig. 5.10 Plot of the resulting average velocity as a function of the pressure, with the best linear fit that is forced to go through (0,0). The best fit is $v = 4.136 \cdot p$, where v is the velocity and p the pressure.

Other experiments have been carried out in which the processing was continued for longer time intervals. These experiments have shown that no material removal is observed for 6 μm diameter aluminum oxide particles for pressures below 1 bar, which corresponds to a velocity of 6.6 m/s for the nozzle that was used in the setup. It is interesting to use this information to compute the response time from Equation (4.20). This response time is a time scale over which particles respond to changes in the flow conditions. For a radius of the abrasive of 6 μm , an abrasive density of 3930 kg/m^3 , a kinematic fluid viscosity of $1.0 \cdot 10^{-6} \text{ m}^2/\text{s}$ and a fluid density of 998 kg/m^3 , this results in a response time of 0.5 μs . With a velocity of 6.6 m/s a particle can travel 3.3 μm within the response time.

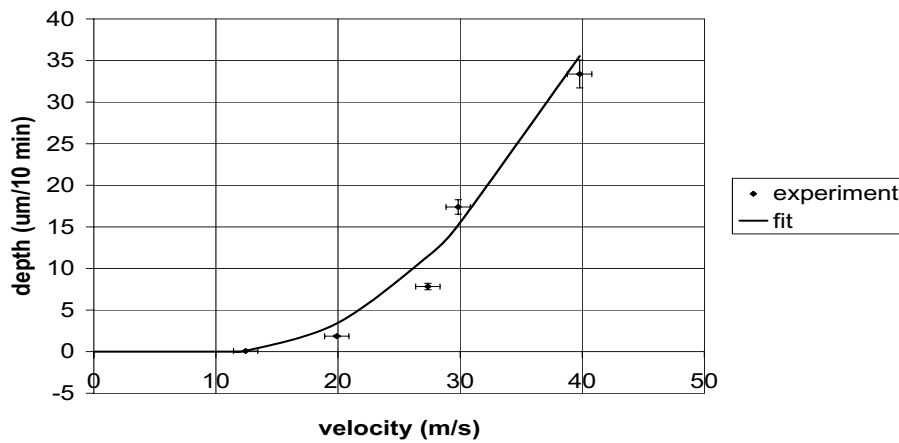


Fig. 5.11 Dependence of the material removal on the average particle velocity for a processing time of 10 minutes, on float glass, with a 20% 6 μm Al_2O_3 slurry. The fit is the best fitting quadratic term with an offset $d=(0.207 \cdot v - 2.275)^2$ for $v > 11$ and $d=0$ for $v < 11$, where d is the depth and v the velocity.

5.2 Stand-off distance

The material removal should not depend on the distance between the cylindrical nozzle and the surface within a limited range of distances, as long as the slurry does not diverge, and does not lose energy. In practical situations the jet will lose energy due to the friction between the jet and the surrounding medium (air). This friction can be seen in the visualisation of the jet in Figure 5.7. An experiment was conducted in which the cylindrical nozzle was directed at perpendicular incidence at a BK7 sample, for 2 minutes, at 4.5 bar, and with a 10% #800 SiC slurry. In 10 different experiments the stand-off distance was chosen to be 1, 5, 10 and 20 mm. In Figure 5.12 the depth of the stationary spots is plotted as a function of the stand-off distance. The removal shows a large spread, but no clear correlation between the removal and the stand-off distance can be observed.

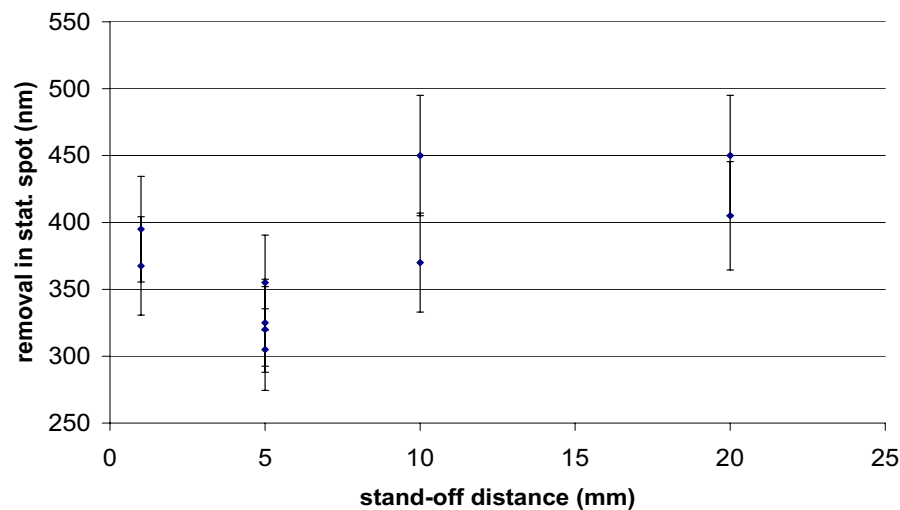


Fig. 5.12 The material removal depth in a stationary spot, as a function of the stand-off distance, with error bars.

5.3 Processing time

The amount of removed material depends linearly on the processing time, because the removal is caused by the total number of impacts of abrasive particles. To check this dependence some experiments were carried out. In the first case material was removed from a BK7 glass substrate for a relatively short period of time, between 10 and 150 seconds. This was done with a 5 wt.% #1200 SiC-water-slurry, and for two impact angles: 90° (perpendicular to the surface) and 45°. The average diameter of the #1200 SiC particles is 3 μm . The processed sample and the material removal as a function of the processing time are shown in part a) and b) of Figure 5.13.

Another experiment was carried out to investigate the time dependence for relatively long times, up to one hour. This was done using a 10 wt.% SiC #800 slurry (average particle diameter of 7 μm), and processing times between 60 and 3600 seconds. In Figure 5.13 c) the maximum depth of the removal profiles is plotted against the processing time.

All the experiments carried out validate the assumption that the time-dependence is linear. The slope of the maximum depth against time curve depends on the chosen parameters such as the type and concentration of slurry, the impact angle etc.

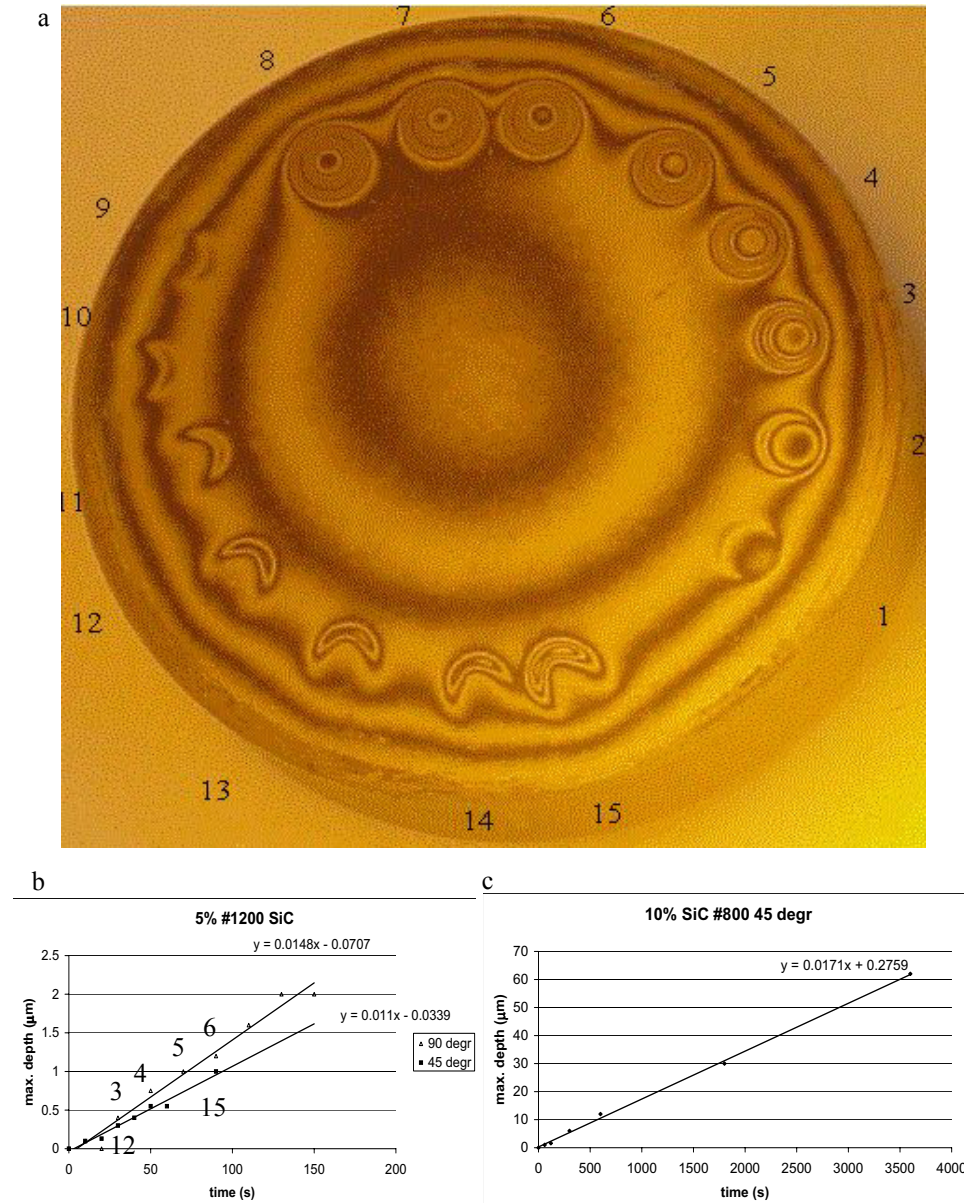


Fig. 5.13 a) A picture of a processed piece of BK7 glass, b) a graph of the maximum depth as a function of the processing time, for impact angles of, 90° and 45° respectively. The numbers indicated around the sample correspond to the numbers in the graph. c) The material removal depth is shown as a function of time for times up to one hour. The error bars are smaller than the size of the measurement points.

5.4 Processed material

The amount of removed material depends on the type of material that is being processed. Lambropoulos [lam97] derives an equation for material removal as a function of some sample material properties in the case of loose abrasive micro grinding, or lapping at fixed nominal pressure. This is a three-body process, where the particles are pressed against the surface by a lap. The total load is distributed over the abrasives. In the case of FJP, particles are accelerated towards the surface with an average velocity. To get an idea of the influence of the type of material that is being processed Lambropoulos's equation is given here

$$\Delta V \propto \left(\frac{E}{H}\right)^{1+\frac{m}{2}} \frac{(\cot\Psi_p)^{7/6}}{K_c H^{3/4}} P^{7/4}. \quad (5.2)$$

In this equation ΔV is the amount of removed material [m³], E is the elastic modulus of the material to be processed [GPa], K_c the fracture toughness [MPa m^{1/2}], H the Knoop hardness [GPa], P the pressure per particle [Pa], Ψ_p the half top angle of the abrasive particles [rad], and m a parameter. In the article it is stated that a value of $m = 1/2$ is used very often [bui93], but a value of $m = 1/3$ is actually better [lam97].

The expression for the volume removal can be simplified by introducing a material parameter M , which results in

$$\Delta V \propto M(\cot\Psi_p)^{7/6} P^{7/4}. \quad (5.3)$$

If the parameter m is chosen to be either 1/2 or 1/3, then the material parameter M becomes

$$M \propto \frac{E^{5/4}}{K_c H^2} \quad m = \frac{1}{2} \quad (5.4)$$

$$M \propto \frac{E^{7/6}}{K_c H^{23/12}} \quad m = \frac{1}{3}.$$

When we apply Equation (5.2) to the FJP process we can see that the material removal depends on the impact of individual particles. More or heavier impacting particles per square meter mean more material removal due to a higher pressure P . The total amount of removed material will increase for longer processing times, because more particles impact the surface. The factor $\cot(\Psi_p)$ decreases with increasing half top angle Ψ_p , and confirms that sharper particles remove more material.

Experiments have been carried out on seven different sample materials with different Knoop hardness values (H), elastic moduli (E), and fracture toughness (K_c) values. Different slurries have been used, on different days, with different processing times, and with different concentrations. The experiment was set up symmetrically, so every type of material has been processed equally long, every slurry has been used on every sample material, and the concentration was identical for all samples, when averaged over all experiments. The average amount of removed material over all of these experiments (indicated by the depth of the generated profiles averaged over the number of experi-

ments) has been measured for all of these materials, and is shown in Table 5.1 along with the material properties [bas95] [dav98] [hus98] [sch91] and the computed M -parameter (see Equation (5.4), where m equals 1/3). The M -parameter has also been plotted versus the amount of removed material in Figure 5.14. A linear relationship between these quantities is suggested by the experiments. When the material removal rate is known for a certain material, an indication of the material removal rate of any other material can be obtained by comparing the M -parameter of both materials.

Table 5.1 Overview of tested sample materials, their properties and the resulting material removal depth on those materials.

material	H (kg/mm ²)	E (GPa)	K _c (MPa√m)	depth (nm)	M (m=1/3)
Aluminum 6082	46	70	30	3515.8	0.00308
SF12	430	60	1	1421.9	0.001064
Steel rvs-304	938	193	150	1026.4	6.22E-06
BK7	610	81	0.86	964.8	0.000899
Si	1056	168	0.7	932.7	0.000903
Zerodur	620	90.3	1	686.1	0.00085
Schott Q0 Quartz	740	76.5	1	614.2	0.000499

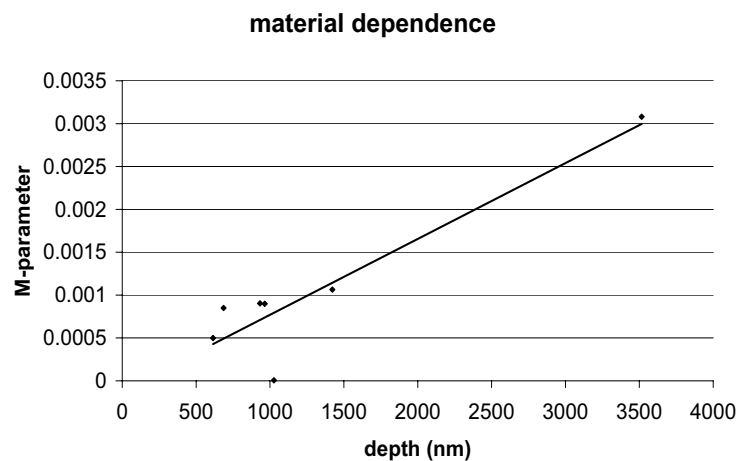


Fig. 5.14 The M -parameter as given by Equation (5.4) with $m = 1/3$ is plotted versus the removal depth for seven different materials, see Table 5.1.

5.5 Impact angle

Various experiments have shown that the material removal footprint depends strongly on the angle at which the slurry approaches the surface. The velocity distribution in the beam will not change significantly due to a surface that is inserted into the slurry, but the horizontal and vertical component of the velocity of the individual particles that hit the surface as a function of the position on the surface does depend on the angle.

If a cylindrical nozzle is used and the slurry strikes the surface perpendicularly, it will generate a ring shaped hollow in the surface. This can be seen in Figure 5.15 a). If a line-scan is made through the center of the depression a w-shaped profile is observed. Intuitively one would expect a depression that is deepest in the center and less deep towards the edges. This is indeed the case if particles are accelerated in air, or if very large particles are used in water. Smaller particles in a water based slurry will however result in a pattern as can be observed in Figure 5.15. The particles can not impact the surface directly because of the water, they are forced to impact in a certain area only, as was described in Subsection 4.4.4.

When the slurry hits the surface at an oblique angle, the ring-shaped hollow changes into a horseshoe-shaped one. As an example we will consider the profile made at an angle of impact of 45° in Figure 5.15 b). The line-scan through the center of the horseshoe consists of one deep hollow, there where the waterfront has hit the surface first and a shallow one further out from the point of impact. The separation between the two hollows gets larger for increasing angles of impact. The reason that this horseshoe shape occurs is the obstruction of the impacting particles on the right by the water flow coming from the left. These experimental observations correspond to the predicted footprints that were presented in Section 4.3.

Now that we have seen that the shape of the footprint changes when the angle of impact is varied we will consider the total amount of material that is removed as a function of this angle. In an experiment, a cylindrical non-expanding jet was aimed at a BK7 surface. The pressure was 6 bar, the stand-off distance 2 cm, the processing time 1 minute, and the slurry was 7% $15\ \mu\text{m}$ Al_2O_3 . For every angle of impact the amount of removed material was evaluated and the depth of the spots was also measured. The measured points are not on a straight line or a quadratic line. We can only say that a small amount of material is removed for small angles, and more material is removed for larger angles. Whether the amount of removed material has its maximum at 80° or at 90° is not clear. At a first instance this seems to contradict Finnie's prediction [fin58]. But Finnie predicts the material removal for single particle impacts at a certain angle, see Subsection 4.5.3. The angle of impact of a particle is not the same as the angle of impact of the jet. Particles in any flow will follow the stream perfectly if the flow does not change its direction. But impacting, jets do change their flow direction. The trajectories of the particles in the slurry can be computed according to Equations 4.19 and 4.20. Their angle of incidence upon impact on the surface can thus be derived. The impact angle of the particles is larger for angles closer to 90° , which causes relatively less material removal according to Finnie. But this effect is overcompensated by the effect that at angles of impact closer to 90° relatively more particles reach the surface, so more removal would be expected.

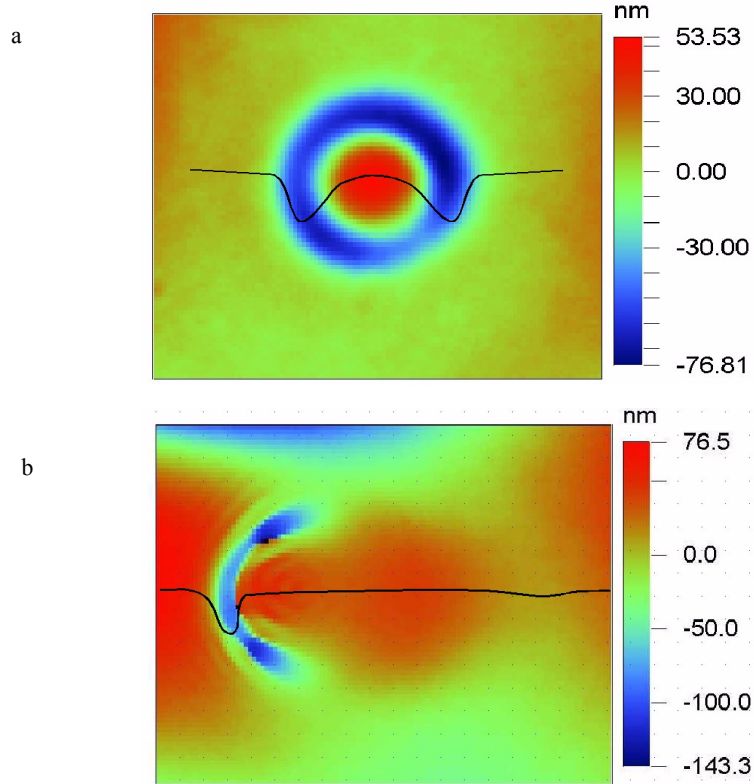


Fig. 5.15 a) A picture of a depression created at perpendicular impact angle (diameter of the spot 3 mm) and b) one created at an angle of impact of 45°. The nozzle was tilted towards the left so most material is removed on that side. The width of the spot is approximately 3 mm.

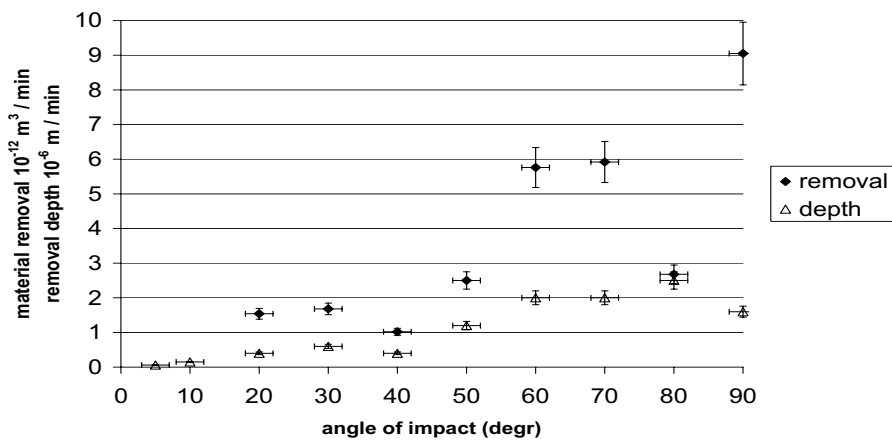


Fig. 5.16 The amount of removed material and the finally reached depth as a function of the angle of impact of the jet.

5.6 Influence of the nozzle shape

The material removal depends on the impact of individual particles in a slurry. The velocity distribution of the abrasive particles in a slurry is determined by the shape of the nozzle and the applied pressure. The flow profile and the shape of our regularly used nozzles will be treated here and an overview of some other possible nozzle shapes will be given. The first type of nozzle that is used very often is a precision nozzle that is usually used for glueing applications, Figure 5.17 a), the flow from it is a solid stream. A solid stream means that the water flowing from the nozzle does not diverge, and no air is mixed into the stream. The second type is sold as a precision spray nozzle by Lechler [www2]. Precision spray nozzles can be split up into a number of categories, depending on the shape of the spray, e.g. flat fan nozzles, see Figure 5.17 b), hollow cone nozzles, see Figure 5.17 c), full cone nozzles, see Figure 5.17 d), and solid stream nozzles, as could be seen in Figure 5.17 a). A flat fan nozzle diverges the slurry in one direction only, and not in the other direction, this results in a line shaped contact area. A hollow cone nozzle sprays the slurry away in the directions of the outer wall of a cone, and not in the center. A full cone nozzle sprays the slurry uniformly in the shape of a cone. In these nozzles that distribute the water over an increasing volume, air must be mixed into the slurry.

A disadvantage of a full cone nozzle is that the water flowing from one part of the nozzle obstructs the water flowing from some other part of it on the surface to be treated. To avoid this a full cone simulation nozzle can be constructed from which water flows in one direction only, as in the solid stream case. By rotation of the nozzle in two directions the flow will resemble that of a full cone nozzle, see Figure 5.17 e). Other nozzle shapes are also possible, e.g. a converging nozzle could be made by directing a stream towards the central axis of rotation of the nozzle itself, see Figure 5.17 f).

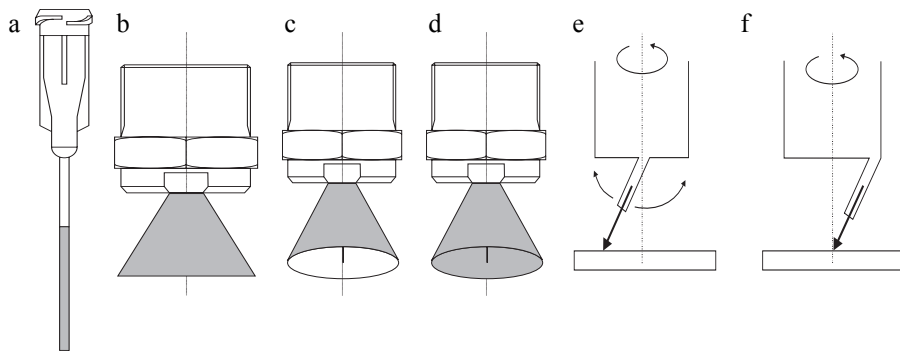


Fig. 5.17 Six different types of nozzles that could be used for FJP. a) A cylindrical nozzle (grey area is slurry), originally used for glueing applications, b) a flat fan nozzle, c) a hollow cone nozzle, d) a full cone nozzle, e) a full cone simulation nozzle, and f) a converging nozzle.

All of these nozzles can be classified according to the angles at which they spray the slurry onto the surface. We will now focus our attention to a point on the surface that is being processed (not the central point). We will investigate the angles (ω , Λ) at which the

slurry approaches this point as a function of the type of nozzle. We will limit ourselves to the case where the nozzle translates with respect to the work piece, the work piece rotates, and the nozzle does not rotate.

The two angles (ω , Λ) have been defined as follows. The angle ω is the angle between the slurry and the sample in the direction of translation (seen from the side), see Figure 5.18 a). The angle Λ is the angle between the possible flow directions of the slurry and the direction of translation of the nozzle, see Figure 5.18 b). To obtain a polishing effect that is as good as possible, in the ideal case we have to polish every point of the surface at every angle.

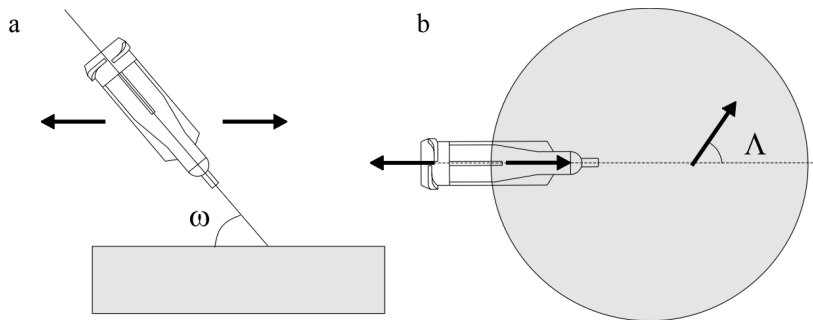


Fig. 5.18 The definition of the angles of the slurry flow. The nozzle and the sample are shown, the nozzle translates over the surface. a) The angle ω is defined in the side-view of the setup. It is the angle between the nozzle and the sample. b) The angle Λ is defined in the top-view of the setup. It is the angle between the possible slurry flow at a point on the surface and the direction of translation of the nozzle.

Solid stream nozzle

In the case of a solid stream nozzle a point on the surface will always see the slurry approaching at $\Lambda = 0$ (the slurry only flows radially towards the center and radially away from it) and it observes two ω -values symmetrically distributed with respect to $\pi/2$ rad, ω and $\pi - \omega$, see Figure 5.19 a).

Flat fan nozzle

For the flat fan nozzle it is important to specify the direction of the nozzle with respect to the direction of translation (Ω). If the plane in which the slurry fans out is in the direction of movement of the nozzle, this will be defined as $\Omega = \pi/2$. In this case the angle Λ will be 0 and the angle ω will be in between its maximum and minimal values. If the plane in which the slurry fans out is rotated $\pi/2$ rad with respect to the previous case ($\Omega = 0$) two ω -values can occur, symmetrically distributed with respect to $\pi/2$ rad, ω and $\pi - \omega$. Λ can take on values between $-\Lambda_{\max}$ and Λ_{\max} , where the subscript max indicates the maximum value that can occur for this nozzle (the maximum expansion angle). For intermediate values of the orientation of the angle of the nozzle w.r.t. the direction of translation ($0 < \Omega < \pi/2$) Λ values can be reached between $-\Lambda_{\max} \cos(\Omega)$ and $+\Lambda_{\max} \cos(\Omega)$. The angle ω can be in an area with a width $\omega_{\max} \sin(\Omega)$, around ω and around $\pi - \omega$, see Figure 5.19 b).

If the flat fan nozzle itself would be rotated during the process, it would have the same effect as a full cone nozzle.

Hollow cone nozzle

When a surface is treated with a hollow cone nozzle values of Λ and ω will be on the rims of two circles, with their centers at $\Lambda = 0$ and $\omega = \omega$ and $\omega = \pi - \omega$. The width and height of the circles will depend on the width and height of the hollow cone spray, see Figure 5.19 c).

Full cone nozzle

The effect of a full cone nozzle is similar to that of a hollow cone nozzle, but now all the values within the circles can also be reached, see Figure 5.19 d).

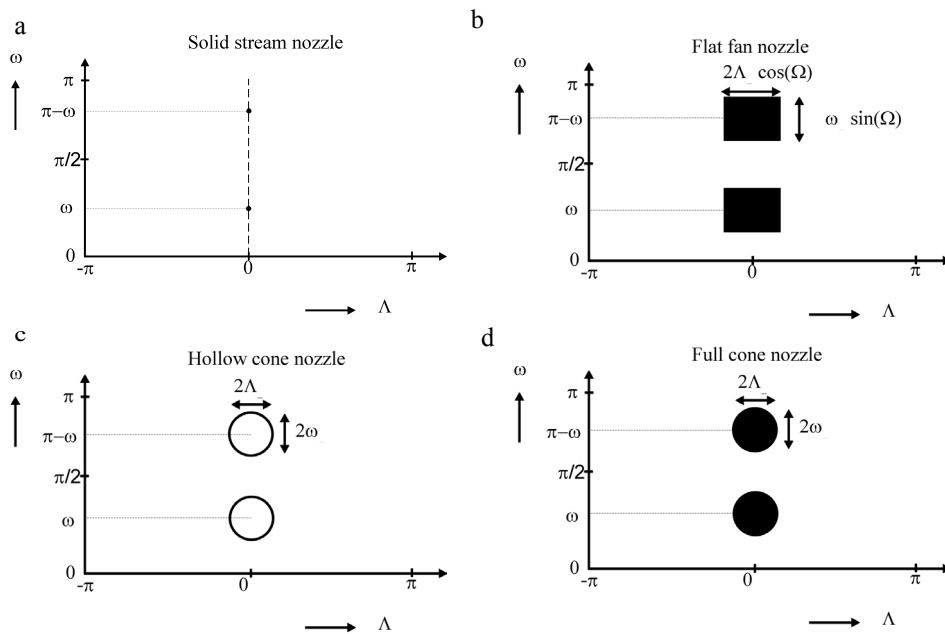


Fig. 5.19 Overview of the angles at which the slurry moves over a point on the surface, for a number of nozzles. a) The solid stream nozzle. b) The flat fan nozzle for fan direction Ω with the plane of translation. c) The hollow cone nozzle and d) the full cone nozzle.

The reason that classical polishing works so well is because of its high degree of random movement. We can therefore assume that the best roughness on a surface will be obtained when the slurry flows over the surface from as many directions as possible. This will maximize the randomness of the process. To obtain the best roughness one should ideally have particles impacting at every possible angle of impact on every part of the surface. This includes both the angle ω between the nozzle and the surface and the angle Λ with respect to the direction of translation of the nozzle. This effect of decreasing

roughness for increasing randomness of the process has been observed experimentally as well.

From this overview we can see that a full cone nozzle that is being translated over the surface, while the sample is rotating will result in the widest range of impact angles. A flat fan nozzle would have the same result if it is rotated around its axis, and has the same effect again as a solid stream nozzle that is rotated and tilted in such a way that it simulates a full cone nozzle.

An experimental verification of this assumption about the roughness as a function of the nozzle shape is very difficult, since it is not trivial which parameters should be kept constant. When the nozzle shape changes, the amount of fluid that flows through it also changes for the same setting of the pressure of the pump. But when the amount of slurry that flows through the nozzle is kept constant the slurry velocity has changed. Which one of these parameters should be kept constant to obtain results that can be compared to each other is open for dispute. In experiments one can observe a preferred direction on a surface when a part of the surface is investigated over which water has been flowing in one direction only. As an example a Nomarski picture of a part of the surface just outside the main processing area is shown in Figure 5.20. For one hour a full cone nozzle was processing the central 2 mm of a rotating BK7 sample at perpendicular incidence, at 5 bar and with a 10% 6 μm Al_2O_3 slurry in water. The surface just outside the central 2 mm diameter area looks like a structure on the beach with sand piling up behind stones or other structures.

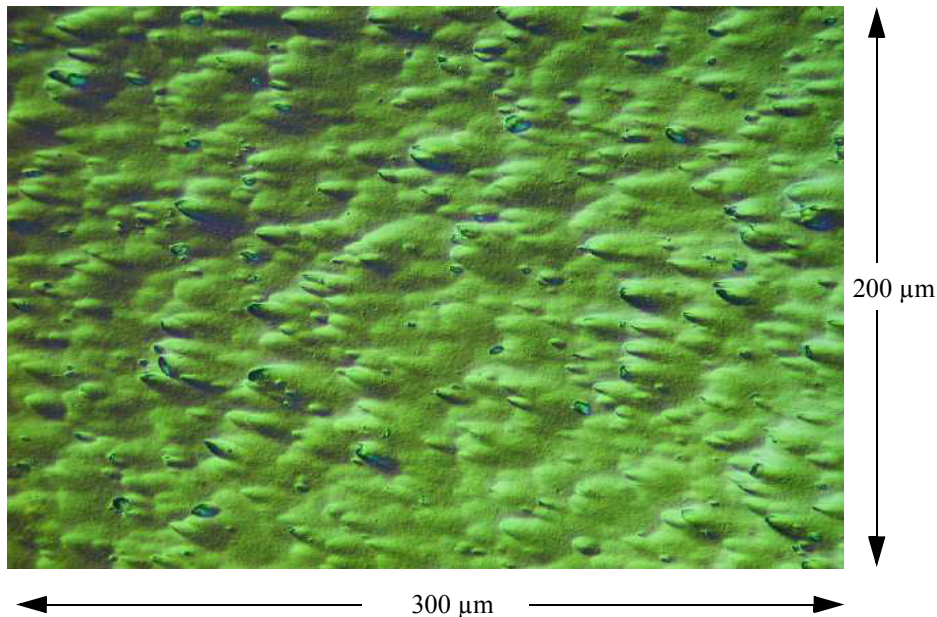


Fig. 5.20 Nomarski image of a part of the surface just outside the center of the sample, where the processing took place. The slurry has only moved over the surface in a radial direction away from the center. This direction can clearly be recognised in this Nomarski image. The average roughness of this surface is 100 nm.

6 Implementation of FJP

This chapter describes the results that were obtained with the FJP technique when applied in a production environment. Unless stated otherwise the setup that was used in this chapter is the one shown schematically in Figure 2.5. In this chapter, we discuss the obtainable shaping accuracy and the actual surface roughness reduction capabilities of the FJP technique.

In Chapter 5 we have seen how the material removal depends on a number of settings. Some introductory experiments have been carried out to see if FJP is applicable to the glass grinding and polishing process. The process should be reproducible (Section 6.1); if the spot moves over the surface the resulting profile should be homogeneous and not influenced by possible process fluctuations (Section 6.2). Another important issue is the recycling of the slurry. In Section 6.3 we will see if the slurry changes its shape or size over time.

Next, some observed phenomena are treated. In Section 6.4 the occurrence of ripples in a stationary spot is explained and the occurrence and removal of mid-spatial frequencies is treated. In Section 6.5 the regime of material removal of FJP is discussed (ductile or brittle). Finally, the shaping and polishing capabilities of FJP are proven by presenting some interferograms of samples along with a description of their production process. In Section 6.6 some examples are given of the shaping capabilities of FJP, and in Section 6.7 some experiments are presented that led to the best results so far. A summary of the capabilities and limitations of FJP will be given in Chapter 7.

6.1 Reproducibility

First an analysis has been conducted of fluctuations that are likely to occur in the setup as it is used. The parameters have been listed in Table 6.1 and an estimation has been made of the accuracy with which they can be set for short and for longer times in the setup. The limitations are caused by the setup components like the pump, the slurry, and the holders that determine the nozzle position, they are not limitations of the process itself. Fluctuations in these process parameters do not necessarily translate into errors in the depth of the generated spots. The effect of the temperature on the accuracy of the process for example will not be very large.

To investigate the variation in depth and width of spots that are supposed to be identical, various experiments have been carried out. In one experiment an attempt was made to produce 5 identical spots with a cylindrical nozzle at 90° and 5 identical spots at 45° . The slurry that was used contained 5% #800 SiC and the processing time was 30 seconds. The

sample was repositioned (both the height and the angle of incidence) after every experiment. The resulting variation in the maximum depth of both types of spots was 30%. This variation is caused by effects that manifest themselves only for short processing times and large removal rates. In 30 seconds the amount of slurry that removes material from the surface is too little to be representative of the total available slurry. Besides, small pressure fluctuations have a relatively large effect on the average pressure during the experiment.

Table 6.1 Overview of the expected errors in the parameters that can be set during an experiment, both for very short and for longer times.

parameter	error for short experiments (a few seconds) (in percentages)	error for long experiments (more than half an hour) (in percentages)	type of error
pressure	8	3	fluctuates around the pressure that is set
angle	2	2	does not change over time
processing time	3	<<1	becomes negligible for larger processing times
concentration		2	for short processing times fluctuations can be high
temperature of the slurry	2	20	after some time the slurry has reached an equilibrium temperature
particle diameter	70	10	for very short times it is possible that only a select group of particles removes material

Another experiment has been conducted in which the processing time was 30 minutes, and the angle of incidence 45°. Seven times a spot was thus produced under identical conditions. The processing time was chosen to be longer than in the previous experiment to minimize the effect that only part of the slurry is used during one experiment. The effect of pressure variations should also average out over the processing time in this experiment. A variation between the spot depths of 10% could be observed. Yet another experiment in which a nozzle was used at perpendicular incidence also showed a variation in spot depth of 10%. The changes over time of the temperature do not influence the depth of the generated depressions much, because FJP does not use pitch and temperature sensitive polishing particles. The variations are probably caused by the spread in the

particle diameter. A 10% variation is too large to apply the process for corrective polishing purposes without a feed-back system. But single spots are not used in corrective polishing, there material is removed over areas that are larger.

When we focus our attention on the removal of material over larger areas, e.g. by scanning the nozzle back and forth in one direction only, we see that the finally resulting shape reproduces very well. The result of five repeated experiments showed that the maximum depth of the shape varied between 4.4 and 4.6 μm , which is a total fluctuation of 4%, or a fluctuation of $\pm 2.2\%$. For the production of optics it is important to reach a very well defined final surface shape. For low end optics one to a few λ is good enough, for high end optics $\lambda/5$ to $\lambda/10$ is needed. In the polishing step of optics, a typical removal of 10 μm depth occurs. When this is done with a 4% accuracy this corresponds to 0.4 μm , which is somewhat smaller than λ . This is good enough for low end optics. This is fortunately not a limitation of the FJP method, but only of the setup. The tolerance on the center thickness of a standard optical component usually is 100 μm . One rarely removes more than 100 μm of material in the final shaping or shape correction step of optical components (10 to 20 μm is a more realistic estimate). A variation of material removal of 4% on this value would therefore not be too large to meet with the tolerances on the center thickness.

6.2 Homogeneity of a translating spot

The previous section reported on the reproducibility of the process. The homogeneity of a translating spot is the logical next step to investigate. If a stationary spot is translated over the surface with a constant dwell time the expected result is a profile that is homogeneous in the lateral direction. In order to carry out the scanning as linearly as possible, the CNC setup as shown in Figure 2.7 was used. A scan was made on a piece of BK7 with a flat fan nozzle and a 10% #800 SiC slurry for 30 minutes; the scanning back and forth was carried out several times. The resulting profile is indeed virtually shift-invariant. A two centimeter wide part of the profile is shown in Figure 6.1. Through this profile (with a maximum depth of 3.5 μm) six cross-sections have been made (see Figure 6.1). The deviation from the average shape of the profiles in the various cross-sections is less than 40 nm. This is a very promising result, which enables the predictable processing of larger areas. A cross section has been made in the direction of translation as well, see Figure 6.2. This shows that the variation in the maximum depth is indeed in the order of 40 nm.

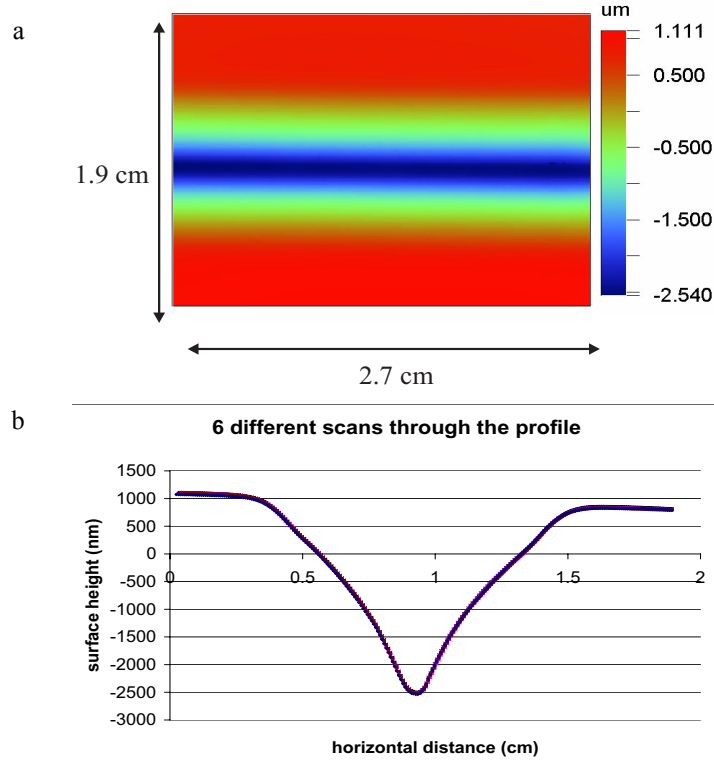


Fig. 6.1 a) Part of the generated homogeneous profile with a maximum depth of $3.5 \mu\text{m}$. b) Six different scans through the profile in a). The deviation from the average is less than 20 nm for the six scanned profiles.

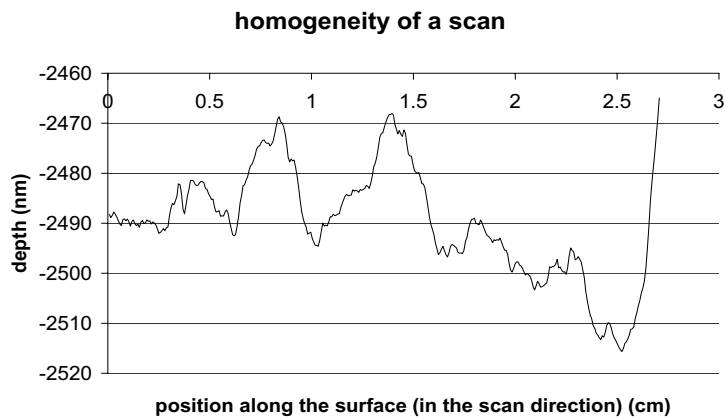


Fig. 6.2 The depth profile as a function of the position in the homogeneous profile. The cross section is taken in the scanning direction.

6.3 Slurry degradation

In the FJP process the slurry is used in a closed-loop setup, so the same abrasive particles are repeatedly used. Therefore, it is important to investigate if the slurry particles are noticeably damaged by the FJP process. The slurry is not filtered in this setup, so contaminations with dust should be avoided and abraded pieces of glass or other parts of the setup that end up in the slurry should be small. When too many contaminations are present in the slurry it should be replaced. When the material removal is in the ductile regime, 64 nm can be taken as a first estimation of the diameter of the glass particles that contaminate the slurry, which is the critical depth for BK7 according to Bifano [bif91], see Equation (6.1).

An experiment was set up that ran for eight hours. During the entire experiment the slurry impinged on a BK7 sample. Every hour the material removal rate was measured, the pH value and the temperature of the slurry, and the size and shape of the #800 SiC abrasive particles; the results have been summarised in Table 6.2. The shape of the particles did not change visibly (with a SEM). The particles have a three-dimensional structure and sharp corners. A typical picture of the abrasive particles can be found in Appendix II. The pH value also did not change during the experiment, see Table 6.2. The temperature slowly increased from 22°C and stabilised at 35°C. The material removal rate per minute was calculated from an experiment that ran for 10 minutes. The removal rate is not very constant, as can be seen in Table 6.2. This is probably caused by fluctuations in the pressure.

The diameter of the abrasive particles was measured with a Mastersizer from Malvern Instruments [www11] whose measurement principle is based on the laser diffraction technique. The particle diameter distribution that results is based on the assumption that the particles are perfect spheres. Three parameters are specified to characterise the diameter distribution: D10, D50 and D90. D10 means that 10% of the particles have an average diameter smaller than the indicated value. Three repetitions of the measurement of the abrasive particle diameter showed a spreading of results of approximately 7%.

Measurements were also carried out on different batches of the same type of abrasives. Batch 2 was unused #800 SiC material. Batch 3 was an #800 SiC slurry that had been used for a very long time. The particle diameter of batch 2 should correspond to the $t = 0$ hours batch. The difference between the diameters of these two batches as well as the difference between the diameters at different times of the batch that was used a number of hours are both smaller than 7%, which is the spreading of repeated measurements. If every particle would fracture, the D10, D50 and D90 values would decrease. If only the largest particles would fracture the D90 value would decrease, and the D50 value and D10 value could decrease depending on the number and size of the resulting fractured particles. As can be seen in Table 6.2 the particle diameter does not decrease continuously as a function of time (a decrease would be expected if the particles would fracture). We can therefore conclude that during a typical experiment that lasts up to 8 hours the fracturing of particles does not occur even though the slurry is recycled. Buijs and Pasmans draw a similar conclusion in their article in *Wear* [bui95]. They state that damaging of erosive particles occurs only at high speeds (brittle conditions) and not in the ductile regime. Since FJP operates in the ductile regime, as will be shown in Section 6.5,

particle fracture is not expected to occur. Pictures of a slurry before and after having been used at a pressure of 1960 bar can be found in the article by Kiyoshige [kiy88].

Table 6.2 Slurry degradation test results.

start time (hours)	mat. rem. rate ($\mu\text{m}/\text{min.}$)	pH value	slurry tem- perature ($^{\circ}\text{C}$)	D10* (μm)	D50* (μm)	D90* (μm)
0	2.0	8.2 +/- 0.1	22	4.93	8.69	14.16
1	1.5	8.2 +/- 0.1	28.5	5.01	8.53	13.44
2	1.5	8.2 +/- 0.1	31.5	5.06	8.60	13.49
4	0.9	8.2 +/- 0.1	34	4.78	8.66	14.32
8	1.5	8.2 +/- 0.1	35	4.84	8.90	14.93
batch 2				5.08	8.59	13.28
batch 3				5.29	9.44	14.95

*DN: N% of the total number of particles has a diameter smaller than this value

6.4 Ripple formation / mid-spatial frequencies

One of the phenomena that can occasionally be observed on samples that have been treated with FJP is the formation of ripples. Ripples are patterns showing a typical periodicity. Two different types of ripples can occur. The first case is when the nozzle and the work piece are not moving with respect to each other and the second case is when they are moving. The resulting surface in the latter case is said to contain mid-spatial frequencies. The two phenomena have completely different causes. With FJP it is also possible to remove ripples. This will be shown at the end of this section.

First the stationary case will be described. A Nomarski image of the occurring ripple pattern can be seen in Figure 6.3. The depression was created under stationary conditions in 15 minutes using a 10% #800 SiC slurry on a BK7 sample, at an angle of 25° , while using a cylindrical nozzle. The depression is $35 \mu\text{m}$ deep and $1000 \mu\text{m}$ wide. The height of the ripples is $0.1 \mu\text{m}$. To understand this phenomenon the relation between the material removal and the angle of impact has to be understood for ductile materials. In 1965 Finnie and Kabil [fin65] report on their findings of surface ripple formation with sand in air on aluminum samples. They observed this phenomenon only for ductile materials and only if the angle of impact is not too large. Their explanation is based on the angle

dependence of the material removal, see Equation (4.25) and Figure 4.17. When particles impact on a hilly surface (or when a number of particles have impacted on a flat surface), their real angle of impact will depend on the side of the hill they are impacting on. They deduce that at small angles of impact the peaks of a surface will erode less rapidly than the valleys. This causes the ripple formation.

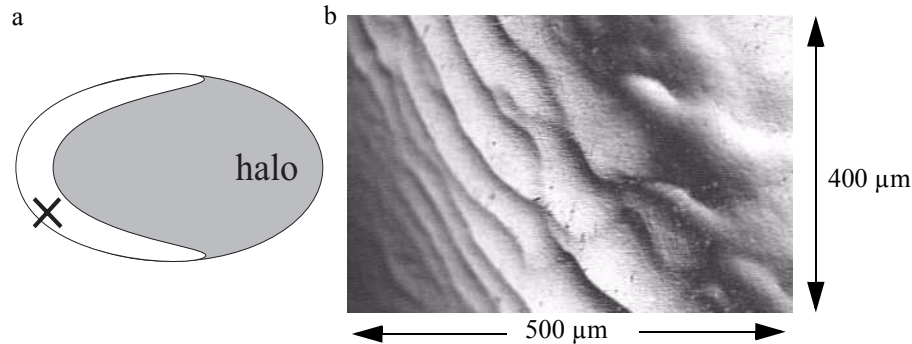


Fig. 6.3 a) Schematic picture of the stationary footprint with the part of the spot that is referred to as the halo. b) A picture of the observed ripple pattern, visualised using a Nomarski microscope around the location in a) marked with a cross (x). The height of the ripples is approximately $0.1 \mu\text{m}$.

Fang et. al. [fan98] mention that the ripple formation can also occur on brittle materials, and even in the case of erosion by pure water, without abrasives. They studied the formation of ripples on ceramic surfaces by a solid-liquid slurry. Their jet velocity was 7.3 m/s and their abrasives were $600\text{--}850 \mu\text{m}$ rounded silica sand particles. From their experiments they find that no ripples occur for erosion times up to 5 hours. For times in the order of 8 hours ripples form, but only if the angle of impact is not perpendicular to the surface. They postulate that the material removal is caused by ploughing of the abrasive particles over the surface and by cracks that are caused by the particles. The removal will be in one of these two modes depending on the angle of impact. Once a hill is created on a surface, it protects the area in the shadow of the hill, and the hills or ripples will become larger.

The angle dependence will definitely play an important role in the formation of ripples. The picture shown in Figure 6.3 clearly shows that ripples can form for erosion times much smaller than 8 hours. Ripples can also occur for impact directions that are perpendicular to the surface, but this is due to the fact that the water impacts perpendicularly, and it flows away parallel to the surface, so the effective angle of impact of the abrasive particles is somewhere in between these two extreme values. Similar ripple patterns can be seen in deserts, in river beds, and on the road near traffic lights ('washboards'). The main difference between ripples in glass or ceramics and those in sand, asphalt or metals is that material can easily be pushed up out of the surface for metals and asphalt, it can re-deposit for sand, but both effects are not possible for glass and ceramics on a large scale. During polishing, some glass parts can leave their place in the glass structure and be re-deposited somewhere else, but this can not occur on such a large scale that ripples are formed.

Secondly, we consider the translating case, where mid-spatial frequencies can appear. When the nozzle and the work piece are moving with respect to each other ripples will not occur due to any phenomenon that causes ripples in the stationary case, since these effects will average out over the distance of translation. But if the translation is not carried out uniformly a ripple pattern can occur. A typical example of such an unwanted periodic effect on the surface can be seen in Figure 6.4, where a calcium fluoride sample has been treated for 90 minutes with a cylindrical nozzle at 45° that was scanned over the surface for 28 mm. The scanning was carried out with the FJP setup from Figure 2.5 with step engines that carry out the translation. In Figure 6.4 a periodic structure can be observed with a repetition distance of 0.94 mm, so 1.07 periods occur per mm. This is caused by the non uniform scanning of the stepping motors in the setup for this particular velocity. The proof that the ripple-phenomenon is not an intrinsic problem for FJP can be found in Section 6.2 and in Section 6.6, where examples are given of surfaces that are treated with FJP and that do not suffer from such a periodic structure.

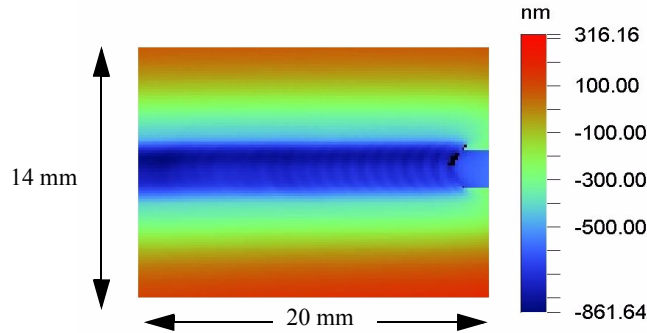


Fig. 6.4 A 14 x 20 mm part of a CaF_2 sample, clearly showing the occurrence of a repeating pattern (mid-spatial frequency). The nozzle has been scanned over the sample in the horizontal direction using stepping motors that cause the inhomogeneous pattern.

It is also possible to remove ripples with FJP. This has been demonstrated by the following experiment in which a stationary spot has been processing a diamond turned steel sample for 15 minutes. A cylindrical nozzle was used at an angle of 70° with the surface, a stand-off distance of a few millimeters, and a 10% #800 SiC slurry. The magnitude of the surface ripples has been reduced considerably, as can be seen in Figure 6.5. The best surface was obtained in the halo of the generated spot. The halo is the area behind the deepest processed area over which the water flows away, see Figure 6.3.

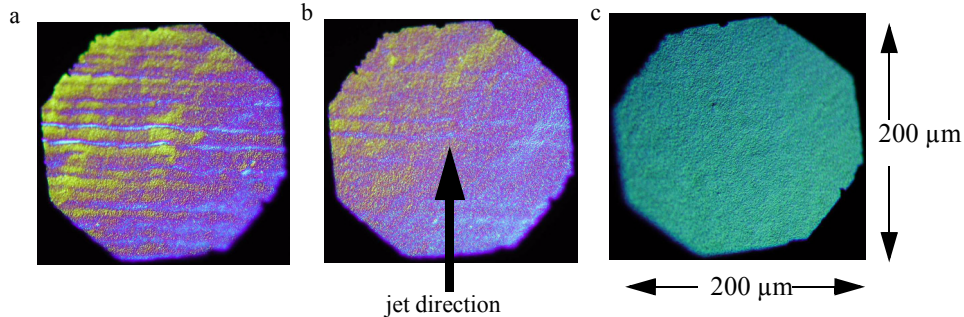


Fig. 6.5 Removal of diamond turning grooves from a steel surface by FJP. Three Nomarski images show a) the initial surface, b) a part of the treated surface, c) the best part of the treated surface (in the halo of the spot).

6.5 Ductile or brittle removal?

Material can be removed in two different regimes: either the ductile or the brittle regime. In the brittle regime the impact of one single particle will cause cracks to appear in the material. If those cracks intersect, large parts of material are removed at once. The typical surface roughness associated with this process is much larger than that of a ductile process. In a ductile process the impact energy of one particle is smaller. The particle does not have enough energy to initiate cracks, it can only remove a small amount of material by scraping over the surface.

The transition between the two types of material removal is at a certain particle energy. This energy can be translated into a critical depth. If particles penetrate deeper into the material than this depth the removal will be brittle, if they can not penetrate this deep the removal will be ductile. According to Bifano [bif91] the critical depth d_c can be expressed as

$$d_c = 0.15 \left(\frac{E}{H} \right) \left(\frac{K_c}{H} \right)^2, \quad (6.1)$$

in which E is the elastic modulus, H the hardness and K_c the fracture toughness.

In this section we will show that the material removal with FJP can be in the ductile regime if the parameters are chosen correctly. The critical depth for BK7 can be calculated to be 64 nm, since the material properties of BK7 are: $E=81$ GPa, $H=5.2$ GPa, and $K=0.86$ MPa m^{1/2}. From an experiment that was conducted, the spot profile in Figure 6.6 resulted. A low concentration opaline slurry (100 gr. in 15 liter water) was sprayed on the surface for 3 hours with a pressure of 3 bar, at an angle of 45° and a stand-off distance of 2 cm. The resulting spot is 44 nm deep, which comes down to a material removal rate of 0.2 nm/min. We know that the shape was created by very many impacts, so the material removal caused by one impact is much smaller than 44 nm. This removal is much smaller than the critical depth, so the removal is in the ductile regime.

The FJP process can operate in the ductile as well as in the brittle regime. The conditions under which the transition occurs is determined by the amount of material that is removed per impacting particle, which is the wear rate. The effect of the relevant process parameters on the wear rate can be found in the previous chapter. Experiments have shown that 30 μm Al_2O_3 particles at 20 m/s remove material in the ductile regime. When 63 μm SiC particles are used the material removal is brittle. The transition occurs somewhere in between.

The FJP process can also be used in the brittle regime. When a 5% SiC #220 (average diameter 63 μm) slurry was sprayed onto a polished surface for 5 minutes, a 23 μm deep profile resulted with a roughness of 600 nm. The lateral dimensions of the spot were 10 x 30 mm, due to scanning of the spot in one direction. The depth of the profile is created by overlapping impacts from the abrasive particles. The roughness is an indication of the removal effect of one single particle. Since the roughness obtained with the SiC #220 slurry is much larger than the critical depth, the removal must have taken place in the brittle regime. The argument that the material removal is in the brittle regime is also supported by the deep pits that can be observed at the edges of the generated spot, where single impacts occurred.

An example of the difference between rapid removal which will be in the brittle regime and slow removal in the ductile regime can be seen in Figure 6.7. In this case a scan was carried out over the surface for 2 cm until a depth of 350 nm was reached. At approximately 0.5 cm from the right hand side of the depression an area can be seen that is 100 nm deeper than the rest of the scan. This part of the surface was damaged when the setup was switched on. The first slurry that flows out of the nozzle still contains some air. This causes the particles to move faster than they would in water, and this causes a higher removal rate. In the Nomarski images shown in Figure 6.7 b) and c) the final surface state of the main part of the processed area (b) can be compared to the state of the deeper area (c). Measurements of the main part show an R_a -value of 2.2 nm, an R_q -value of 2.8 nm, an R_z -value of 20.6 nm and an R_f -value of 27.9 nm. The deeper area clearly is much rougher ($R_a = 70$ nm).

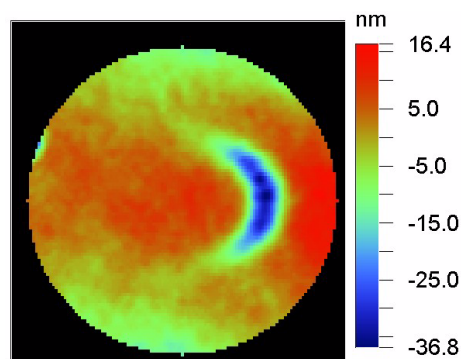


Fig. 6.6 Removal spot after 3 hours of processing with a 0.67% opaline slurry at 5 bar. The diameter of the masking circle is 9 mm.

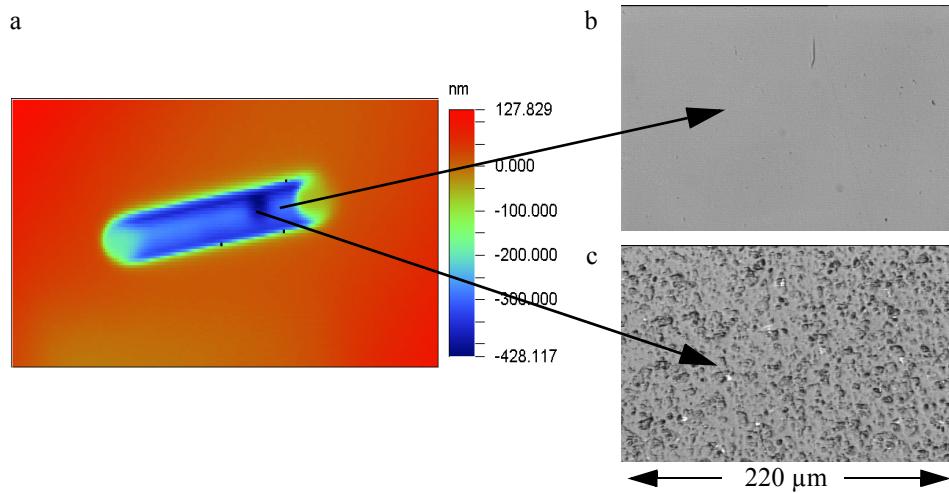


Fig. 6.7 a) A 2 cm long scan on a pre-polished BK7 surface (initial average roughness 1 nm) shows a constant profile (350 nm deep) in most places. At approx. 1/4 of the length from the right hand side a deeper area (450 nm deep) can be observed. b) A Nomarski picture of 160 x 220 μm of the processed area of the spot in a), with an average roughness of 2.2 nm. The deeper area is much rougher ($R_a=70$ nm) than the rest of the spot as can be seen from the Nomarski image in c).

6.6 Shaping

Three examples of surfaces that were shaped with FJP will be given in this section. In Section 6.2 the possibility of uniformly translating a spot over a surface has already been demonstrated. In this section a ring-shaped area will first be shown to demonstrate the possibility of constant rotation (Subsection 6.6.1), followed by a whole surface that has been processed, which resulted in a flat center area (Subsection 6.6.2). In Subsection 6.6.3 three examples will be presented of prescribed surfaces that have been produced.

6.6.1 Rotation only

The nozzle with the coil inside, that has been described in Section 4.6 was used for the first experiment. A 10% #1200 SiC slurry was sprayed perpendicularly onto the surface (9 mm out of the center of the sample) for one hour, at 10 bar, and with 1 cm stand-off distance while the surface rotated at 2 Hz. The resulting 600 nm deep ring-shaped profile can be seen in Figure 6.8. In the center of the sample another experiment has been conducted that is not relevant for this experiment. The amount of removed material is independent of the position on the sample. It is also clearly visible that more material is removed from the area closer to the center of the sample. This is caused by the fact that the area over which material was removed is smaller there.

In principle when both translation and rotation are possible, the processing of an entire surface should also be possible when the correct dwell time is taken into account. But when processing an entire surface the center is always a large concern. A dip or a hill can occur in the center, as was described in Subsection 4.6.2.

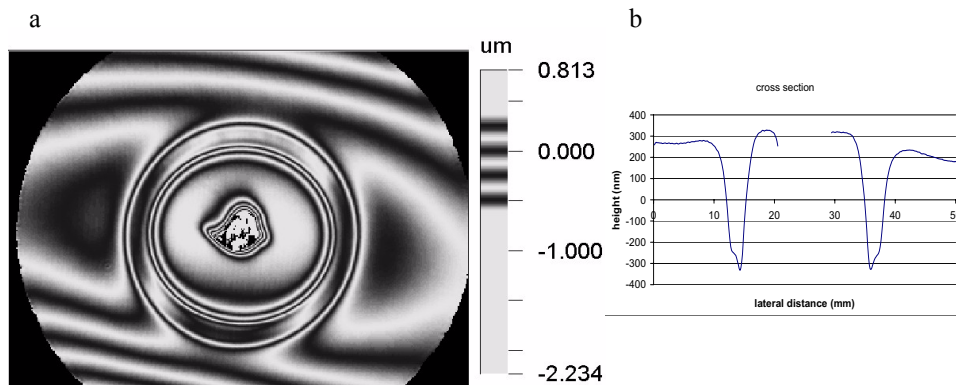


Fig. 6.8 A ring-shaped processed area. The sample in a) has a diameter of 50 mm; in the center a separate stationary experiment has been conducted and only the ring-shaped area around it is of interest to us in this case. b) A cross-section through the sample in a) in the horizontal direction and going through the center of the sample.

6.6.2 Flat center area

Removing material uniformly over a large area with a small contact area is a challenge, especially when the removal should take place from a rotating sample. It is difficult to remove the correct amount of material from the central part of the surface. When a small spot is moved with constant velocity over a rotating surface a dip will result in the center, as could be seen in Figure 4.20 a). To avoid this deeper area in the center the most obvious solution is to increase the velocity of the nozzle when it is moving over the center, which reduces its dwell time there, so less material is removed. Since it can be difficult to set this velocity sufficiently accurate we had to come up with a different solution. We propose to use a spot that is larger. In Figure 6.9 the surface and the nozzle are drawn. For convenience of explanation the nozzle has been divided into three areas: 1, 2, and 3. The surface is divided into four areas: 1, 2, 3, and 4. The effect of using a larger nozzle is that different parts of the spot will simultaneously remove material from different parts of the surface. The center of the nozzle will remove material from the entire sample. That part of the nozzle at the transition between 2 and 3 will follow the trajectory as indicated by the arrow. Because the sample rotates in the mean time this part of the nozzle can only reach those parts of the surface indicated by 3 and 4.

It should be possible to match the removal in the outer area to the removal that would occur in the center in such a way that the removal is constant over a larger area. The simulation program that was described in Subsection 4.6.2 was used to compute the resulting surface when the round, rotating surface is 40 x 40 elements large while the spot is 3 x 10 elements and removes the same amount of material over its entire area and it moves over

the entire sample from left to right. The finally resulting surface, and a cross-section through the center can be found in Figure 6.10.

In Figure 6.11 four examples are shown of nozzles with a footprint that have the same width as the surface to be processed. The nozzle scans over the surface with a constant velocity, while the surface is rotating. Material is removed from the surface. The resulting surface can be found next to each nozzle. Figure 6.11 a) shows that when scanning over a sample with a rectangular nozzle of the same size as the sample the resulting surface is flat.

To check if the simulated result for the flat central area could be obtained in practise, a 5% #800 SiC slurry was sprayed onto a pre-polished sample for 45 minutes. The nozzle was a flat fan type, the pressure was 5 bar and translation was carried out over 25 mm with a constant velocity of 5 mm/s. The sample rotated with 2 Hz. The stationary footprint of a flat fan nozzle is rectangularly shaped, with its deepest part in the center, see Figure 6.12. The resulting shape on the sample can be seen in Figure 6.13. The discontinuous change of the slope of the resulting shape is caused by the fact that the surface is divided in a finite number of elements. The material removal is determined per element, continuous removal does not occur. In a real experiment such sharp transitions will not occur. The removal and the slopes are limited by the size of the footprint.

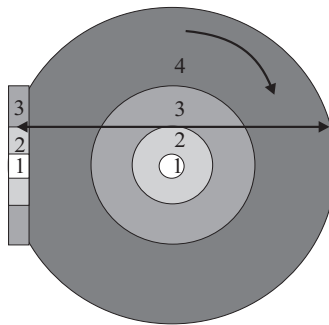


Fig. 6.9 Top view of a rotating sample (the round grey object) and a scanning nozzle (the rectangular grey object). The straight arrow indicates the movement of that part of the nozzle that removes material from the areas 3 and 4 of the surface.

According to the Wyko interferometer, the entire surface (40 mm diameter) has a peak to valley value of 857 nm. This is the maximum height range, so the maximum depth of the area that was processed, since the surface was initially flat. The area in the center with a diameter of 15 mm gives a form error of $3 / 0.062$ (0.273). This notation means that the shape (indicated by the 3) deviates 0.062 fringes from a reference flat, with an irregularity or un-roundness of 0.273 fringes. Since the ISO 10110 norm works with a standard wavelength of 546.1 nm and the Wyko interferometer with 632.8 nm a factor of 1.16 has to be accounted for. The form error of the central 15 mm according to the ISO norm would thus be: $3 / 0.0719$ (0.32). According to the ISO norm this surface is flat to $\lambda/14$ and has an irregularity of $\lambda/3$.

From this experiment we can conclude that it is possible to predict the removal over an area larger than this spot when taking the dwell time into account. It is also possible to produce flat surfaces to $\lambda/3$. With the correct dwell time distribution and translation and rotation equipment it should therefore be possible to produce any arbitrary shape with lateral spatial variations of the order of the spot size.

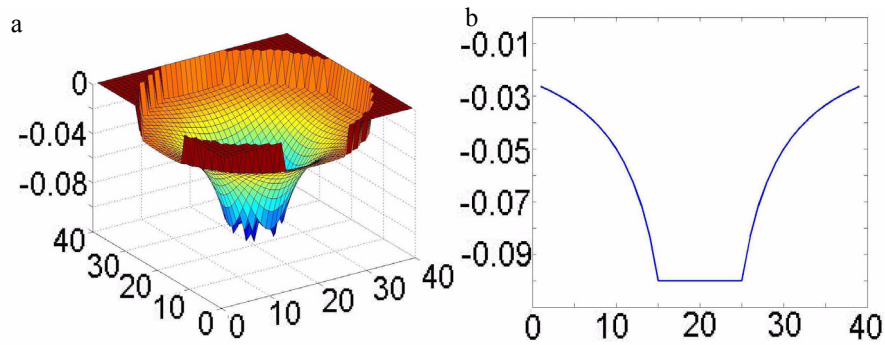


Fig. 6.10 a) 3D view and b) radial cross-section through the simulated surface profile (40 x 40 elements large) that will result when a spot with a 3 x 10 elements large footprint is scanned over the surface with a constant velocity.

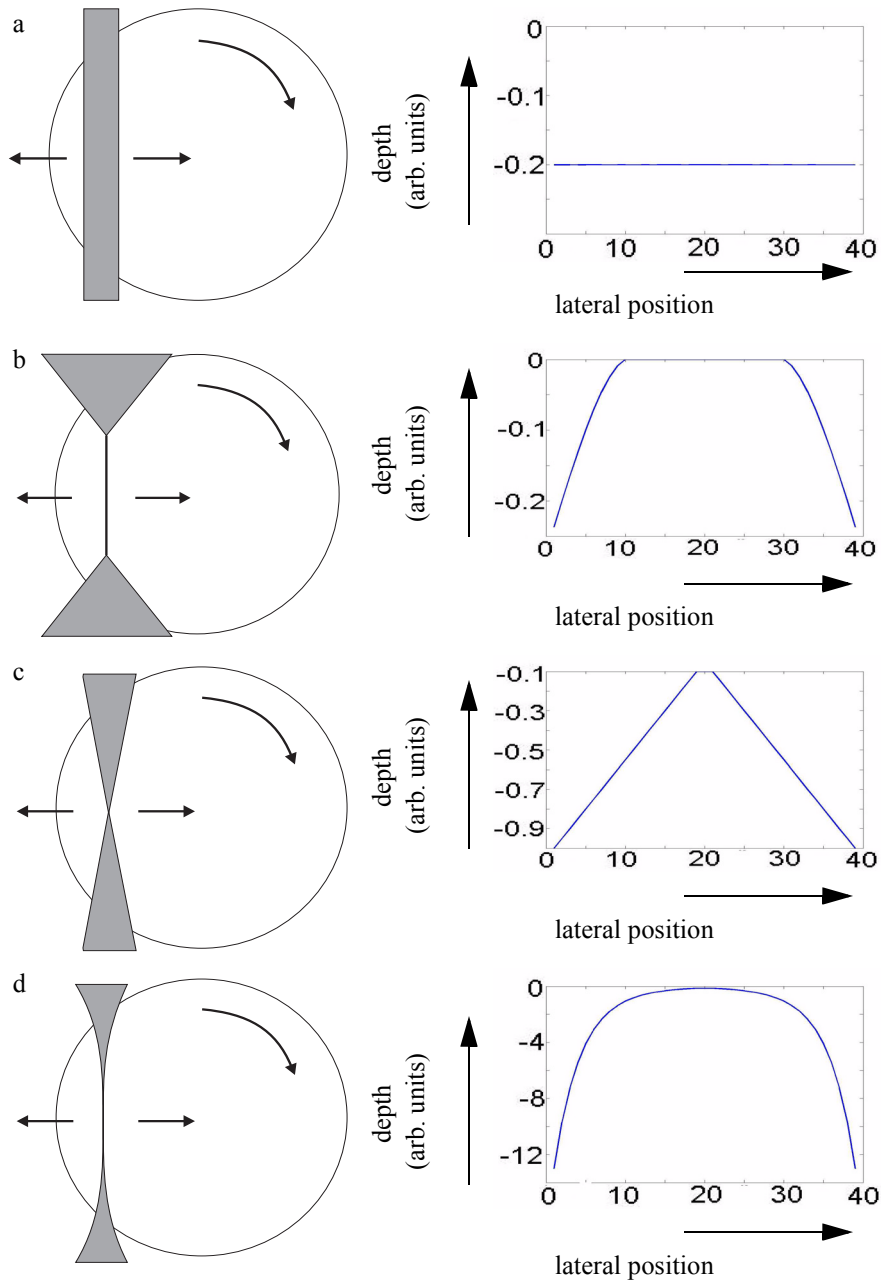


Fig. 6.11 Four examples of nozzles with special footprints that remove material from a rotating surface. The nozzles are indicated in grey, they scan over the surface while the surface rotates. A one-dimensional radial section through the profile can be found on the right-hand side.

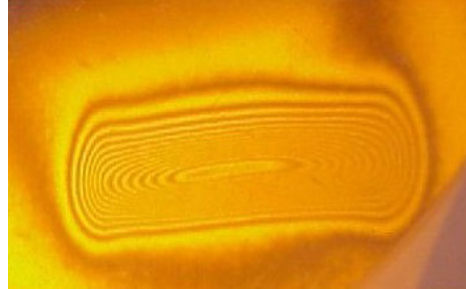


Fig. 6.12 Stationary footprint of the flat fan nozzle. At four cm distance from the nozzle a rectangular spot results of approximately 0.5 x 1 cm. The deepest point of the spot is found in the center of the depression.

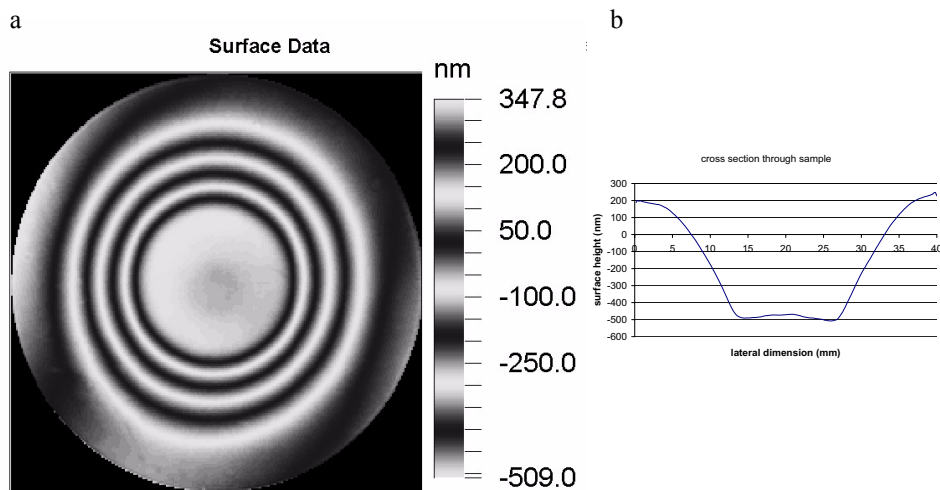


Fig. 6.13 The 4 cm diameter pre-polished sample has been processed in the central area with a diameter of 25 mm. The 15 mm diameter area in the center is flat to $\lambda/14$ (PV-value), with a non-rotationally symmetric deviation in depth of $\lambda/3$. a) Overview of the entire sample (Wyko interferometer) b) Cross-section in the horizontal direction.

6.6.3 Producing some typical prescribed surfaces

The model that is described in Subsection 4.6.2 predicts the amount of removed material in a certain point from the position on the sample and the velocity function of the nozzle with respect to the surface. This section will compare the results of three computed and three produced and measured surfaces. Firstly, the effect of translating a nozzle over a rotating surface with a constant velocity is computed and tested, secondly, the position-dependent velocity is computed that is needed to produce a spherical shape and a shape is produced according to the computed velocity distribution, and, finally, a shape is produced that shows a fourth order dependence on the radial coordinate.

Case 1: Constant radial velocity

The first case applies to a constant radial velocity. A 50 mm diameter round BK7 sample is rotating while a cylindrical nozzle is translated repeatedly back and forth over the surface with a constant velocity of 10 mm/s. The angle between the nozzle and the sample is 45°, its stand-off distance is 1 cm, the processing time 60 minutes, and the pressure is 5 bar. The predicted and the resulting surfaces can be found in Figure 6.14. The shape has been correctly predicted to within 5%. The predicted material removal does not give accurate predictions for the amount of removal in the center, as will be discussed after the third case.

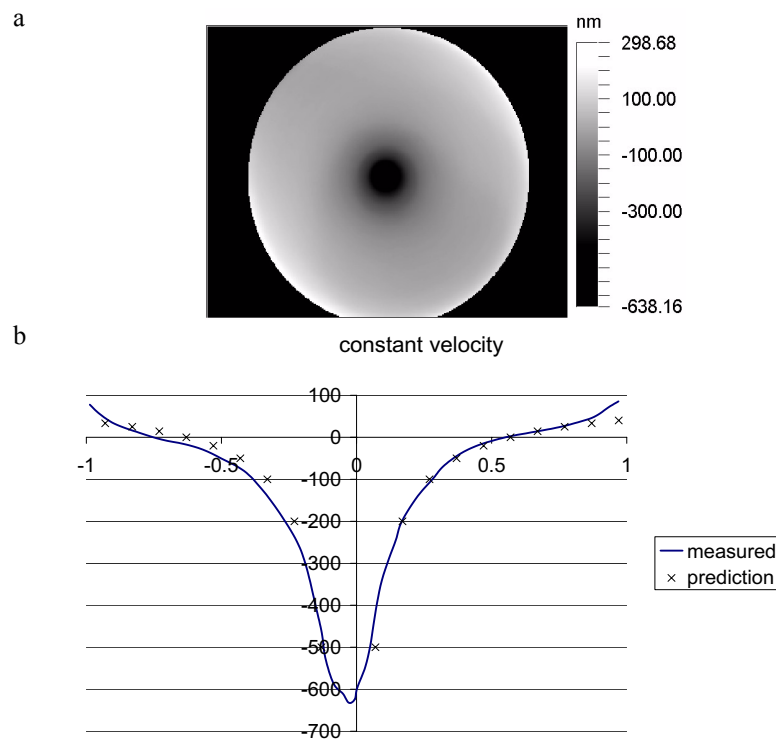


Fig. 6.14 Material removal over a 50 mm diameter rotating sample with a constant velocity of the nozzle with respect to the surface. a) Overview of the entire sample with a grey-scale coding of the amount of removal. b) Profile of the sample in a cross-section through the axis of the sample, showing a maximal depth of almost 700 nm; crosses indicate the predicted material removal.

Case 2: Spherical surface

In the second case the goal was to produce a spherical surface. The necessary velocity was computed as a function of the distance to the center. Then the restrictions of the possible velocities in the setup were taken into account, and based on those velocities a prediction of the resultant shape was made. Due to these restrictions and the discrete steps in the velocity a not-perfect sphere is predicted. Especially close to the center the shape

deviates from a sphere. Then the experiment was carried out, see Figure 6.15. A flat fan nozzle was used, at a stand-off distance of 4 cm, at perpendicular incidence, a 10% #800 SiC slurry, the processing time was 2 hours, the sample was rotating, the pressure was 2 bar, and the velocity can be found in Table 6.3. The position of the center of the nozzle has been given with its corresponding velocity. The velocity changes every 2 millimeter from the center to 22 millimeters away from the center. The last step indicates that the velocity of the nozzle when going back from 22 mm to the center is 50 mm/s. The nozzle moved over the surface many times. The prediction is correct to within approximately 5% again. The inaccuracy in the center will be explained in the section about case 3.

Table 6.3 Velocity of the nozzle with respect to the surface, as a function of its radial position (r is the radial position with respect to the center of the sample, v the velocity).

r (mm)	0-2	2-4	4-6	6-8	8-10	10-12	12-14	14-16	16-18	18-20	20-22	22-0
v (mm/s)	50	25.6	14.8	9.3	6.2	4.4	3.2	2.4	1.8	1.4	1.2	50

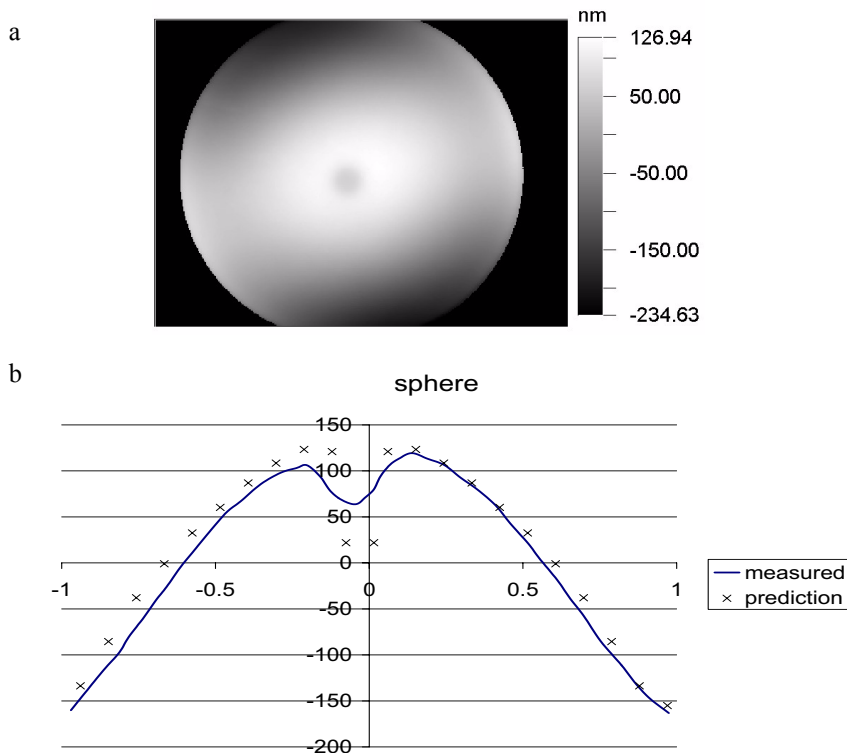


Fig. 6.15 Material removal over a 50 mm diameter rotating sample with a variable velocity of the nozzle with respect to the surface. The velocity is chosen in such a way that a spherical sample should result. a) Overview of the entire sample, b) profile in a section through the center axis of the sample, showing a maximum depth of more than 250 nm; the crosses represent the predicted material removal.

Case 3: Shape with a fourth order component

In the third case the goal was to produce a profile with a fourth order component, since these shapes can be interesting for surface corrections (a surface with the shape $C_1[r^4-r^2]$). The necessary velocity was computed as a function of the distance to the center. Taking the velocity limitations of the setup into account, we made a prediction of the expected shape, see Figure 6.17. The processing time was 1 hour, the slurry a 10% #800 SiC one, a cylindrical nozzle was used at perpendicular incidence, the stand-off distance was 1 cm, the pressure 5 bar, and the velocity can be found in Table 6.4. The nozzle translated over the surface many times. The resulting surface shows some steps that occur at the transition of one velocity to the other, see Figure 6.17. The predicted surface and the measured one do not coincide perfectly. A difference up to 15% can be observed, although the required shape can be clearly recognised in the picture. These deviations have a number of causes. The position of the nozzle is difficult to set accurately with respect to the center of the surface. When an error in the position is made in the direction of the scanning motion, the center will be treated too much, or not enough, depending on the direction of the error. The radial velocity also becomes incorrect due to this off-set. An error in the position perpendicular to the scanning movement can also be made. The effect will be that the center of the work piece is not processed enough. Another cause of the difference between the prediction and the measured results occurs when the velocity that is set does not correspond to the realised velocity. To investigate this the velocity of the scanning table has been measured as a function of its position, with a laser position transducer. The resulting velocity has been plotted together with the set velocity in Figure 6.16. The position -35 corresponds to the center of the work piece, the position -15 corresponds to the edge of the sample. One can observe that the velocity of 50 mm/s from the edge to the center is not constant, it fluctuates somewhat. The velocity of 50 mm/s is also not reached instantaneously, it takes approximately 5 mm to reach this velocity. The table overshoots a bit, goes to the 50 mm/s velocity in the other direction. The step-wise velocity decrease that is supposed to follow is replaced by a continuous velocity decrease, until the velocity of 1.4 mm/s is reached. Then the velocity follows the set velocity again, until the edge of the sample is reached.

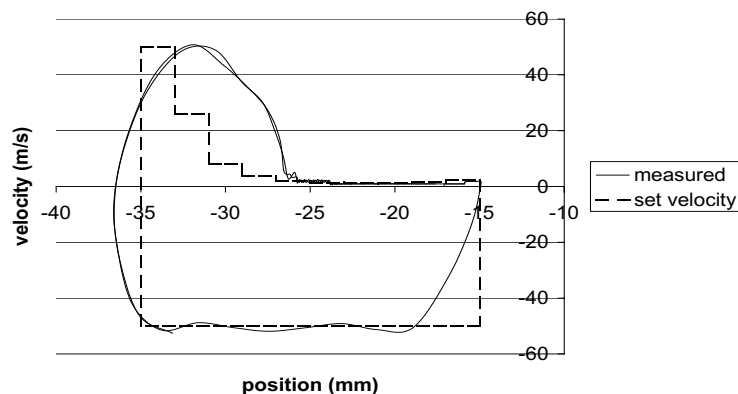


Fig. 6.16 The realised velocity (measured) of the scanning table of the FJP setup during a little more than one period and the velocity that was set.

Table 6.4 Set velocity of the nozzle with respect to the surface, as a function of its radial position (r is the position, v the velocity).

r (mm)	0-2	2-4	4-6	6-8	8-10	10-12	12-14	14-16	16-18	18-19	19-0
v (mm/s)	50	26	8.1	3.7	2.1	1.4	1.14	1.08	1.44	2.39	50

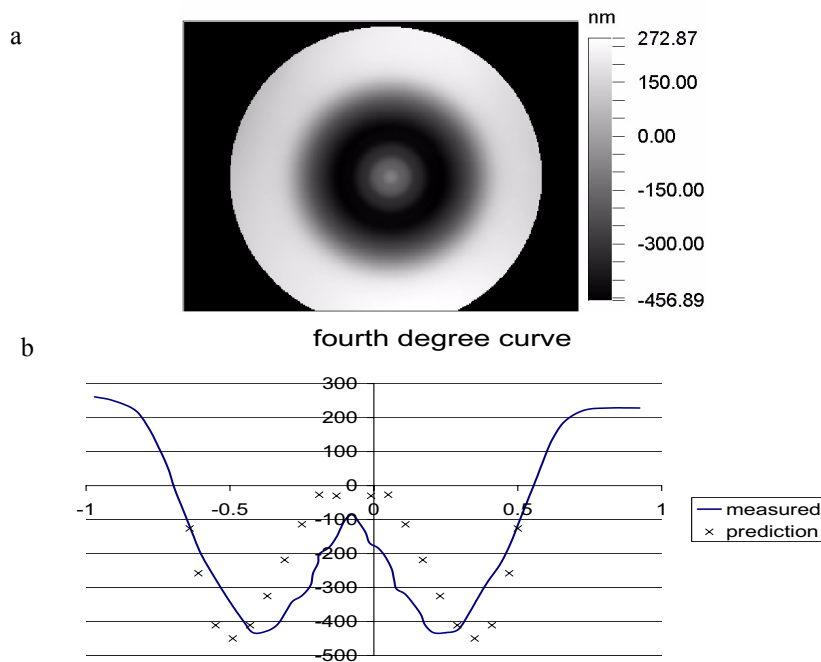


Fig. 6.17 Material removal over a 50 mm diameter rotating sample with a varying velocity of the nozzle with respect to the surface. a) Overview of the entire sample, b) section through the axis of the sample in the horizontal direction, showing a maximum depth of more than 700 nm; the crosses represent the predicted removal profile.

As a general conclusion we can say that it is possible to predict the shape of a surface to within 5% when the velocity of the nozzle with respect to the surface is known. Limitations imposed by the setup are the setting of the velocity which can only be done in a discrete number of steps (only 15 intervals with a different velocity can be set) and the fact that only values between 1 and 50 mm/s are permitted, lower velocities result in a complete stop of the translation and higher velocities cause the translation to continue beyond the allowed interval. It is desirable to have a setup in which the center of the work piece can be found with a high accuracy, and the velocity can be accurately set as a function of the radial position, without limitations on the number of different velocities that can be set. The accuracy with which the translation is carried out depends in practise on the velocity. The transition between two consecutive velocities will in practise be contin-

uous and not discrete, while we assume a discrete transition in the simulation. When the nozzle changes its direction of motion (in our case 1 at the outer edges of the sample, and in case 2 and 3 in the center and at the outer rim of the area that is processed) it will slow down, come to a stop, speed up and translate in the opposite direction. The nozzle needs a finite time for this in practise, while we assume an instantaneous direction change in the simulation, see Figure 6.16. To obtain a correct prediction the number of changes in the velocity should be as low as possible, or the realised velocity should be measured and a prediction should be made based on the actual velocity. The fact that the nozzle changes direction in the center of the work piece is caused by the fact that we can only set a limited number of intervals with a certain velocity and by the fact that we want to have a certain number of intervals with a different velocity. If scanning would be carried out from one edge of the sample to the other edge the number of intervals would be twice as high as when we only scan over half of the sample. A disadvantage of scanning from the center to the edge is that the error in the realised velocity in the center is relatively high.

The three prescribed surfaces and the flat surface that was presented in Subsection 6.6.2 show that it is possible to adjust the amount of removed material by changing the dwell time or by changing the position or shape of the stationary footprint. Another possibility is to change the pressure (so the depth of the footprint per unit time). The choice of which one of these controlling parameters is used depends on the accuracy and ease with which each parameter can be set.

6.7 Polishing

In Section 4.7 a model was presented that describes the surface roughness as a function of the number of impacts when the impacts of abrasives are assumed to be at random locations on the surface. Some qualitative theoretical considerations were presented for the dependence of the final roughness on the initial roughness, on the effect of one impact, and on the diameter of an abrasive particle. In this section some experimental data will be presented for the roughness as a function of the processing time and the effect of the initial roughness of a surface on the final roughness in Subsection 6.7.1, in Subsection 6.7.2, the effect of the pressure on the roughness will be discussed. Some pictures of surfaces will be presented in Subsection 6.7.3 from which the surface structure becomes visible. Subsection 6.7.4 will conclude with the lowest roughness that has been obtained to date when starting from a fine-ground surface.

6.7.1 Roughness as a function of time and initial roughness

To investigate the influence of the FJP process on the roughness of a surface as a function of time the following experiment has been carried out. With a 5% #1200 SiC slurry three different BK7 samples were treated. The first sample was polished ($R_a < 1$ nm) the second was pre-ground with #800 SiC ($R_a = 400$ nm), and the third was pre-ground with SiC #400 ($R_a = 600$ nm). The amount of removed material and the roughness of the samples was measured after 1, 2, 5, 10, 30, and 60 minutes. The resulting graphs can be seen in Figure 6.18 and some pictures of the initially roughest sample can be found in Figure 6.19. From these experiments one can conclude that the material removal depends

on the initial roughness. The material removal is the highest for the roughest surfaces. This can be explained from the fact that abrasive particles in the flow that move parallel to the surface can more easily remove material from a very hilly surface with protruding peaks than from a perfectly flat surface. Particles that impact nearly perpendicular on the surface will not notice any difference. It could also be explained from the fact that the rough surface causes more turbulence in the flow, which increases the material removal rate [fin60]. The roughness of both rough surfaces decreases as a function of time, while the roughness of the smooth surface increases. These results agree with the computed roughness as a function of the number of impacting particles.

In Section 4.7 it was shown that in theory the final roughness of a surface will converge to one equilibrium value independent of the initial surface roughness, for identical experimental conditions. The equilibrium value of the roughness depends on the type of slurry that is used, the pressure, and the other process parameters. This has also been confirmed experimentally. From an #800 SiC ground BK7 surface with an initial average roughness of 300 nm 20.4 μm was removed with a 10% #800 SiC slurry. This resulted in a surface with an $R_a = 6.4$ nm, $R_q = 8.3$ nm, $R_z = 60.3$ nm, and $R_t = 76.0$ nm. From a polished surface with an initial roughness of $R_a = 1$ nm 19 μm was removed, which resulted in a surface with an $R_a = 6.0$ nm, $R_q = 7.8$ nm, $R_z = 61.2$ nm, and $R_t = 89.6$ nm. The Wyko roughness measurements of both samples can be found in Figure 6.20.

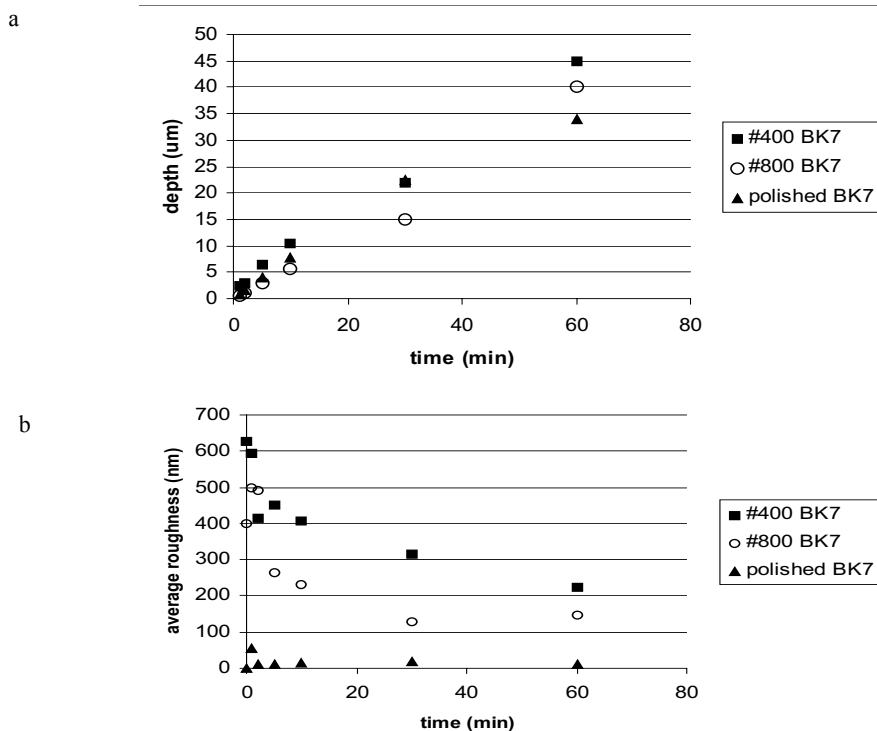


Fig. 6.18 a) Material removal and b) roughness as a function of time for three different initial surface roughness values.

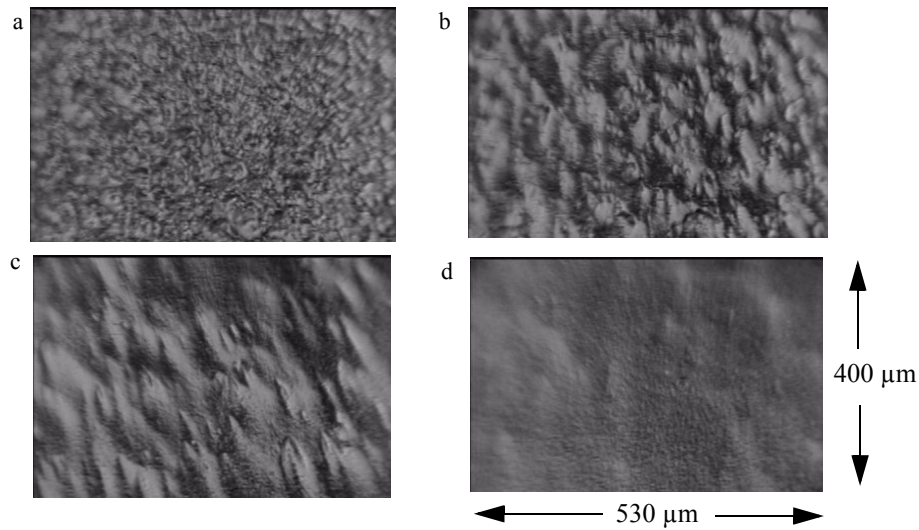


Fig. 6.19 Four Nomarski pictures of the #400 SiC pre-ground surface, after a) 1 min, b) 10 min, c) 30 min and d) 60 minutes of processing. The R_a -values are respectively 625 nm, 405 nm, 315 nm, and 225 nm.

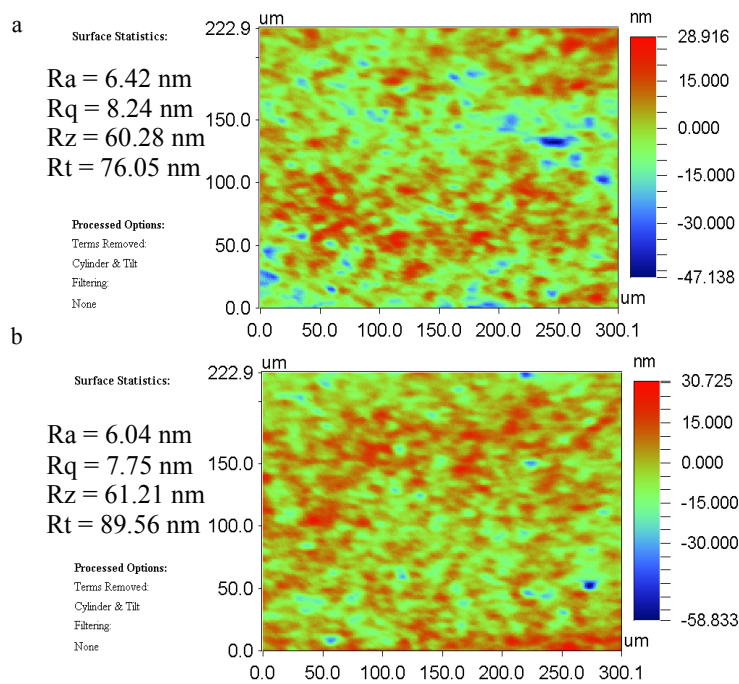


Fig. 6.20 Comparison of surface structure and roughness values for two samples that were treated identically, but had a different initial surface roughness. Wyko measurements of the final states of a) the initially ground surface and b) the initially polished surface.

6.7.2 Roughness as a function of the pressure

In Section 4.7 a dependence was predicted of the roughness on the pressure. Higher pressures were predicted to result in higher roughness values, due to the higher kinetic energy per impacting particle, which can cause deeper depressions in the surface. To investigate this dependence, an experiment was conducted in which stationary spots were created under identical conditions on an initially polished BK7 sample ($R_a = 1$ nm). The only parameter that was changed was the pressure (7, 14, and 27 bar). This was done for three different processing times (1, 5 and 10 minutes). A cylindrical nozzle was used with an inner diameter of 3 mm, the nozzle was perpendicular to the surface, the stand-off distance was 1 cm, a 10% #800 SiC slurry in 50% water and 50% glycerin was used. The amount of removed material has been plotted versus the processing time for the three pressures in Figure 6.22 a). From this plot we can see that higher pressures cause more material removal per unit of time. The resulting roughness could be caused by the amount of material that is removed, by the processing time, or by the pressure. In Figure 6.22 b) one can see that the roughness clearly depends on the pressure. Higher pressures result in higher roughness values. In Figure 6.22 c) the roughness has been plotted as a function of the processing time. The highest pressure (27 bar) increases the roughness more rapidly than the lower pressures. Each combination of experimental conditions will correspond to an equilibrium roughness value. When the processing is continued long enough this value will be reached.

In Figure 6.22 d) the roughness has been plotted as a function of the pressure, both experimental values and a quadratic fit are shown. The fit is obtained based on the following idea. The roughness is caused by material removal. The material removal rate depends on v^2 , according to Finnie's equation (Equation (4.25)). The force a particle exerts on the surface is equal to the pressure times the contact area. The following relation between the force on the surface and the change of velocity of the particle should also hold (see Equation (2.4))

$$F_t \cdot \Delta t = m \cdot \Delta v. \quad (6.2)$$

This equation shows that the force is proportional to the particle velocity. Therefore the pressure is proportional to the velocity. The roughness is proportional to the material removal rate, which is proportional to v^2 , which is proportional to p^2 . For a pressure of 0 the roughness should not change. Therefore a quadratic fit through (0,0) was carried out on the measured roughness values. This resulted in

$$R_a = 0.0345p^2. \quad (6.3)$$

This fit is valid for the experimental conditions given here only. The spread in the measured values is caused by the different processing times. Longer processing times cause higher roughness values, because the initial roughness value was smaller than the equilibrium value for this slurry.

The experiments should be continued until the final roughness is reached, for a number of pressures, a quadratic fit could then be carried out on these final values to obtain information on the dependence of the final roughness on the pressure.

6.7.3 Surface structure

In order to get a better understanding of the structure of a surface that was treated with FJP a Nomarski picture was made of the footprint of a spot that was created with a cylindrical nozzle at perpendicular incidence and at an angle of 45° , as can be seen in Figure 6.21. A number of pictures was taken of parts of the spot and they are combined to form the whole image.

From these Nomarski pictures one can see that at perpendicular incidence a circular symmetric deformation results. In a ring-shaped area the material is removed, while little material is removed from the center. At an angle of incidence of 45° the material removal occurs in a horse-shoe shaped area. In both cases pits are created in the initially polished surface. Observations have been made that the amount of pits does not increase with increasing processing time, but more pits do occur for higher slurry velocities. This led to the idea that the pits are caused by single abrasive particles that have a large velocity component perpendicular to the surface, and thus have enough energy to create a small crater in the surface. The fact that the number of pits does not increase with time must mean that the pits are also removed by the rest of the fluid.

One cause of the occurrence of pits is the high velocity of particles. The slurry flows out of the nozzle with a certain velocity. The velocity of the surrounding medium in which the slurry is ejected is zero. This velocity difference causes the outer layer of the slurry to mix with the surrounding air. This can also cause particles to end up in the air. These particles still have a velocity in the direction of the jet. If these particles approach the surface, they are not slowed down like other particles that are surrounded by water. This can cause the damage that is observed. In order to investigate if the occurrence of air is indeed responsible for the pits in the surface two identically polished surfaces were treated, one with the normal slurry and one in which extra air bubbles were introduced into the slurry. The surface which was treated with the slurry with extra air bubbles has more pits in it.

Another cause for the pits in a surface is that some particles have too much energy. This could either be caused by the velocity distribution in the flow (not all particles have an identical velocity, but this depends on their position in the beam) or by the mass distribution of the particles (not all particles have the same diameter). Particles with a different density could theoretically also be present in the slurry.

To reduce the perpendicular velocity component one could reduce the angle between the slurry and the surface, but this would change the stationary footprint to a large elongated one which is less practical. Another possibility is to increase the viscosity of the slurry. This forces the particles to follow the streamlines more closely, so they impact the surface at a more oblique angle. The viscosity can be increased by changing the carrier of the fluid from water to glycerin (=glycerol), or by using a mixture of glycerin and water.

Experiments in which only glycerin was used showed that it is difficult to pump this viscous fluid through the setup. Adding some water decreases the viscosity and makes it easier to pump the liquid around. A comparison of the reachable surface roughness was made for identical process parameters while comparing the effect of using a slurry of water only and when using a mixture of water and glycerin (50%). This shows that the number of deep craters on the surface is less in the case of a glycerin slurry. This is caused by the fact that the particles have a lower impact velocity and angle upon impact.

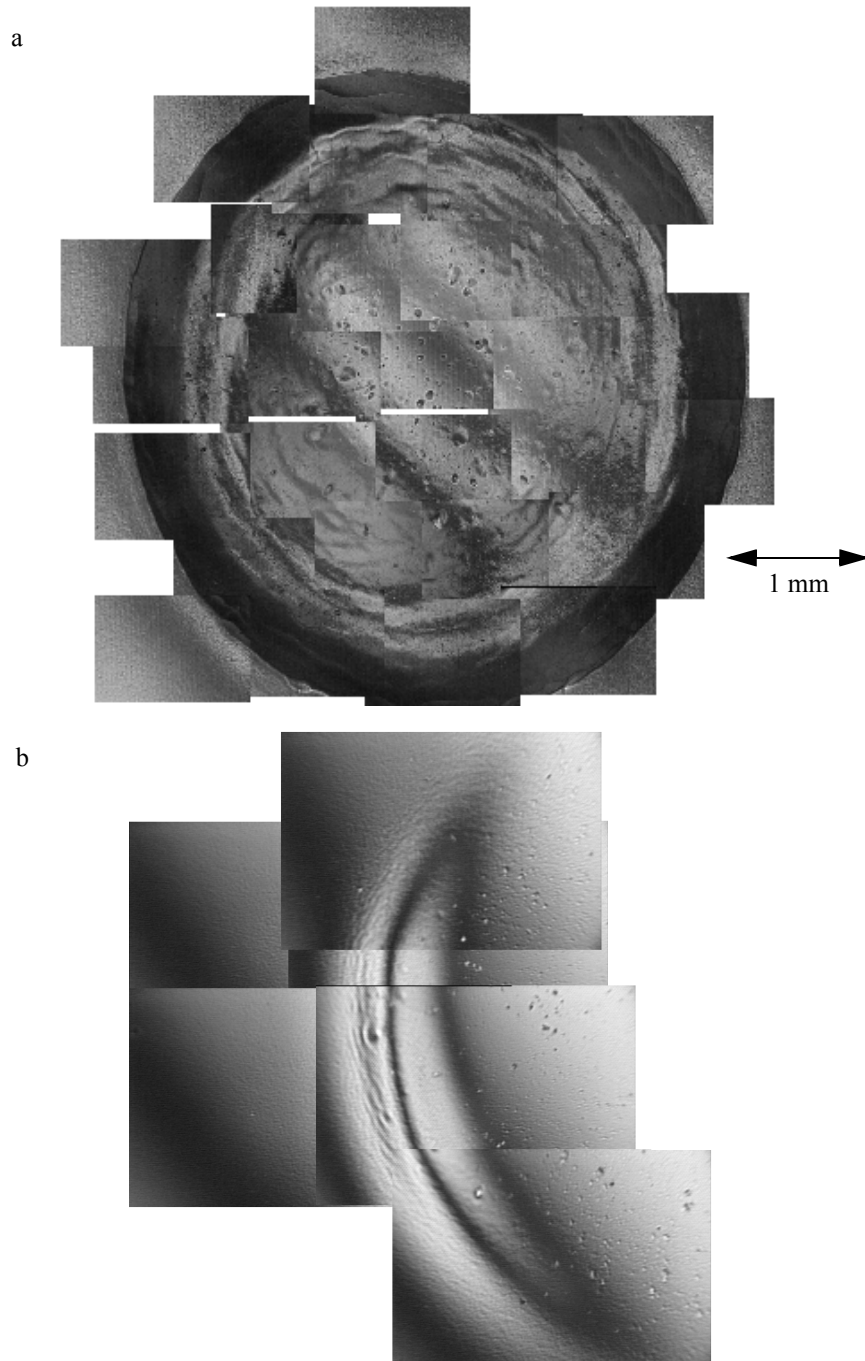


Fig. 6.21 a) Nomarski pictures of a spot created under perpendicular incidence and b) at an angle of 45° .

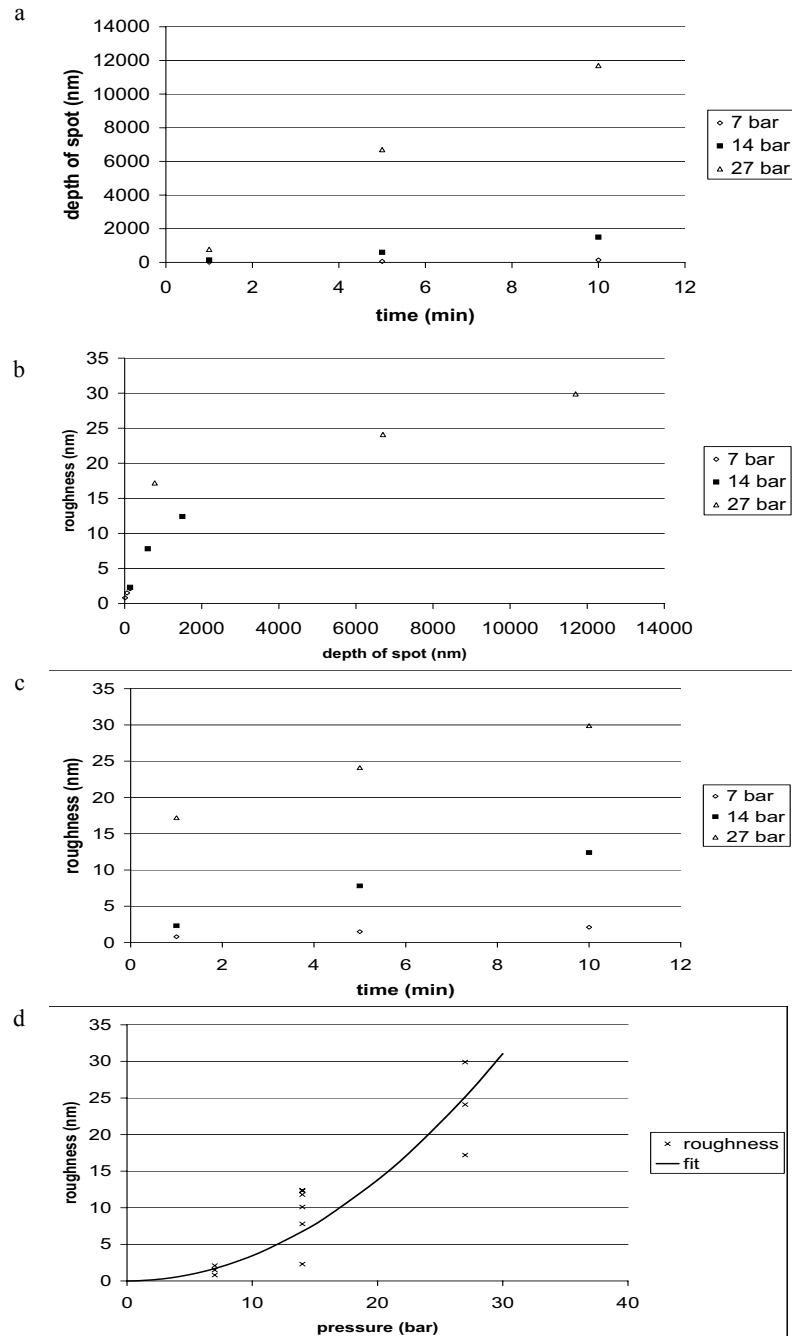


Fig. 6.22 a) Amount of removed material as a function of the processing time for various pressure values (7, 14, and 27 bar). b) Roughness as a function of the amount of removed material. c) Roughness as a function of the processing time. d) Roughness as a function of the pressure, both the measured values and the quadratic fit are shown.

6.7.4 Best roughness obtained

In this chapter some experimental relations have been described between the roughness and some parameters that can be set, like the processing time (Section 6.7.1), the initial roughness (Section 6.7.1), and the pressure (Section 6.7.2). In Chapter 4 some theoretical relations between the final roughness and the particles velocity, their diameter, and the initial surface roughness have been discussed. This subsection will show an interferogram of the best roughness that has been obtained on a fine ground (300 nm average roughness) BK7 surface. The final R_a -value equals 3.6 nm, the R_q value equals 4.7 nm, the R_z value equals 34.6 nm, and the R_t value equals 40.6 nm. To obtain this lowest roughness value a flat fan nozzle was used that is rotated around its own center with 75 rot/min. The work piece rotated with 200 rot/min. The work piece was translated 3 mm back and forth for one hour. The angle between the nozzle and the sample was 80°. The slurry that was used was a 10% #1000 SiC slurry in water (5 μm diameter). The pressure behind the slurry was 5 bar.

Theoretically, an even better result would be obtained if the particle diameter was increased and the velocity decreased, but, in practice, one also has to remove a certain amount of material in order to remove the roughness, and decreasing the velocity would slow down this process. In practical situations a trade-off should always be made between the result that can be obtained and the amount of time it will take.

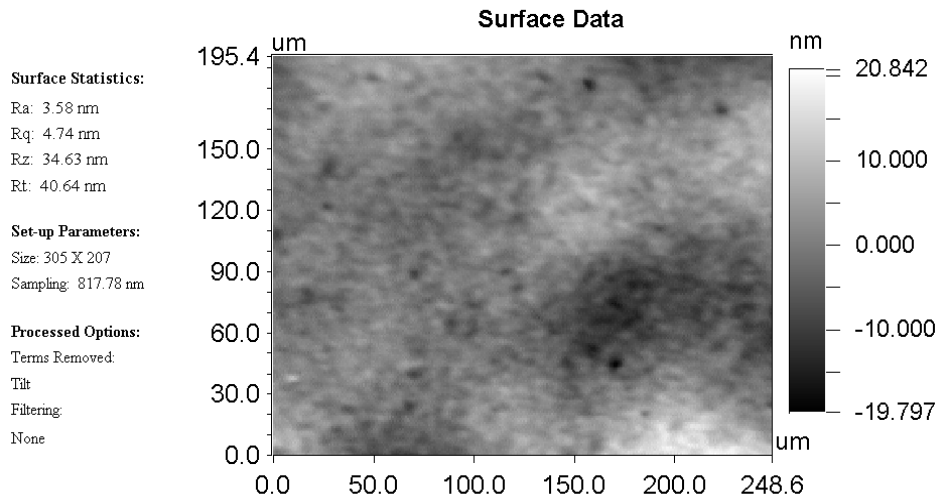


Fig. 6.23 Wyko interferogram of the best roughness reduction obtained so far on BK7, starting from a fine ground (300 nm average roughness) surface.

7 Conclusions and suggestions

Fluid Jet Polishing (FJP) is a shape correction and/or roughness reduction technique. FJP uses a slurry that flows out of a nozzle to process the surface, therefore it is a contactless machining technique and it is more suited to treat hard-to-reach areas of a surface than existing techniques. It could for example be used to treat the insides of moulds, or to treat steep (a)spherical surfaces. This thesis has mainly described the application of FJP to glass surfaces, more research is needed to investigate the applicability to metals, plastics etc.

In Section 7.1 a summary of the possibilities and limitations will be presented of the measurement techniques that were described in this thesis, of the presented models, and of the FJP technique. Some suggestions for possible improvements will be done as well. Then two alternative techniques will be suggested. The idea of chemically assisted FJP will be discussed in Section 7.2, and a close contact variant of FJP, called Jules Verne, will be discussed in Section 7.3 with some initial tests that have been carried out.

7.1 Conclusions

The conclusions that were drawn in this thesis are brought together in this section. First, the two presented in-process measurement methods will be described. Then the models that have been developed for the prediction of material removal and the resulting roughness will be mentioned. Finally, the applicability and limitations of the FJP technique will be discussed in eight categories that each describe an issue relevant for processing techniques; we treat the accuracy of shape corrections, the reduction of roughness, the material removal versus process parameters, the processable area, the deterioration and contamination of the slurry, the influence of the sample material, the properties of the slurry, and, finally, we present some comments concerning mid-spatial frequencies.

In-process measuring

The possibility of carrying out in-process measurements has been demonstrated in this thesis. In Section 3.3 the iTIRM (intensity-detecting Total Internal Reflection Microscopy) technique is described. iTIRM is a technique for in-process monitoring of the total surface quality of flat surfaces, which includes the surface roughness, sub surface damage, and scratches in the surface. The iTIRM technique can measure the surface quality over a wide range from very rough to very smooth surfaces (some μm to well below 1 nm). Surface roughness improvements of 0.1 nm rms can be detected with this technique. In order to measure the surface quality of non-flat surfaces some modifications

have to be made to the setup. The direction under which the internally reflected beam will leave the sample depends on the slope of the part of the surface that is measured. The position of the detector has to be adjusted accordingly. For rotationally symmetric parts annular rings could be measured for each detector position. The measurement spot would have to be moved over the surface (while adjusting the detector position), and then the measurements have to be stitched together.

The surface shape can also be measured in-process. In Section 3.4 a measurement technique based on the interference of an object and a reference beam was described. Both beams reflect from the inside of the surface to be measured at the total internal reflection condition. The information on the surface shape is obtained from the reflected beams via a temporal phase unwrapping method. Unwrapping problems are avoided by comparing successive images instead of comparing any image to the first image. Only single spots can be monitored with the current setup. In order to measure an entire surface scanning will have to be implemented and the reference spot has to be chosen in an intelligent way. Only when every part of the image is processed simultaneously, it is not possible to choose a reference spot that does not change.

Models for removal and roughness prediction

In order to obtain a better understanding of the FJP process and to be able to predict the material removal as a function of the process parameters without extensive experimental testing, several models have been developed.

In Section 4.3 a model for the pressure distribution in the jet has been described. From this model the footprints that occur for cylindrical nozzles can be predicted for every angle of impact.

In Section 4.4 a model is presented that computes the position and velocity of the particles in a slurry. This model can be used to determine the number of impacting particles per second and the angle and velocity of the abrasive particles upon impact on a surface. Section 4.5 describes three models for the material removal from a surface on the microscopic level: the finite element approach is discussed, a simple estimation of the amount of removed material is derived from a SEM picture of a sample, and Finnie's model is discussed.

Section 4.6 describes how the material removal can be predicted from the stationary footprint and the movement of the nozzle with respect to the surface. When a certain final surface shape is desired the position-dependent velocity can be deduced. Flat and curved surfaces have been produced and they correspond to the predicted shapes to within 5%, as was shown in Subsection 6.6.3. For shapes that require more changes in the radial velocity of the nozzle the deviation is higher. These deviations are caused by the inaccuracy of the translation of the setup.

A model that predicts the roughness is presented in Section 4.7. This model is based on the assumption that impacts occur at random locations on the surface, where they remove a certain amount of material, if there are no obstructions on the surface that prevent the particle from reaching this random position. The surface roughness can be computed from the final surface height distribution. The final roughness that can be reached on a surface is shown not to depend on the initial roughness, both theoretically (see Section 4.7) and experimentally (see Subsection 6.7.1). The final roughness increases for

increasing pressure. This has been discussed theoretically (see Section 4.7) and experimentally (see Subsection 6.7.2).

Accuracy of shape corrections

Section 6.1 has shown that with FJP shape corrections can be carried out over an area larger than the footprint of the nozzle. In the setup that is used at this moment these corrections are limited to an accuracy of 4% in depth. This limitation is caused by a combination of the in-accuracies of all the elements that are present in the setup, and by the drift of some of the process parameters, as has been summarised in Table 6.1.

In the fine grinding step, when starting from a rough ground surface, a material removal of 100 μm is very common. When a surface is fine ground and only polishing has to be done removal rates rarely exceed 10 to 15 μm . When removing 10 μm of material a 4% accuracy corresponds to 0.4 μm , which is somewhat smaller than the reference wavelength λ_0 ($\lambda_0 = 546.1$ nm according to the ISO specifications). The shaping accuracy of the current setup is good enough for low-end optics, but for high-end optics $\lambda/5$ to $\lambda/10$ is needed. The obtained accuracy is fortunately not a limitation of the FJP method, but only of the setup. This is proven by the experiment in Section 6.2, which shows that a deviation from the average shape of approximately 1% can be obtained.

In the setup used for the experiments discussed in this thesis, the most important limiting factors for the accuracy of shaping are the fluctuation of the abrasive particle diameter and the pressure fluctuations. The fluctuation of the temperature of the slurry is also very large, especially over a few hours, but as in classical grinding its influence is not that large, as was proven by experiments.

The shaping accuracy can be improved when the width of the diameter distribution of the abrasive particles is reduced, or when the largest particles are removed from the slurry. The number of pits that are created in the surface is also smaller for a narrower distribution, because less excessively large particles that have more energy to damage the surface will be present in the slurry. In more expensive batches of abrasives this width is smaller than in cheaper batches. By filtering the initial abrasives the distribution width of the abrasives can also be reduced.

The demands that we place on a pumping system is that it should be capable of reaching a certain stable output pressure (maximally 20 bar with a fluctuation of less than 2.5%), and a flow rate of at least 10 l/min. The system should also be capable of pumping abrasive slurries, without being damaged by them. To reduce the pressure fluctuations in the setup an alternative should be found for the presently used pumps. Both the used peristaltic pumps and the membrane pump show a relatively large fluctuation of the output pressure. These fluctuations are only partially damped by pressure stabilisers, like a membrane in a cavity. A different type of pump that could be used is the gear pump. This type of pump seems to be capable of delivering a constant output pressure. A big problem with these pump systems is that they are sensitive to wear. To avoid the wear in the pump the slurry could be mixed at the last moment, in the nozzle. The rest of the system would only come into contact with clean water or any other medium that is used. The problem that arises in such a setup is that the slurry can not simply be recycled, because the abrasive particles have to be separated from the water. One should also make sure that the particle distribution is homogeneous in the jet when mixing the abrasives with the liq-

uid at the last moment, this is not a trivial issue. An advantage of mixing the abrasives with the liquid in the nozzle is that the concentration can easily be varied during the process. A different type of membrane pump could be used for pumping slurries at a constant pressure. Pump systems exist with three membranes that are capable of producing a constant output pressure. The pressure in this system can be adjusted by changing the air pressure behind two of the membranes, which can be set very accurately. Small adjustments can be made to the pump which ensure that the elements of the pump that are sensitive to wear (like membranes and valves) are only in contact with the water, and not with the abrasives when the system is turned off. Thereto small chambers should be present below the sensitive areas, where the abrasives can settle down.

Another way of reducing the fluctuations could be the storing of the slurry in a vessel that is under pressure. Because of the pressure, the slurry flows out of the nozzle that is connected to the vessel. To return the slurry to the vessel only a small over-pressure is needed. When the process is temporarily interrupted when the slurry is pumped back the constancy of this over-pressure is not important for the final stability of the pressure at the output of the nozzle.

The expected spread in particle diameter (currently some tens of percents, see Figure 5.3) and the pressure fluctuations (currently some tens of percents, see Subsection 5.1.4) can be reduced to at least 25% of their current values.

The deviation from the average shape within a profile that has been created by repeatedly translating a spot over the surface is less than 1%, see Section 6.2. This proves that the material removal is accurate to 1% when the effects of the pressure fluctuation and of the abrasive particle diameter average out by ‘machining’ the surface in a repeated way.

Roughness reduction

When material has to be removed from glass with a high accuracy it should be done in the ductile regime. In Section 6.5 it has been shown that FJP can operate in the ductile regime, when the process parameters are chosen correctly. A roughness reduction on BK7 can be obtained in a one-step process (one slurry, one fixed pressure during the entire process) from a fine-ground surface (average roughness $R_a = 300$ nm) to $R_a = 3.6$ nm, see Subsection 6.7.4. This roughness reduction is limited by the fact that pits are sometimes generated by particles with a high velocity. In order to reduce the velocity component of the abrasives in the direction perpendicular to the surface, glycerin could be used in stead of water as the medium in which the abrasives are mixed. Since glycerin has a higher viscosity, particles will follow the streamlines of the flow more closely, and the angle between the impacting particles and the surface will be smaller.

Another unwanted phenomenon in the setup that increases the surface roughness is the mixing of air with the water jet. In the case of FJP the turbulent water jet travels through a surrounding medium (air). The fact that the jet is turbulent and the fact that the velocity of the jet and the surrounding medium differ causes some of the air to be mixed into the jet. As a result some of the abrasive particles will not be slowed down in the vertical direction upon impact by the surrounding water since it is replaced by air. Because of their higher perpendicular velocity component they will remove more material. To avoid the mixing in of air some solutions have been found. A first solution is that the medium through which the jet travels is replaced by water. The jet will behave differ-

ently as a whole now. It will be slowed down more than in air if the water does not move with the same speed as the jet. Hence the processing should be done closer to the end of the nozzle. The removal will be more dependent on the stand-off distance. The slurry can not be directly recycled, because the concentration has been reduced by the water surrounding the jet.

A second solution is that the outside part of the jet is blocked by a mask, see Figure 7.1 a). This has to be done close to the surface that is treated. If it is done too far away from the surface you are effectively creating a new jet, with the same problems.

Another solution is encapsulation of the jet by a co-flowing jet that consists of water only, as shown in Figure 7.1 b). This would cause the air to be mixed into the co-flowing water, before it is mixed with the slurry with the abrasives. This will result in a larger area over which the jet can be used without rapidly moving abrasives in air. The difficulty that still has to be solved is that this changes the particle concentration in the slurry, so simple recycling systems are not sufficient anymore.

Air can also be present in the hoses or the nozzle before the processing begins. When the slurry begins to flow out of the nozzle this air will be dragged along. This can be prevented by pumping the slurry around for some time before the processing begins. This could be done by placing a shutter between the nozzle and the sample.

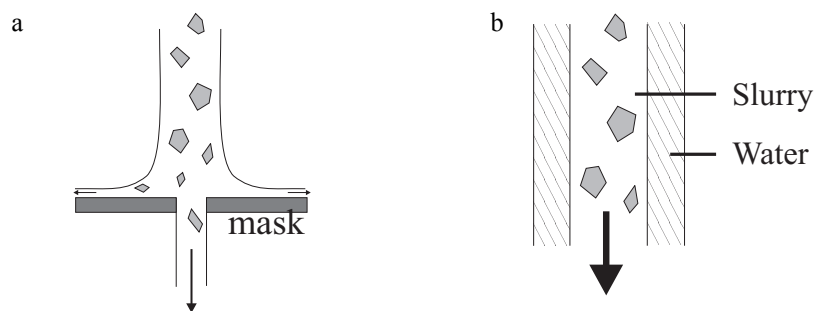


Fig. 7.1 Suggested alternatives for the flow that should prevent the mixing in of air in the flow. This can be done by a) blocking the outside part of the beam, or by b) using the slurry with abrasives in the center and adding a co-flowing jet of pure water at the outside of the stream.

Material removal vs. process parameters

The material removal in the FJP process depends on a number of parameters. A short summary of the dependencies and a reference to the section in which a more detailed description is given, is listed here.

- The erosion depends linearly upon the concentration (Subsection 5.1.1).
- The material removal scales quadratically with the radius of the impacting particles; the material type and the shape of the particles are less important than the radius of the particles (Subsection 5.1.2).
- The temperature of the slurry does not influence the material removal rate (Subsection 5.1.3).

- The material removal depends on the square of the average abrasive particle velocity, and shows a velocity offset (Subsection 5.1.4).
- The material removal rate is not critically dependent on the stand-off distance, when a cylindrical nozzle is used that does not diverge and when the loss of energy of the jet is not too large (Section 5.2).
- The amount of removed material depends linearly on the processing time (Section 5.3).
- The amount of removed material depends on the elasticity, the hardness, and the fracture toughness of the sample material according to Equation (5.2) as proposed by Lambropoulos [lam97].
- The material removal footprint depends on the angle at which the slurry approaches the surface, see Section 5.5. The shape of the nozzle is important for the resulting velocity distribution of the fluid, and therefore it determines the material removal footprint, see Section 5.6.
- A drastically higher material removal rate can be achieved by using a high pressure, but this results in a relatively high final roughness; an optically acceptable final surface roughness can be achieved by using a pressure of typically 5 to 10 bar at the expense of a lower material removal rate.

Processable area

The minimal width of the processing area is approximately 1 mm due to the nozzle diameter. This nozzle diameter can not be chosen infinitely small, because the nozzle will then get blocked by glass debris, contaminating particles and the slurry particles flowing through it and sticking together.

Slurry deterioration and contamination

The slurry that is used has been shown not to deteriorate during a processing time of 8 hours at five bar (20 m/s), see Section 6.3. The slurry will be contaminated by glass particles that have been removed from the sample surfaces, but also by dust particles, abraded particles of the inside of the pump, the hoses, and the tank, and by oil particles that are present in the pump. Particles of previously used slurries can also be found in the slurry. When particles of 7 μm are used for the processing, smaller particles will not be an issue for the contamination. This means that FJP can be operated at a cleanliness level comparable to that in the case of normal grinding, instead of the level required for standard polishing.

To determine the importance of contaminating particles it is recommended to carry out some experiments with different concentrations of particles with a certain diameter and hardness. One should investigate when and if the presence of these particles becomes noticeable. Measures should be taken against noticeable contamination levels, e.g. by filtering the slurry.

Sample material

Various materials can be treated with FJP so that shape correction and roughness reduction are possible. In order to know the exact removal rates and the reachable roughness of each material, more research is needed. In Section 5.4, data of the material removal rate

of seven different materials is presented. A theoretical dependence of the material removal rate on the samples material properties is also presented.

Slurry properties

A drift in some of the slurry properties like temperature, viscosity and pH value can occur during an experiment. Even though the change of the temperature does not influence the material removal rate much, see Subsection 5.1.3, it can be controlled using a commercially available machine that controls the temperature. The optimum temperature should be investigated and set for the specific application (type of material). To get a more reproducible process, the viscosity and pH value of the slurry should also be monitored and controlled.

Sub-aperture technique / mid-spatial frequencies

Usually, FJP is applied as a sub-aperture technique. In the special case that the footprint of the nozzle is larger than the optic, FJP no longer is a sub-aperture technique. A problem that often arises in sub-aperture techniques is the occurrence of mid-spatial frequencies. It has been shown in Section 6.4 that this does not occur in the case of FJP. It has even been shown that the amplitude of existing mid-spatial frequencies can be reduced (Section 6.4).

General conclusions

At this moment FJP can be applied to make shape corrections to surfaces with an accuracy of approximately λ , see Section 6.1. With some more research and some improvements to the setup this accuracy can be increased by a factor of four. Roughness reduction to a few nanometers is possible at this moment. More research should show if this can be reduced to 1 nm, which is needed for many high-end applications. At this moment it is possible to apply small shape changes without increasing the roughness of the initially polished surface to values above 1 nm. This is limited by the amount of material that should be removed from the surface. The application of FJP to BK7 glass and other hard materials is the most promising one. Using FJP for soft materials like CR39 is more difficult, due to pits that easily occur in the surface.

7.2 Alternative setup 1: Chemically assisted FJP etching

When processing silicon dioxide or certain plastics a possible variation on the FJP technique is the addition of an etchant to the slurry. The slurry could be used with or without abrasives. One possibility would be to aim a hydrogen fluoride (HF) slurry at a glass surface that is protected by a water film. Material will only be etched away exactly there where the HF slurry penetrates through the water film. The correct pressure can be set by inspecting the back side of the water film as a function of the pressure of the HF slurry. See Figure 7.2. When the surface that is treated is monitored in real time the removal can be watched more closely. The nozzle will have to be made of a HF resistant material.

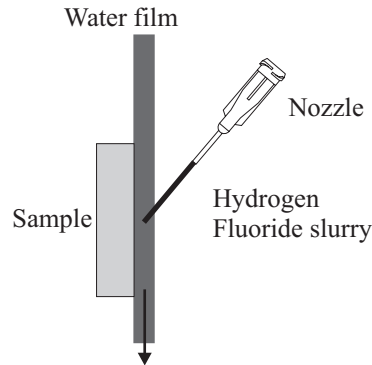


Fig. 7.2 The suggested setup for chemical FJP etching.

7.3 Alternative setup 2: The Jules Verne setup

A close contact alternative to FJP has been invented, and is arbitrarily named Jules Verne (JV). While FJP is used in the regime where the nozzle has a stand-off distance of some millimeters to some centimeters, the regime where the stand-off distance is typically smaller than $100\ \mu\text{m}$ can also be explored. The advantage of this alternative setup is that the slurry flows more parallel to the surface, which is more favorable for roughness reductions. Another advantage is that the slurry does not come into contact with the air before or while it removes material. Air can not be mixed into the slurry to cause pits in the surface. To investigate this alternative a setup has been built on a computer numerically controlled LOH polishing machine [www14]. The reason to build the setup on this machine is because of its accurate control possibilities. A slurry of abrasives in water is pumped out of a nozzle that is very close to the surface to be treated (typical stand-off distance of $50\ \mu\text{m}$). This distance could be controlled by a feed-back system that measures the pressure. It would be even better to adjust this distance by using a force controlled tool or work piece. The slurry velocity in the main chamber of the nozzle is not high enough to remove material, but when the slurry leaves the nozzle it is accelerated on passing through the tiny gap between the nozzle edge and the surface, see Figure 7.3. The material removal occurs in a ring-shaped area, like in the case of a curve generator of the FAUST-type (Fabrication of Aspherical Ultra-precise Surfaces using a Tube) [fah97] [fah98]. Since the slurry removes material before it comes into contact with the surrounding medium air, this medium can not influence the removal process, unless it was already in the slurry. The nozzle is rotated to average out any irregularities in the rim of the nozzle geometry. With a rotational speed of 1000 rotations per minute and a diameter of 16 mm, the nozzle edge has a velocity of 0.8 m/s. This is chosen to be small compared to the radial velocity of the water which is, depending on the distance between the nozzle and the surface, in the order of 20 m/s.

Various nozzle geometries and materials and many different types of slurries can be used. The processing can be done on many different sample materials. An advantage of using ceramic or sapphire nozzles is that they do not wear rapidly. An advantage of using plastic nozzles is the low risk when contact accidentally occurs between the nozzle and the surface. Since the material removal depends on the pressure build-up caused by the small distance between the nozzle and the work piece, the process has a built in maximum depth it can reach for a stationary nozzle.

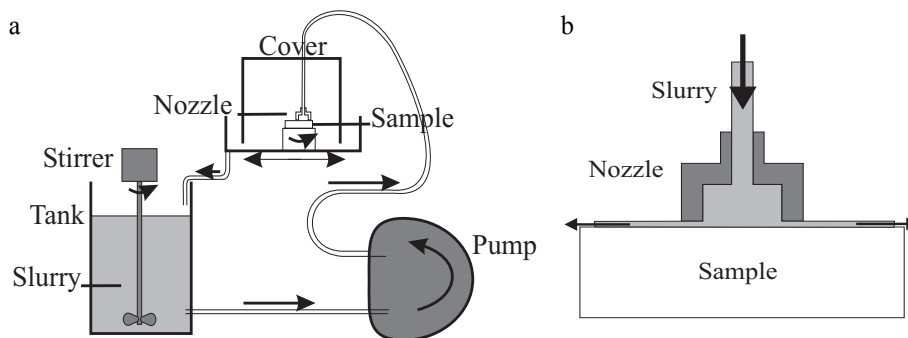


Fig. 7.3 a) Schematic picture of the Jules Verne setup and b) a detail of the circular symmetric nozzle. The slurry flows into the nozzle from above. The velocity is at its maximum where the nozzle and the surface are closest to each other. The slurry flows away in a radial direction after leaving the nozzle.

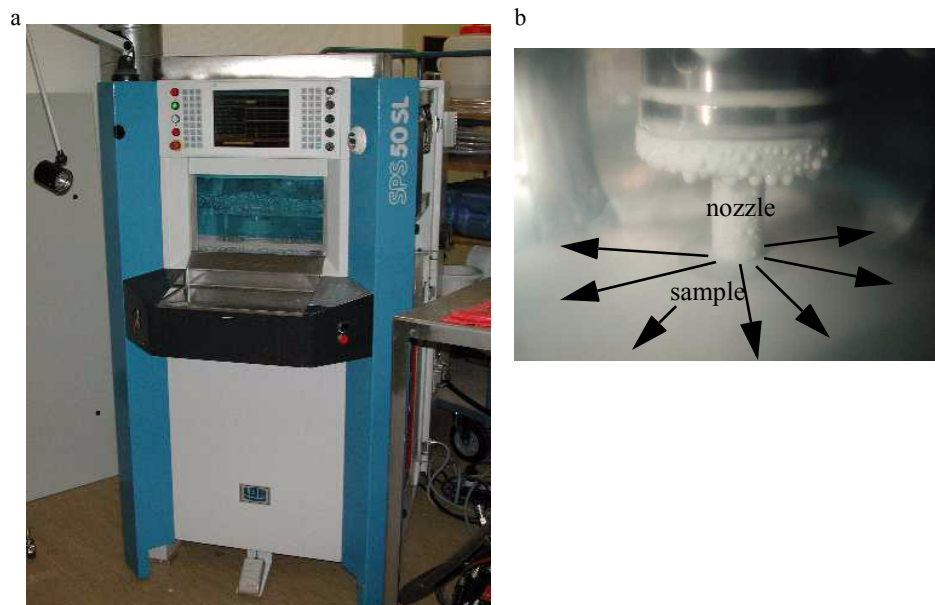


Fig. 7.4 Picture of the experimental Jules Verne setup. a) The modified Loh machine. b) Detailed picture of the nozzle, while it is processing a flat BK7 sample. The arrows indicate the slurry flow.

7.3.1 Principle of material removal

The material removal in the Jules Verne case will be in the ductile regime up to much higher velocities than in the case of FJP. For BK7 glass the critical depth of cut is 64 nm, as was explained in Section 6.5. This means that if more material is removed by one particle the removal will be in the brittle regime [bif91]. The penetration depth of the particles depends on their velocity perpendicular to the surface. In Section 6.5 it has been shown that the material removal for FJP is in the ductile regime. When the total velocity in the case of JV is in the same regime as was the case with FJP then the JV process will also be in the ductile regime since for JV the particle velocity component perpendicular to the surface is lower than for FJP.

A coarse estimate of the average velocity of the slurry can be obtained from the mass balance. The water flux into the nozzle should equal the outflow. The average slurry velocity depends on the surface area through which the slurry leaves the nozzle. If we assume a constant flow of 10 liter per minute ($=1/6 \cdot 10^{-3} \text{ m}^3/\text{s}$), and an inner diameter of the nozzle of 6 mm this results in a velocity through the nozzle of 5.9 m/s. When an outer diameter of 10 mm is assumed the velocity of the slurry at the rim of the nozzle will depend on the distance Δ from the surface according to

$$v = \frac{1}{60\pi} \left(\frac{1}{\Delta} \right). \quad (7.1)$$

This is graphically represented in Figure 7.5.

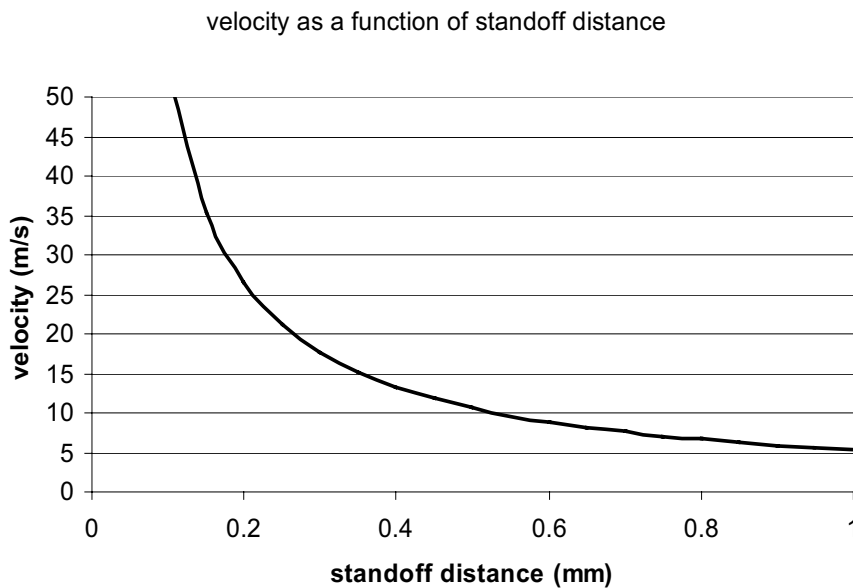


Fig. 7.5 The average slurry velocity as a function of the distance to the surface for a flow of 10 l/min., an inner diameter of the nozzle of 6 mm and an outer diameter of 10 mm.

7.3.2 Advantages and disadvantages of Jules Verne

Advantages:

- Nozzle diameter can be chosen freely
- Non circular nozzles can be used (possibility of making aspheres).
- The type, concentration and diameter of abrasives in the slurry can be chosen.
- The pH value and viscosity of the slurry can be optimised to suit the process.
- The process is sensitive to stand-off distance. This means that a natural limit of removal depth exists. When the nozzle is close to the surface material is removed. This removed material causes the gap between the nozzle and the surface to increase, and this reduces the material removal speed. This makes it possible to remove e.g. diamond turning grooves, because the higher parts of the grooves are removed, while the lower parts can not be removed.
- Better roughness obtainable than in the case of FJP owing to the fact that the slurry moves parallel over the surface in every radial direction.

Disadvantages:

- The z controlling is more severe than in the case of FJP, because the distance to the surface should be controlled very accurately. The position control for processing non-flat surfaces is not trivial.
- The process is sensitive to stand-off distance, therefore deep areas not easily reachable.
- There is a limitation on the shapes that can be produced, depending on the diameter of the nozzle that is used. This can partially be overcome by combining the FJP and the JV technique. Deeper areas can be treated by FJP (higher flow rate) and better reachable areas can be treated in the JV mode.

7.3.3 Simulation of the flow

The flow pattern in the Jules Verne (JV) case has been simulated in a two dimensional simulation. To get information on the distribution of impact position and impact velocity of the abrasive particles, the following scheme has been followed. The area of interest is defined and then divided into small rectangular areas, boundary conditions are imposed, the streamlines are computed over the entire area of interest, the velocity is computed from the streamlines, and particles are released in this flow. Each of these concepts has been explained in Section 4.4.

Boundary conditions

The flow in the nozzle was assumed to be according to the picture shown in Figure 7.6. The slurry flows into the nozzle from the top and flows away to the left and right hand side. Because the flow is symmetrical, no slurry can flow across the center line, and the area of interest is thus limited to the grey area. Now the concept of streamlines comes into the picture. The definition of a streamline is a curved continuous space curve on which the tangent of any point is parallel to the velocity at that point. It coincides with the trajectory of an elementary mass element of the flowing liquid. To follow the mass flow, we consider some specific streamlines, numbered from 0 to 10 that are equally spaced at

one half of the inlet of the nozzle in the cross-section (see Figure 7.6). The value of the outermost streamlines is arbitrarily chosen to be zero at the sample (bottom) and on the center line (left) and it is chosen to be $10 \text{ m}^2/\text{s}$ per unit depth at the nozzle surface. At the in- and outflow it increases linearly from the value zero to ten.

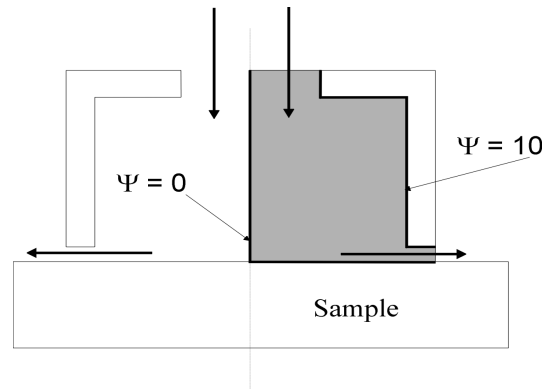


Fig. 7.6 A cross-section through the axis of symmetry of the JV nozzle with the area of interest highlighted in grey. The value of the boundary streamlines Ψ are indicated. The arrows indicate the flow direction.

A simulation of the streamlines and of the particles that are released in the flow has been carried out according to the model described in Section 4.4. A number of particles is released in the flow and their trajectories are computed until the moment that they reach the surface. An example of the calculated particle trajectories is given in Figure 7.7 b). The number of particles that is released is reduced in the right half of the inlet opening, because those particles will not reach the surface anyway. In Figure 7.7 c) the histogram of the position of impact is presented. In Figure 7.7 d) the velocity of the particles upon impact is shown, both in horizontal and vertical direction. The maximum number of impacts occur in the area between the nozzle and the surface, some impacts occur in the large chamber.

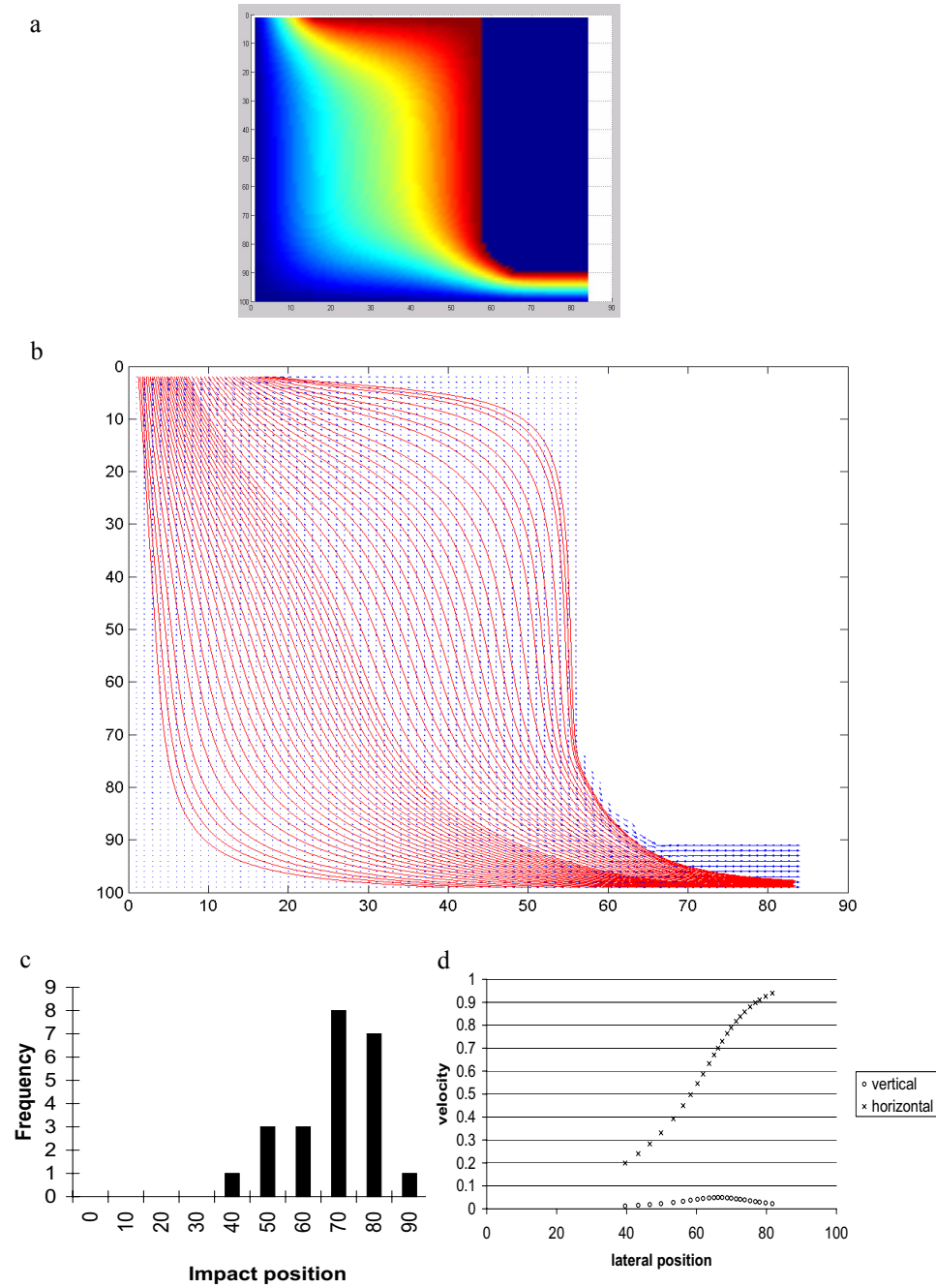


Fig. 7.7 a) The computed potential flow profile. b) The trajectory that particles with a certain mass would follow in this flow (more particles are released in the left part of the figure). c) Histogram of the impact position of the particles that impact on the surface. d) The horizontal and vertical velocity of the particles upon impact.

7.3.4 Initial experiments with JV

Proof of principle

As a proof of the JV principle the pressure in the hose leading to the nozzle has been measured as a function of the distance between the nozzle and the surface for a number of different settings of the pump pressure. The pressure indeed increases when the distance gets smaller, and higher pressures can be reached if a larger part of the pump power is used, as can be seen in Figure 7.8.

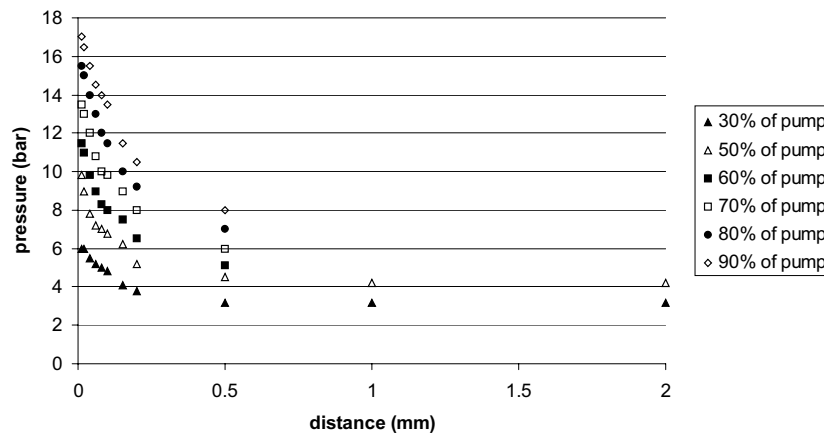


Fig. 7.8 Pressure as a function of the distance between the nozzle and the surface at 30, 50, 60, 70, 80, and 90% of the pump power.

Stationary spot

The next test has been to remove material from one location on a flat, pre-polished 40 mm diameter BK7 sample. The pressure was 8 bar, the standoff distance 0.05 mm, the slurry 10% #1000 SiC, and the processing time 30 minutes. The sample did not rotate or translate, but the nozzle did rotate in order to average out any inhomogeneities in the nozzle's edge (500 rot/min). The nozzle that was used was made of Teflon and had an inner diameter of 6 mm and an outer diameter of 16 mm. The shape of the wall was spherical, as can be seen in Figure 7.9 a). The resulting fringes (after 30 minutes of processing) can be seen in Figure 7.9 b). In the ring shaped area where the nozzle and the work piece were closest together (11 mm diameter) the largest amount of material has been removed. In the center, no material has been removed. This corresponds well to the prediction that was given in Figure 7.7. The nozzle did not show much wear from this experiment, but after a number of hours of processing the Teflon nozzle shows wear. That part of the nozzle that comes closest to the sample shows most wear. In following experiments a ceramic nozzle has been used, since it does not wear as much as Teflon.

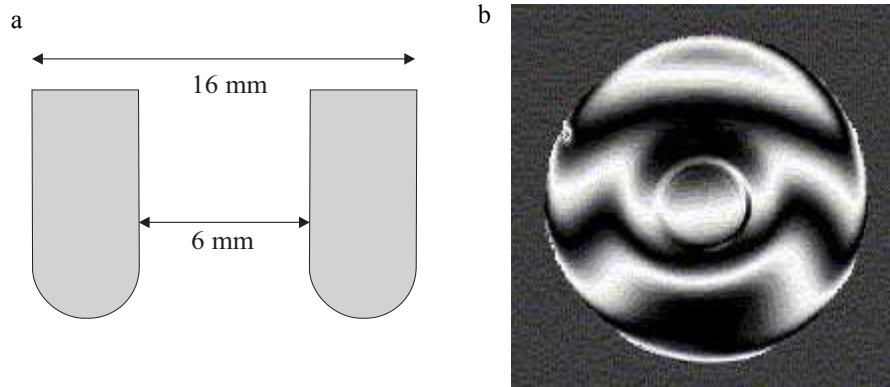


Fig. 7.9 a) Cross section of the JV nozzle that was used, with dimensions indicated. b) Footprint created by the JV nozzle in the stationary mode on a pre-polished 40 mm diameter BK7 sample.

Future experiments

Only a small number of experiments has been conducted so far. The material removal should still be investigated for larger areas of contact (the nozzle should move with respect to the surface), and for non-flat surfaces. The control of the distance between the nozzle and the surface should be controlled very accurately, while the nozzle and the sample can be rotating and they can be translating with respect to each other. When this control is not accurate enough the nozzle can come into contact with the surface and cause scratches. The reachable roughness should also be investigated for a number of different slurries and pressures.

When looking at the material removal principle and the initial results of Jules Verne, this technique has the potential to remove material from glass surfaces and possibly to reach even lower roughness values than FJP, because of the direction of flow of the slurry. JV can be used as a curve generator. Difficulties that will have to be solved in order for the technique to work reliably are the accurate positioning of the nozzle that is necessary, and assuring that no clogging up of slurry occurs.

I Proof that the particle velocity equals the slurry velocity

A calculation based on the balance of forces shows that the particle velocity equals the slurry velocity in the case of FJP [akk96]. We suppose the abrasive particle to be a perfect sphere. To compute the relative speed between the particle and the surrounding water, we can assume that the water is not moving. The forces that act on the particle are the gravitational force F_g , the drag force F_d , and the upward force F_u , see Fig. I.1.

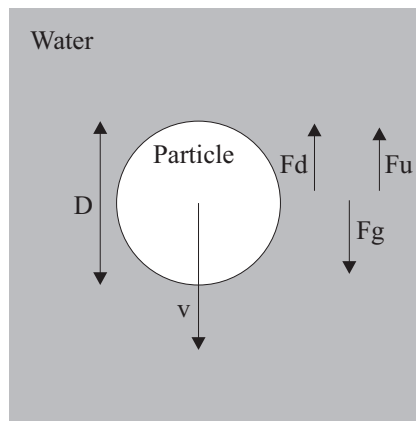


Fig. I.1 Schematic view of an abrasive particle with diameter D falling through the surrounding water with velocity v , and the forces acting on it: the gravitational force F_g , the drag force F_d and the upward force F_u .

We take for the density of the water $\rho_w = 1000 \text{ kg/m}^3$, the density of the abrasive $\rho_a = 4000 \text{ kg/m}^3$, the gravitational acceleration $g = 9.81 \text{ m/s}^2$, and the abrasive diameter $D = 15 \text{ }\mu\text{m}$.

The drag force is given by

$$F_d = C_D \frac{\pi}{4} D^2 \frac{1}{2} \rho_w v^2 \quad , \quad (\text{I.1})$$

in which C_D is the drag coefficient, a velocity dependent constant, which is tabulated in many transport phenomena books (Janssen [jan87]). The upward force is

$$F_u = \frac{\pi}{6} D^3 \rho_w g \quad , \quad (1.2)$$

and the gravitational force equals

$$F_g = -\frac{\pi}{6} D^3 \rho_a g \quad . \quad (1.3)$$

Because the sum of all the forces acting on the particle has to equal zero, we find

$$F_d + F_u + F_g = 0 \quad , \quad (1.4)$$

and, consequently,

$$v = \sqrt{\frac{4Dg(\rho_a - \rho_w)}{3C_D\rho_w}} \quad . \quad (1.5)$$

After some iterations, we find that the particle velocity with respect to the water is $4.4 \cdot 10^{-4}$ m/s. Since the water speed is in the order of 20 m/s, the particles can be assumed to move at the same speed as the water.

II Glass and abrasive properties

In this appendix some useful properties of both glasses and abrasives will be given.

II.1 Properties of glasses

What is glass? A definition or description that could be given is the following. Any of a large class of materials with highly variable mechanical and optical properties that solidify from the molten state without crystallization, that are typically based on silicon dioxide, boric oxide, aluminium oxide, or phosphorus pentoxide that form the network, and many elements that can modify the network, such as Na, K, Cu, Ba. It is a hard, brittle, translucent, and commonly transparent substance, white or colored, made by fusing together sand or silica with lime, potash, soda, or lead oxide. Glass is variously colored by the metallic oxides; thus, manganese colors it violet; copper (cuprous), red, or (cupric) green; cobalt, blue; uranium, yellowish green or canary yellow; iron, green or brown; gold, purple or red; tin, opaque white; chromium, emerald green; antimony, yellow [web13].

Glass is an amorphous solid, it is isotropic and homogeneous. A material is amorphous when it has no long-range order, that is, when there is no regularity in the arrangement of its molecular constituents on a scale larger than a few times the size of these groups [dor94].

Many different types of glass exist, and every manufacturer has its own name for each specific type. The various types can be classified in a two dimensional chart called the glass map according to their refractive index n_d and their Abbe number v_A . The Abbe number expresses the reciprocal of the dispersion of an optical medium. Its value is given by

$$v_A = \frac{n_d - 1}{n_F - n_c}, \quad (\text{II.1})$$

where n_d , n_F and n_c are the refractive indices that belong to the Fraunhofer lines of 587.6 (yellow helium line), 486.1 (blue hydrogen line), and 656.3 nanometers (red hydrogen line) respectively [kar93].

Some important properties of glasses are [ban86]:

- optical properties
 - refractive index, this depends on wavelength and temperature
 - internal transmittance
 - Abbe number
- chemical properties
 - durability with respect to water
 - durability with respect to certain chemicals
- thermal properties
 - melting temperature
 - thermal conductivity
 - specific heat
 - thermal expansion
- mechanical properties
 - hardness
 - elasticity
 - density
 - fracture toughness

As a comparison, some different materials have been listed in the table below. Their density, several measures of hardness (hardness H , Knoop hardness HK , Mohs hardness $Mohs$), the fracture toughness K , the elasticity E and the critical depth d_c are listed as well [bas95] [dav98] [hus98] [sch91]. The calculation of the critical depth has been performed according to Equation (6.1).

Table II.1 Overview of mechanical properties of some glasses and other materials.

Material	ρ (kg/m ³)	H (GPa)	HK (kg/mm ²)	Mohs	K (MPa \sqrt{m})	E (GPa)	d_c (m)
Schott Q0 Quartz	2200		740	7		76.5	
BK7	2510	5.2	610	4.5 to 6.5	0.86	81	$63.9 \cdot 10^{-9}$
Steel rvs-304	8000	8	938	5 to 8.5	130 to 180	193	$1.27 \cdot 10^{-3}$
SF12	3740		430			60	
Zerodur	2530		620			90.3	
Al 6082	2710	0.4	46	2 to 2.5	22 to 40	70	$148 \cdot 10^{-3}$
Si	2320	9	740	7	0.7	168	$16.9 \cdot 10^{-9}$
Ge		9			0.5	140	$7.2 \cdot 10^{-9}$

II.2 Properties of abrasives

Many different abrasives exist for grinding and polishing applications. On the internet and in catalogs the material properties of specific batches of the powders can be found [www17]. For grinding the main powders that are available are carborundum (silicon carbide / SiC), emery (iron spinel, hercynite), corundum (aluminum oxide / Al₂O₃), garnet (iron aluminum silicate), diamond (C), and boron carbide (B₄C). For polishing the four main powders used are rouge (red oxide of iron / ferric oxide / Fe₂O₃), cerium oxide (CeO₂), aluminum oxide (Al₂O₃), and putty powder (tin oxide).

For polishing applications the abrasives should not be too soft (then they will only deform and not remove material) and they should not be too hard either. The hardness of the polishing particles has to be matched to the hardness of the hydrated layer of the glass that is processed.

For grinding applications the choice of abrasives is a trade-off between rapidly removing material and obtaining an acceptable final roughness.

Table II.2 Overview of grinding and polishing particles and some of their properties.

	type of abrasive	density (gr/cm ³)	hardness (Mohs)	shape
grinding	carborundum	3.21	9-10	
	emery		8	blocky + sharp edges
	corundum	3.93	9	rhombohedral
	garnet		8-9	cubic
	diamond	2.26	10	hexagonal
	boron carbide	2.52	2750 Knoop	irregular, platelets, and whiskers
polishing	rouge			
	cerium oxide		6	cubic face centered
	aluminum oxide	3.93	9	rhombohedral
	putty powder	6.45		

In the following table the particle diameter of various mesh sizes of silicon carbide, aluminum oxide and cerium oxide particles will be given.

Table II.3 Diameter v.s. mesh size of some abrasives.

SiC	Particle diameter (μm)	Al ₂ O ₃	Particle diameter (μm)	Cerium oxide	Particle diameter (μm)
#60	250	#1200	1	Opaline	1
#80	177	#1500	0.7	CERI 2035	2.5
#100	125	#2000	0.3	CERI 1800	7.5
#120	105	#2500	0.1	CERI 3000G	1.2
#150	88	#3000	0.05		
#180	74				
#220	63				
F230	53				
F240	45				
F280	37				
F320	29				
F360	23				
F400	17				
F500	13				
F600	9				
F800	7				
F1000	5				
F1200	3				

As an illustration of the shape of some commonly used abrasives, some SEM images are shown in Figure II.1. Note the large difference between the three-dimensional structure of Boron carbide, SiC and Garnet (a, b, e and f) and the flat structure of aluminum oxide particles (c and d).

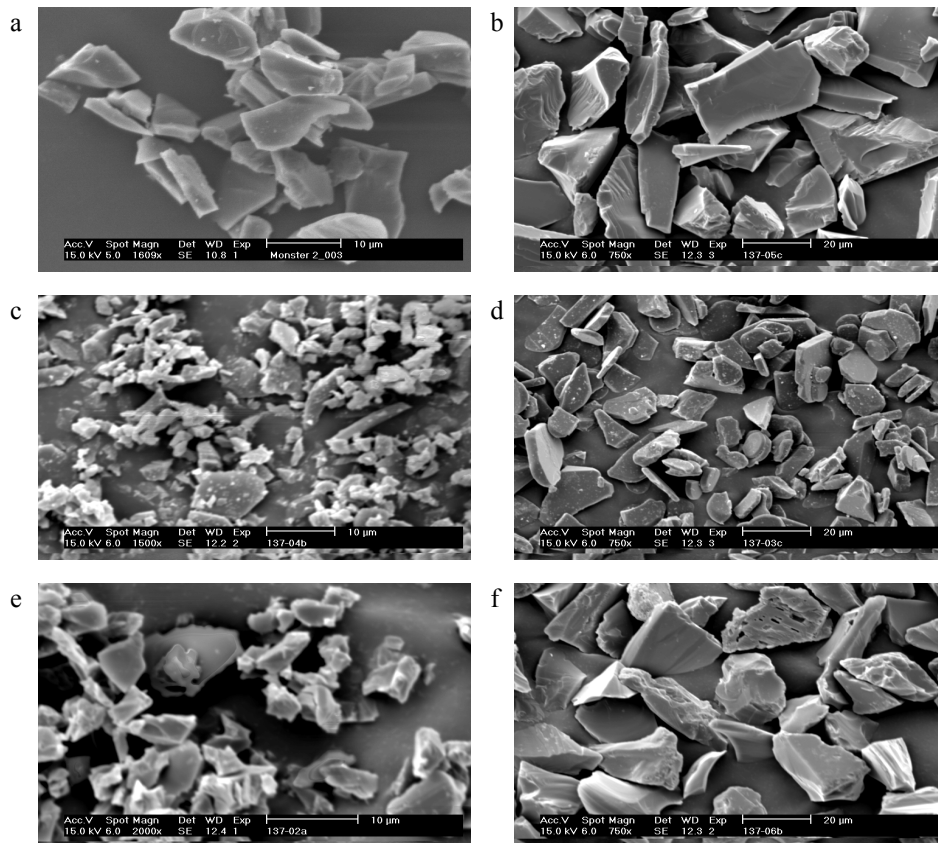


Fig. II.1 A SEM picture of #800 SiC grains (a), SiC #400 (b), 5 μm Al₂O₃ (c), 15 μm Al₂O₃ (d), Emery BM304 (e) and Borcarbid F400 (f).

III Process parameters

In order to enable the reproduction of an experiment, the process parameters in Table III.1 should be written down. An example is given to show some realistic values of the parameters.

Table III.1 Typical values of the process parameters during an experiment.

parameter	value	unit
type of abrasives	Al ₂ O ₃ (7 μm average diameter)	
concentration of abrasives	5	wt.%
slurry medium	50% tap water and 50% glycerin	
work piece material	BK7	
type of nozzle	cylindrical	
nozzle diameter	1.36	mm
pressure	5	bar
angle of incidence	45	°
stand-off distance	10	mm
processing time	30	min.
scanning velocity of the nozzle	5	mm/s
scanning distance	10	mm
rotation of the nozzle	none	
rotation of the work piece	3	Hz
positioning of the nozzle w.r.t. the center of the work piece	0	m

IV Finnie's model for material removal

Finnie has developed a model [fin58] that describes the material removal caused by one impacting particle as a function of the angle of impact. His model predicts the amount of removed material using the equations of motion of a single particle and assuming that the removal occurs in a ductile way. As can be seen in Figure IV.1, a particle is defined as an irregularly shaped object that scrapes away material in a ductile way. The particle's front face is assumed to be flat up to at least the contact height l , the width of the cutting particle is uniform and equals b . The distance from the center of gravity to the edge of the particle equals r . The particle approaches with a velocity v at an angle α . The position of the particle tip is denoted by (x_t, y_t) , the time at which the cutting begins is $t = 0$, the time at which the particle ceases to cut is defined as t_c . The ratio of the vertical and the horizontal force component of the total force acting on the particle is constant and equal to K_f . During the entire cutting process elastic deformation is neglected and crack initiation does not occur. This leaves us with plastic flow only. From the center of gravity of the particle at the moment that the particle begins to cut the x - and y axes originate. These axes are fixed in space. In this coordinate system the equations of motion in the x - and y direction, and the relation between the angular acceleration ϕ'' and the torque T can be written

$$\begin{aligned} F_x &= ma_x \\ F_y &= ma_y \\ T &= I\phi'' \end{aligned} \tag{IV.1}$$

in which F_i is the force acting on the particle in the x or y direction, m the mass of the impacting particle, a the acceleration of the particle, and I the moment of inertia of the particle.

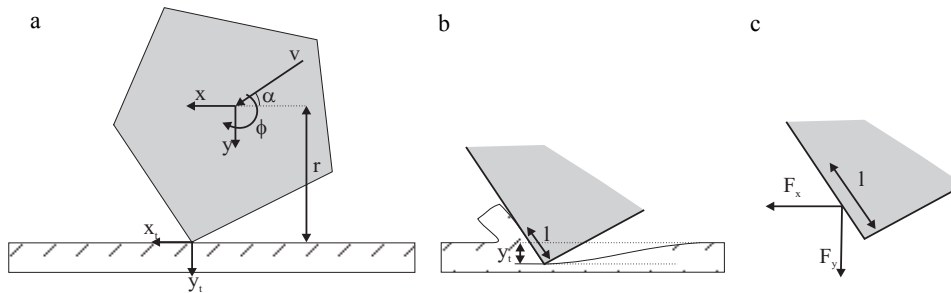


Fig. IV.1 Schematic view of the impact of a particle (grey) on a surface (white) and the amount of material that is being removed, according to Finnie's model. a) At $t = 0$, b) when $0 < t < t_c$, c) overview of the forces acting on the particle.

Assume that p_c , the constant horizontal component of the contact stress in the glass at the interface between the particle and the surface, is constant, limited by the strength of the surface. The vertical component of the contact stress is assumed to be equal to K_f times that in the horizontal direction. The area over which the forces act is $l \cdot b$. For convenience of notation we define

$$\Psi = \frac{l}{y_t}, \quad (IV.2)$$

and we write for the horizontal and vertical force components

$$F_x = -p_c \Psi b y \quad (IV.3)$$

$$F_y = -p_c K_f \Psi b y.$$

The particle is assumed to carry out a rotation around its center of gravity. Therefore the external moment or torque is equal to the moment of inertia of the particle times its angular acceleration. This torque originates from the force on the particle in the horizontal direction at a distance r from its center of gravity. The effect of the vertical component has been assumed to be very much less than the horizontal one.

The equations of motion can be written as

$$\begin{aligned} m y'' + p_c K_f \Psi b y &= 0 \\ m x'' + p_c \Psi b y &= 0 \\ I \phi'' + p_c \Psi b r y &= 0. \end{aligned} \quad (IV.4)$$

These equations can be solved when the following initial conditions are used. Accents denote the time derivatives.

$$x(0) = 0$$

$$y(0) = 0$$

Contact between the particle and the surface starts at $t = 0$

$$x'(0) = v(0) \cos(\alpha) = v_0 \cos(\alpha)$$

$$y'(0) = v(0) \sin(\alpha) = v_0 \sin(\alpha)$$

$$\phi'(0) = \phi_0'$$

This results in

$$\begin{aligned} y &= \left\{ \frac{v_0 \sin \alpha}{\beta} \right\} \sin \beta t \\ x &= \left\{ \frac{v_0 \sin \alpha}{\beta K_f} \right\} \sin \beta t + \left\{ v_0 \cos \alpha - \frac{v_0 \sin \alpha}{K_f} \right\} t \\ \phi &= \left\{ \frac{m r v_0 \sin \alpha}{\beta K_f I} \right\} [\sin(\beta t) - \beta t] + \phi_0' t, \end{aligned} \quad (IV.5)$$

where $\beta = \sqrt{\frac{\rho_c \Psi b K_f}{m}}$, v_0 is the initial particle velocity and α the angle of impact. For the moment of inertia I the value of $mr^2/2$ is taken, which is that of a cylinder, with m the mass of the impacting particle. For K_f a value of 2 is taken. This value is in agreement with results that were obtained from measurements carried out by Finnie [fin58].

The cutting starts at $t = 0$ and stops when $t = t_c$. The cutting process stops when the horizontal motion of the particle tip becomes zero ($x_t' = x' = 0$), or when the particle tip leaves the surface ($y_t = y = 0$). This results in two conditions

$$\begin{aligned} x_t' = 0 & \Rightarrow \cos \beta t_c = 1 - \frac{K_f}{3 \tan \alpha}, \\ y_t = 0 & \Rightarrow \beta t_c = \pi. \end{aligned} \quad (\text{IV.6})$$

Depending on the angle of impact, one of these two conditions applies. For very small angles of impact the particle will leave the surface while it still has a velocity in the horizontal direction, so in that case we should monitor when the particle tip leaves the surface. For large angles of impact the particle will be slowed down by the material it removes, and its velocity will therefore become zero. In this case the zero velocity in the horizontal direction will be the reason the particle stops removing material. At the transition angle both conditions apply, so the particle tip leaves the surface while the horizontal motion of the tip becomes zero. The amount of material removed by one particle W_p is proportional to the volume that was swept out

$$W_p = \rho b \int_0^{t_c} y_t dx_t, \quad (\text{IV.7})$$

where ρ is the density. We will only look at the case where $\phi_0' = 0$, this means that the particles have no initial rotation, or when many particles are investigated the average of the initial particle rotation is zero. The total amount of removed material W is equal to the number of impacting particles times the volume removed by one single particle, or when the mass of all the particles equals M , the removal that results is

$$\begin{aligned} W &= \frac{\rho}{\rho_c \Psi} \frac{M v_0^2}{K_f} \left[\sin 2\alpha - \frac{6}{K_f} \sin^2 \alpha \right] & \text{if } \tan \alpha \leq \frac{K_f}{6}, \\ W &= \frac{\rho}{\rho_c \Psi} \frac{M v_0^2}{K_f} \left[\frac{K_f \cos^2 \alpha}{6} \right] & \text{if } \tan \alpha \geq \frac{K_f}{6}, \end{aligned} \quad (\text{IV.8})$$

The function W has been plotted in Figure IV.2. The predicted weight loss is continuous at the limiting angle given by

$$\tan \alpha = \frac{K_f}{6} \quad (\text{IV.9})$$

and equals

$$W = \frac{\rho M v_0^2}{p_c \Psi K_f} \left[\frac{6K_f}{36 + K_f^2} \right]. \quad (\text{IV.10})$$

The first derivatives of both functions are also identical at this angle and they equal:

$$\left. \frac{dW}{d\alpha} \right|_{\alpha = \arctan\left(\frac{K_f}{6}\right)} = \frac{-2\rho M v_0^2 K_f}{p_c \Psi (36 + K_f^2)}. \quad (\text{IV.11})$$

The maximum erosion occurs at a slightly lower angle,

$$\tan(2\alpha) = \frac{K_f}{3}. \quad (\text{IV.12})$$

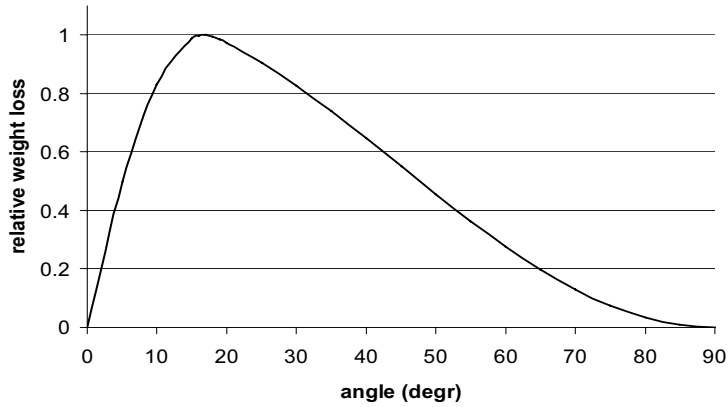


Fig. IV.2 Normalised relative weight loss as a function of the angle of impact of a single particle according to Finnie's model.

Index of symbols and subscripts

Index of symbols

Symbol	meaning	units
a	jet radius	m
A	surface area	m ²
a_x, a_y	acceleration in the x and y direction	m/s ²
b	width of cutting particle	m
c	concentration	weight %
C_i	constant	-
C	radial coordinate	m
d	particle or fluid stream diameter	m
d_c	critical depth	m
E	elastic modulus	GPa
$f(x,y)$	height profile of a stationary footprint	m
F_i	force	N
F	load	kg
g	gravitational acceleration	m/s ²
h	height	m
H	hardness	GPa
HK	Knoop hardness	kg/mm ²
I	moment of inertia	kg m ²
I_B	background intensity	W/m ²
K	Preston's coefficient	m ³ s ² /kg

Symbol	meaning	units
K_c	fracture toughness	MPa \sqrt{m}
K_f	ratio of vertical to horizontal force components in cutting process	-
l	length	m
m	mass of one particle	kg
M	total mass of all impacting particles	kg
M_d	modulation depth	-
n	number of impacting particles	-
$n_{\#}$	refractive index	-
p	pressure	Pa
p_c	contact stress	kg/ms ²
p_0	ambient pressure	Pa
$q(x,y)$	height of a surface as a function of x and y	m
r	radial coordinate	m
r	distance from center of gravity of the particle to the contact point	m
R	radial distance where $p \approx p_0$	m
Re	Reynolds' number	-
s	shape factor	-
t	processing time	s
t_c	duration after which cutting stops	s
T	torque	N m
u	average fluid velocity	m/s
v	particle velocity	m/s
V	volume	m ³
w	width	m

Symbol	meaning	units
W	wear, volume removed or depth of removal	m^3 or m
x,y,z	cartesian system of coordinates	m
α	angle of impact	$^\circ$
β	asymptotic direction of stream B_1	$^\circ$
γ	asymptotic direction of stream B_2	$^\circ$
Δ	distance between nozzle and surface	m
η	dynamic viscosity	Pa s
η_f	kinematic viscosity	m^2/s
θ	parameter indicating the direction of the velocity	-
λ	wavelength of light	m
Λ	angle of the slurry with respect to the translation direction of the nozzle, seen from above	rad
v_A	Abbe number	-
ρ	density	kg/m^3
τ	response time	s
v	average velocity	m/s
ϕ	particle rotation	$^\circ$
ω	angle of the slurry with respect to the sample, seen from the side	rad
φ	phase	rad
$\Delta\Phi$	phase difference	rad
ψ	stream function	m^2/s per unit depth
Ψ_p	half top angle of a particle	rad

Symbol	meaning	units
Ψ	ratio of contact length to depth of material removal	-
ω	angle between slurry and surface	rad
Ω	angle between fan out plane and translation direction of the nozzle	rad

Index of subscripts

Subscript	meaning
f	fluid
max	maximal value
p	particle
t	tip of the abrasive
0	initial value

References

- [akk96] H.E.A. van den Akker and R.F. Mudde, 'Fysische transport verschijnselen,' Delft University Press, Delft (1996)
- [ban86] N.P. Bansal and R.H. Doremus, 'Handbook of glass properties,' Academic Press Inc., Orlando, FL (1986)
- [bas95] Bass, 'Handbook of Optics Vol 1 and 2,' McGraw-Hill (1995)
- [ben89] Jean M. Bennett and Lars Mattsson, 'Introduction to surface roughness and scattering,' Optical Society of America, Washington D.C. (1989)
- [bif91] T.G. Bifano, T.A. Dow, and R.O. Scattergood, 'Ductile regime grinding: a new technology for machining brittle materials,' J. of Eng. for Ind., Trans. of the ASME, **113**, pp.184-189 (1991)
- [bij01] R.M. van der Bijl, Hedser van Brug, Oliver W. Faehnle, and Joseph J. M. Braat, 'Applicability of iTIRM for roughness reduction monitoring,' SPIE Annual Meeting 2001, in SPIE Proc. **4451**, pp.340-344 (2001)
- [bij99] R.M. van der Bijl, O. W. Fahnle, and H. van Brug, 'Subsurface damage measurements as tool for process monitoring,' the fourteenth ASPE Annual Meeting, **20**, pp.606-609 (1999)
- [bjo98] John E. Bjorkholm, 'EUV Lithography - the successor to optical lithography?,' Intel Technology Journal, Q3 (1998)
- [boo00] Silvia M. Booij, Hedser van Brug, and Oliver W. Fahnle, 'A mathematical model for machining spot in Fluid Jet Polishing,' Optical Fabrication and Testing, OSA Technical Digest, Opt. Soc. of Am., Washington DC, pp.70-72 (2000)
- [bru02] Hedser van Brug, Mietta Groeneveld, Silvia M. Booij, and Joseph J.M. Braat, 'In-process measurements of material removal in fluid jet polishing,' SPIE conference, W. Osten (ed.), ISBN 8194-4545-2, Seattle, USA, pp.243-250 (2002)
- [bru98] Hedser van Brug, 'Temporal phase unwrapping and its application in shearography systems,' Appl. Opt., **37**, pp.6701-6706 (1998)
- [bui93] M. Buijs and K. Korpel-van Houten, 'A model for lapping of glass,' J. of Mat. Sci., **28**, pp.3014-3020 (1993)
- [bui95] M. Buijs and J.M.M. Pasmans, 'Erosion of glass by alumina particles: transitions and exponents,' Wear, **184**, pp.61-65 (1995)
- [cog94] Carol J. Cogswell, Kieran G. Larkin, John W. O'Byrne, and Matthew Arnison, 'High-resolution, multiple optical-mode confocal microscope: I, Three-Dimensional Microscopy: Image Acquisition and Processing,' **2184**, pp.48-54 (1994)

- [coo90] Lee M. Cook, 'Chemical processes in glass polishing,' *Journal of Non-Crystalline Solids*, **120**, pp.152-171 (1990)
- [coo91] Cooke, 'Optics Cooke book,' Opt. Soc. of Am., Washington DC (1991)
- [cum95] M.J. Cumbo, D. Fairhurst, S.D. Jacobs, and B.E. Puciebner, 'Slurry particle size evolution during the polishing of optical glass,' *Appl. Opt.*, **34**, pp.3743-3755 (1995)
- [dav98] J.R. Davis, 'Metals handbook,' Metals Park: ASM International (1998)
- [din01] DIN Taschenbuch 304, Technische Produktionsdokumentation, Beuth Bln., ISBN 3-410-14866-3, Dec. 2001
- [dor94] R.H. Doremus, 'Glass Science,' John Wiley & Sons, New York (1994)
- [dyk82] Milton Van Dyke, 'An album of fluid motion,' The parabolic press, Stanford, California (1982)
- [fah02b] Oliver W. Föhnle, Torsten Wons, Evelyn Koch, Sébastien Debruyne, Mark Meeder, Silvia M. Booij, and Joseph J.M. Braat, 'iTIRM as a tool for qualifying polishing processes,' *Appl. Opt.*, **41**, pp.4036-4038 (2002)
- [fah97] O.W. Föhnle, H. van Brug, C.J. van der Laan, and H.J. Frankena, 'Loose abrasive line-contact machining of aspherical optical surfaces of revolution,' *Appl. Opt.*, **36**, pp.4483-4489 (1997)
- [fah98] Oliver W. Föhnle, 'Shaping and finishing of aspherical optical surfaces,' PhD thesis, Eburon P&L, Delft, ISBN 9056510576, TU Delft (1998)
- [fah98b] Oliver W. Föhnle, Hedser van Brug, and Hans J. Frankena, 'Fluid jet polishing of optical surfaces,' *Appl. Opt.*, **37**, pp.6771-6773 (1998)
- [fah99a] Oliver W. Föhnle and Hedser van Brug, 'Novel approaches to generate aspherical optical surfaces,' *Optical Manufacturing and Testing III*, in Proc. SPIE **3782**, pp.170-180 (1999)
- [fan98] Q. Fang, P.S. Sidky, and M.G. Hocking, 'Micro-ripple formation and removal mechanism of ceramic materials by solid-liquid slurry erosion,' *Wear*, **223**, pp.93-101 (1998)
- [fin58] Iain Finnie, 'The mechanism of erosion of ductile metals,' *Proc. of the third U.S. Int. Congres of Appl. Mech.*, pp.527-532 (1958)
- [fin60] I. Finnie, 'Erosion of surfaces by solid particles,' *Wear*, **3**, pp.87-103 (1960)
- [fin65] I. Finnie and Y.H. Kabil, 'On the formation of surface ripples during erosion,' *Wear*, **8**, pp.60-69 (1965)
- [fin95] Iain Finnie, 'Some reflections on the past and future of erosion,' *Wear*, **186-187**, pp.1-10 (1995)
- [fin03] Personal communication with professor Finnie
- [gol90] Donald Golini and Stephen D. Jacobs, 'Chemo-mechanical effects in loose abrasive grinding of ULE,' *Science of optical finishing, OSA technical digest*, **9**, pp.25-28 (1990)
- [haa00] Bas Adriaan van Haarlem, 'The dynamics of particles and droplets in atmospheric turbulence, a numerical study,' PhD thesis, Delft University of Technology, Ponsen & Looijen, (2000)
- [hoo00] A.M. Hoogstrate, 'Towards high-definition abrasive waterjet cutting: a model based approach to plan small-batch cutting operations of advanced materials'

- by high-pressure abrasive waterjets,' PhD thesis, Delft University of Technology, ISBN: 90-90138887-0 (2000)
- [hor72] D.F. Horne (M.B.E.), 'Optical Production Technology,' Adam Hilger, London (1972)
- [hoy77] J.W. Hoyt and J.J. Taylor, 'Waves on water jets,' *Journal of Fluid Mechanics*, **83**, pp.119-127 (1977)
- [hus98] Bob Hussey and Jo Wilson, 'Advanced technical ceramics directory and databook,' London: Chapman and Hall (1998)
- [jac99] S.D. Jacobs, S.R. Arrasmith, I.A. Kozhinova, L.L. Gregg, A.B. Shorey, H.J. Romanofsky, D. Golini, W.I. Kordonski, P. Dumas, and S. Hogan, 'MRF: Computer-Controlled Optics Manufacturing,' *The American Ceramic Society Bulletin*, (1999)
- [jan87] L.P.B.M. Janssen and M.M.C.G. Warmoeskerken, 'Transport phenomena data companion,' Delftse Uitgevers Maatschappij, Delft (1987)
- [jon82] Robert A. Jones, 'Computer-controlled grinding of optical surfaces,' *Appl. Opt.*, **21**, pp.874-877 (1982)
- [jon98] A.R. Jones and J.B. Hull, 'Ultrasonic flow polishing,' *Ultrasonics*, **36**, pp.97-101 (1998)
- [kal91] Adolf Kaller, 'On the polishing of glass, particularly the precision polishing of optical surfaces,' *Glastech. Ber.*, **64** (9), pp.241-252 (1991)
- [kar93] Hank H. Karow, 'Fabrication methods for precision optics,' John Wiley and sons, Inc., New York, ISBN 0 471 51222 2, (1993)
- [kir94] N.B. Kirk and J.V. Wood, 'Glass polishing,' *British Ceramic Transactions*, **93**, pp.25-30 (1994)
- [kiy88] M. Kiyoshige, H. Matsumura, Y. Ikemoto, and T. Okada, 'A study of abrasive waterjet cutting using slurried abrasives,' 9th International symposium on Jet Cutting Technology, pp.61-73 (1988)
- [koe96] Wilfried Koenig and Fritz Klocke, 'Fertigungsverfahren Band 2, Schleifen, Honen, Laeppen,' VDI-Verlag, Duesseldorf (1996)
- [lam97] John C. Lambropoulos, Su Xu, and Tong Fang, 'Loose abrasive lapping hardness of optical glasses and its interpretation,' *Appl. Opt.*, **36**, pp.1501-1516 (1997)
- [lam99] John C. Lambropoulos, Yi Li, Paul Funkenbusch, and Jeff Ruckman, 'Non-contact estimate of grinding-induced subsurface damage,' *SPIE Conference on Optical Manufacturing and Testing III*, **3782**, pp.41-50 (1999)
- [law75] B.R. Lawn and R. Wilshaw, 'Review: Indentation fracture, principles and applications,' *J. of Mat. Sci.*, **10**, pp.1049-1081 (1975)
- [lea66] S.J. Leach and G.L. Walker, 'The application of high speed liquid jets to cutting,' *Phil. Trans. Royal Society of London*, **260 A**, pp.295-308 (1966)
- [mil77] L.M. Milne-Thomson, 'Theoretical hydrodynamics,' The Macmillan Press Ltd., London (1977)
- [pat1] Mohamed Ahmed Hashish, David Arthur Crowe, and Dean Armstrong, 'Abrasive-liquid polishing and compensating nozzle,' U.S. Patent 5700181, Dec. 23 (1997)

- [pau98] S. Paul, A.M. Hoogstrate, C.A. van Luttervelt, and H.J.J. Kals, 'Analytical and experimental modelling of the abrasive water jet cutting of ductile materials,' *J. Mat. Process. Tech.*, **73**, pp.189-199 (1998)
- [pre27] F.W. Preston, 'The theory and design of plate glass polishing machines,' *Journal of the Society of Glass Technology*, **11**, pp.214-256 (1927)
- [reh76] G. Rehbinder, 'Some aspects on the mechanism of erosion of rock with a high speed water jet,' *Third International Symposium on Jet Cutting Technology*, paper E1, pp.E1-1 E1-20 (1976)
- [sch01] Axel Schindler, Georg Boehm, Thomas Haensel, Wilfried Frank, Andreas Nickel, Bernd Rausschenbach, and Frieder Bigl, 'Precision optical asphere fabrication by plasma jet chemical etching (PJCE) and ion beam figuring,' *Proceedings of the SPIE; Optical manufacturing and testing IV*, **4451**, pp.242-248 (2001)
- [sch91] S.J. Schneider, 'Engineered Materials Handbook, volume 4: Ceramics and glasses,' *Materials park: ASM International* (1991)
- [sha00] Prashant M. Shanbhag, Michael R. Feinberg, Guido Sandri, Mark N. Horenstein, and Thomas G. Bifano, 'Ion-beam machining of millimeter scale optics,' *Appl. Opt.*, **39**, pp.599-611 (2000)
- [she66a] G.L. Sheldon and I. Finnie, 'On the ductile behavior of nominally brittle materials during erosive cutting,' *Transactions of the ASME, J. of Eng. for Ind.*, pp.387-392 (1966)
- [she66b] G.L. Sheldon and I. Finnie, 'The mechanism of material removal in the erosive cutting of brittle materials,' *Trans. of the ASME, J. of Eng. for Ind.*, **88**, pp.393-400 (1966)
- [sum95] David A. Summers, 'Waterjetting technology,' E&FN Spon, London (1995)
- [tem81] P. Temple, 'Total Internal Reflection Microscopy: A Surface Inspection Technique,' *Appl. Opt.*, **20**, pp.2656-2664 (1981)
- [toe00] Helmut Hermann Toeppen, 'Charakterisierung superglatte Oberflaechen,' PhD thesis, ISSN 1434 8454 Deutsches Zentrum fuer Luft- und Raumfahrt e.V., Köln (2000)
- [twy42] F. Twyman, 'Prism and lens making,' Adam Hilger, Bristol and New York (1942)
- [veg98] F. Vega, N. Lupón, J.A. Cebrian, and F. Laguarda, 'Laser application for optical glass polishing,' *Opt. Eng.*, **37**, pp.272-279 (1998)
- [web13] 'Webster's revised unabridged dictionary,' C.&G. Merriam co., Springfield, Mass. (1913)
- [whi94] D.J. Whitehouse, 'Handbook of surface metrology,' IOP Publishing Ltd., Bristol Institute of Physics, ISBN 0 7503 0039 6 (1994)
- [whi99] Frank M. White, 'Fluid Mechanics,' WCB/ McGraw-Hill, Boston, ISBN 0 07 069716 7 (1999)
- [win92] J. van Wingerden, H.J. Frankena, and B.A. van der Zwan, 'Production and measurement of superpolished surfaces,' *Opt. Eng.*, **31**, pp.1086-1092 (1992)
- [wol95] C. R. Wolfe, I. K. Lawson, M. Kellam, R. T. Maney, and A. Demiris, 'Measurement of wavefront structure from large aperture optical components

- by phase shifting,' Proc. of SPIE Vol. **2536**, Optical Manufacturing and Testing (1995)
- [woy99] P.J. Woytowitz and R.H. Richman, 'Modeling of damage from multiple impacts by spherical particles,' *Wear*, **235**, pp.120-133 (1999)
- [www1] '<http://www.glassonline.com/history.html>'
- [www2] '<http://www.lechler.com/>'
- [www3] 'http://www.veeco.com/html/product_bymarket_proddetail.asp?ProductID=132'
- [www4] '<http://www.tencor.com/index-noflash.html>'
- [www5] '<http://www.taylor-hobson.com/>'
- [www6] '<http://www.wyko.com/>'
- [www7] '<http://www.tsi.com/>'
- [www8] '<http://www.efd-inc.com/>'
- [www9] '<http://www.ls-dyna.com/pages/history.shtml>'
- [www10] 'http://www.hhtc.ca/microscopes/electron_microscope.htm'
- [www11] '<http://www.malvern.co.uk/home.htm>'
- [www12] '<http://www.manufacturingit.net/Sections/Formulea/Equations/Fluids/Reynolds%20Number.htm>'
- [www13] 'http://www.efm.leeds.ac.uk/CIVE/CIVE1400/Section4/laminar_turbulent.htm'
- [www14] '<http://www.loh.de>'
- [www15] '<http://www.zygo.com/>'
- [www16] '<http://www.fisbaoptik.ch/>'
- [www17] '<http://www.ceradyne.com/material.htm>'
- [wyk95] Sharon K. Lippold, 'Wyko optical testing, operator's guide,' Wyko Corporation, East Elvira Road, Tucson, Arizona 85706, Edition 1.600
- [zu91] J.B. Zu, G.T. Burstein, and Hutchings, 'A comparative study of the slurry erosion and free-fall particle erosion of aluminum,' *Wear*, **149**, pp.73-84 (1991)

Summary

Summary belonging to the thesis:
Fluid Jet Polishing
S.M. Booij

The goal of this thesis research was to investigate the possibilities and limitations of the Fluid Jet Polishing (FJP) technique. FJP is a new optical fabrication technique that is capable of making shape corrections and reducing the surface roughness of glass and other materials. The principle of operation is that a mixture of water and abrasives (the slurry) is sprayed on the surface at a low pressure. The experimental setup has been described in detail in this thesis. The advantage of FJP over existing techniques is the fact that it can both grind and polish and that areas can be reached that are not accessible with existing techniques.

Measuring techniques are important in order to judge the effect of a shaping or polishing technique. Therefore, special attention has been given to in-process measurement techniques. One of the described techniques is iTIRM (intensity-detecting Total Internal Reflection Microscopy). iTIRM can be used for in-process monitoring of the total surface quality, which includes the surface roughness, sub-surface damage, and scratches in the surface. The iTIRM technique can measure the surface quality of both very rough and very smooth surfaces (total range from some μm to 0.8 nm). Surface roughness improvements of 0.1 nm rms can be detected with this technique.

The surface shape can also be measured in-process. A measurement technique is shown that is based on the interference of an object and a reference beam that both reflect from the inside of the surface to be measured at the total internal reflection condition. The information on the surface shape is obtained from the reflected beams via a temporal phase unwrapping method. Unwrapping problems are avoided by comparing successive images in stead of comparing any image to the first image.

In order to gain a better understanding of the FJP technique several models have been described. Some have been found in literature, others have been developed especially for FJP. The formation of cracks has been described with Lawn's model [law75]. The theoretical pressure distribution in the slurry has been described by the numerical calculation developed by Rehbinder [reh76] and Leach and Walker [lea66]. Based on the pressure distribution as developed by Rehbinder, a prediction of the stationary footprint that occurs in the case of a cylindrical nozzle has been computed for the FJP case.

Based on a general description of flows by Milne-Thomson [mil77] the velocity of the flow in the case of FJP has been computed, the trajectory of the particles in the flow has been derived, and the position and velocity at the moment of impact with the surface has been determined. The interaction between the abrasive particle and the surface of impact has been considered at the microscopic level by a description of three different analysis: first of all, the finite element approach as developed by Woytowicz and co-workers

[woy99], secondly, a very simple estimation derived in this thesis, based on the material removal as observed with a SEM, and finally, Finnie's estimation [fin58] which describes the material removal of a single impacting particle in air as a function of the angle of impact.

Since the material removal should be known over an area larger than the footprint of the nozzle an analysis has been described that explains the material removal in the case of scanning or rotation of the work piece with respect to the nozzle. The shape inaccuracies that can occur in the center of a work piece have been described as well.

In order to get a better understanding of the resulting surface roughness a model has been developed that predicts the roughness as a function of the initial surface and some process parameters. This model is based on the random impacts of particles on a surface.

The effect of various process parameters on the material removal and the surface roughness has been investigated experimentally as well. These parameters include the slurry parameters such as the number of particles, the type and size of the particles, the particle velocity, and several process parameters such as the processing time, the processed material, the impact angle and the nozzle type.

We also report on some relevant experiments that we carried out with the FJP setup, like the reproducibility of the process, the homogeneity of a translating spot, the degradation of the slurry over time, the formation and removal of mid-spatial frequencies, and the detection whether the FJP process is ductile or brittle. The shaping capabilities have been shown, by prescribing a surface and attempting to produce this surface shape. Some roughness experiments have been described, showing a.o. the roughness as a function of time, the effect of the initial roughness on the final roughness, the roughness as a function of the pressure, and the lowest roughness that could be obtained.

Conclusions are drawn and two alternative setups are suggested. The conclusions concerning the shaping accuracy and the roughness reduction are that shape corrections are limited to an accuracy of 4% in depth in the setup that is used at this moment. The material removal is accurate to 1% when the effects of the pressure fluctuation and of the abrasive particle diameter average out by processing the surface several times. A roughness reduction on BK7 can be obtained in a one-step process (one slurry, one fixed pressure during the entire process) from a fine-ground surface (average roughness $R_a = 300$ nm) to $R_a = 3.6$ nm. The first suggestion for comparable techniques that has been described is chemically assisted FJP, the second alternative is a close contact version of FJP. Some initial experiments that have been conducted with this second alternative have been described as well.

Fluid Jet Polishing is a new technique that is well suited for making shape alterations to glass surfaces, and for reducing the surface roughness of glasses to a few nanometers. Especially harder to reach areas can ideally be treated with FJP.

Samenvatting

Samenvatting behorende bij het proefschrift:
Polijsen met een vloeistofstraal
(Fluid Jet Polishing)
S.M. Booij

Het doel van dit proefschrift was het onderzoeken van de mogelijkheden en beperkingen van de Fluid Jet Polishing (FJP) techniek. FJP is een nieuwe optische vervaardigingstechniek die geschikt is om vormcorrecties en een ruwheidsvermindering te realiseren op glas en andere materialen. Het principe van deze techniek is dat een mengsel van water en slijpdeeltjes (de slurry) onder een lage druk op het oppervlak gespoten wordt. De experimentele opstelling staat gedetailleerd beschreven in dit proefschrift. Het voordeel van FJP boven bestaande technieken is dat FJP zowel kan slijpen als polijsten en dat gebieden bewerkt kunnen worden die met bestaande technieken niet bereikbaar zijn.

Meettechnieken zijn nodig om het effect van slijp- en polijsttechnieken te beoordelen. Daarom wordt aandacht besteed aan meettechnieken die tijdens het proces gebruikt kunnen worden. Een van de beschreven technieken is iTIRM (intensiteit-detecterende Totale Interne Reflectie Microscopie). iTIRM is een techniek waarmee tijdens het proces de totale oppervlaktekwaliteit in de gaten gehouden kan worden. De totale oppervlaktekwaliteit bestaat uit oppervlakteruwheid, schade direct onder het oppervlak, en krassen in het oppervlak. Met de iTIRM-techniek kunnen zowel hele ruwe als hele gladde oppervlakken gemeten worden (het totale bereik beslaat het gebied van enkele μm tot 0.8 nm). Ruwheidsverbeteringen van 0.1 nm rms zijn detecteerbaar.

De vorm van een oppervlak kan ook tijdens het proces gemeten worden. Een meettechniek wordt beschreven die gebaseerd is op interferentie van een object- en een referentiebundel die beide aan de onderkant van het te meten oppervlak reflecteren onder de totale-interne-reflectie-conditie. De vorm van het oppervlak wordt uit de gereflecteerde bundels bepaald door middel van de ‘temporal phase unwrapping’ methode. Problemen met ‘unwrapping’ worden voorkomen door telkens twee opeenvolgende beelden te vergelijken, i.p.v. ieder beeld met het allereerste beeld te vergelijken.

Om een beter begrip te krijgen voor de FJP-techniek, wordt een aantal modellen beschreven. Een aantal komt uit de literatuur, andere zijn speciaal voor FJP ontwikkeld. De scheurvorming is met Lawn’s model beschreven [law75]. Voor de theoretische drukverdeling in de slurry worden de beschrijvingen van Rehbinder [reh76] en Leach en Walker [lea66] gegeven. Uitgaande van de drukverdeling volgens Rehbinder is een voorspelling gedaan van de stationaire voetafdruk die ontstaat met FJP wanneer een cilindrische nozzle wordt gebruikt.

De snelheid van de stroming in het geval van FJP, de banen van de deeltjes in de stroming, en de positie en de snelheid van de deeltjes op het moment dat ze het oppervlak raken zijn berekend uitgaande van de stromingsbeschrijving door Milne-Thomson

[mil77]. De interactie tussen de slijpdeeltjes en het oppervlak is op microscopisch niveau beschreven m.b.v. drie verschillende modellen: ten eerste, de eindig-elementen-aanpak ontwikkeld door Woytowitz e.a. [woy99], ten tweede, een eenvoudige afschatting die in dit proefschrift is afgeleid, gebaseerd op de materiaalafname zoals deze met een SEM waargenomen is. En ten slotte, de afschatting van Finnie [fin58], die de afname door een enkel deeltje beschrijft als functie van de hoek van inval.

Om de afname over een groter gebied te kunnen berekenen, is een model beschreven dat de materiaalafname beschrijft voor het geval dat de nozzle en het werkstuk roteren of translateren t.o.v. elkaar.

Om de uiteindelijke oppervlakteruwheid te kunnen verklaren, is een model ontwikkeld dat de resulterende ruwheid beschrijft als functie van de beginruwheid en een aantal procesparameters. Dit model is gebaseerd op inslagen die plaatsvinden op willekeurige posities op het oppervlak.

Een aantal experimenten wordt beschreven die het effect van verschillende procesparameters op de materiaalafname en op de ruwheid laten zien. Deze parameters zijn o.a. de slurry-parameters zoals het aantal deeltjes, de soort en afmeting van de deeltjes en de deeltjessnelheid, en enkele van de procesparameters zoals de bewerkingstijd, het te bewerken materiaal, de hoek van inval en het soort nozzle.

Enkele belangrijke experimenten die met FJP zijn uitgevoerd, worden ook beschreven, zoals de reproduceerbaarheid van het proces, de haalbare homogeniteit van een bewerkt oppervlak, de degradatie van de slurry als functie van de tijd, de vorming en verwijdering van mid-spatieële frequenties, en de observatie of het proces ductiel of bros is. Vervolgens worden de vormingsmogelijkheden van FJP onderzocht door een voorgeschreven oppervlak te produceren. Ten slotte worden enkele ruwheidsexperimenten beschreven, zoals o.a. de ruwheid als functie van de tijd, het effect van de beginruwheid op de uiteindelijke ruwheid, de drukafhankelijkheid van de ruwheid, en de beste ruwheid die tot nu toe bereikt is.

Ten slotte worden conclusies getrokken en er worden twee alternatieve opstellingen voorgesteld. De belangrijkste conclusies gaan over de nauwkeurigheid van vormen en de mogelijke ruwheidsreductie. Vormcorrecties kunnen met een nauwkeurigheid in diepte van 4% worden uitgevoerd met de huidige opstelling. De materiaalafname is tot op 1% nauwkeurig als de drukfluctuaties en de effecten van diameterverdeling van de slijpdeeltjes uitmiddelen door verschillende keren over het oppervlak te bewegen. Een ruwheidsafname op BK7 is in een enkel-staps-proces (één slurry en een vaste druk tijdens het hele proces) mogelijk van een fijngeslepen oppervlak (gemiddelde ruwheid $R_a = 300$ nm) naar $R_a = 3.6$ nm. De eerste suggestie voor alternatieve technieken die beschreven is, is chemisch ondersteund FJP. Het tweede alternatief is een variant van FJP waarbij de afstand tussen de nozzle en het werkstuk erg klein is. Met dit tweede alternatief zijn enkele experimenten uitgevoerd, en deze zijn ook beschreven.

Fluid Jet Polishing is een nieuwe techniek die goed geschikt is voor het aanbrengen van vormveranderingen op glasoppervlakken, en ook geschikt is voor ruwheidsverminderingen op glas tot enkele nanometers. Moeilijk bereikbare gebieden zijn zeer goed bewerkbaar met FJP.

Acknowledgements

During the four years of my promotion many people have helped me in various different ways. I would like to thank all of them, because my research could not have been carried out without them. First of all, I would like to thank my promotor, prof. Braat, for taking so much time to carefully and meticulously read through anything I supplied in written form. Your remarks have always motivated me to continue my work. I would also like to thank my mentor Eddy for reading through and checking my articles and thesis.

Oliver, I would like to thank you for the many hours of discussions, both over the phone and in person (at home, in the office, on mountains, during meetings and while travelling somewhere) that made me enthusiastic about optics and its production, you helped me understand many aspects of fabrication processes. I admire your organising skills that always made it possible for cooperation projects to exist between the university and 'your' company.

Auch mochte ich 'mein' OFT Team herzlich danken für die angenehme Zusammenarbeit, die vernünftigen Diskussionen, und die Gemütlichkeit in der Schweiz: Torsten, Evelyn, Thomas, Vuli, Marco, Mark und Sebastien, vielen Dank!

Ook Bob, Rob, Maarten, Mariet en Ingeborg van de slijperij hier in Delft wil ik bedanken voor hun hulp en begeleiding als ik zelf iets wilde polijsten. En Adrie natuurlijk voor het coaten van sampels, en het regelen van wafers.

Verder is er nog een grote groep mensen binnen de TU die mij tijdens mijn onderzoek heeft geholpen. Aan het begin van mijn onderzoek was Indro altijd degene die ervoor zorgde dat de opstelling het deed. Jij loste alle problemen met de opstelling in no-time op, je kwam met nieuwe ideeën en wist ze ook uit te voeren.

Gerrit van Dijk, mijn mede-weegschaal-gebruiker, bedankt voor de tijd die je genomen hebt om na te denken over allerlei aspecten van mijn opstelling, zoals bijvoorbeeld over deeltjes in een polyurethaan achtergrondmateriaal als alternatief voor de huidige slurries.

Kees Geerse en John Zevenbergen wil ik bedanken voor het feit dat ik gebruik mocht maken van hun laser-doppler-anemometer. En Marcel Achtsnick voor de interessante discussies over zijn airblasting-opstelling.

De aanpak van het theoretische gedeelte van mijn werk is sterk beïnvloed door de verhelderende discussies met prof. René de Borst van Lucht en Ruimtevaart (eindig-elementen-methode) en met prof. Jerry Westerweel van Werktuigbouwkunde (stroomlijnenberekening).

De vakgroep optica is ook erg belangrijk voor me geweest. Bedankt voor alle gezelligheid jongens! Ik heb met plezier de lunch- en koffiepauzes met jullie doorgebracht. Ook waardeer ik het overleg over mogelijke opstellingen en het meedenken met mij naar aanleiding van mijn werkbespreking-praatjes. Peter S., bedankt dat je na wilde denken over het toepassen van jouw meetapparaat voor het meten van mijn sampels, en dat je je opstelling zelfs voor me hebt omgebouwd.

Mietta, het was gezellig om met je samen te werken, je hebt in je eentje de hele interferometrische opstelling voor het FJP-apparaat gebouwd en aan de praat gekregen. Een hele prestatie!

De ex-vakgroep-mensen wil ik hartelijk bedanken voor hun gezelligheid waardoor ik me gelijk thuis voelde bij optica. Carola, bedankt voor de gezelligheid tijdens alle etentjes en bij de biertjes die we samen dronken, en voor de bijzondere vakantie in Schotland. René, bedankt voor het goede lay-out voorbeeld en de discussies waardoor we soms uren voor de Albert Heijn stonden. Peter en Jantien, onze uitjes waren altijd enorm gezellig, en jullie meelevens tijdens drukke periodes heb ik enorm gewaardeerd. Jullie konden je precies inleven in onze situatie. Robert-Jaap, ik heb je een tijd gemist, zonder kamergenoot is het erg stil.

I would like to thank Prof. Dr. Steve Jacobs, for showing interest in my work, having great discussions with, and for sending me a.o. very small polishing powders and his class notes.

Mijn ouders wil ik bedanken voor het vertrouwen dat ze altijd in mij hebben gehad, en de tijd die ze gestoken hebben in het helpen van mij als ik ergens niet uit kwam. De principes die jullie me hebben bijgebracht, zijn essentieel geweest om hier te komen.

Nolanda, bedankt voor het doorlezen en verbeteren van de nederlandse stukken tekst.

Ten slotte wil ik Roelof ook hartelijk bedanken voor de vele uren die je hebt besteed aan het doorlezen van mijn proefversies en voor alle opmerkingen die het stuk leesbaarder gemaakt hebben. Voor de steun en het advies die je me gaf als ik niet meer wist hoe ik de volgende stap moest zetten. Voor het promoveren vlak voor mij, zodat ik inzicht kreeg in de hele planning en alle knelpunten daarin. Voor het schrijven en aanpassen van programma's om een literatuurdatabase bij te houden en om grafiekjes eenvoudig om te zetten naar een bestand met getalwaarden. En ten slotte voor je eindeloze geduld met mij.

Biography and publications



Silvia Booij was born on October 26th 1976 in Delft, the Netherlands. She graduated from high school in 1994. She studied Applied Physics at Delft University of Technology from 1994 till 1999 when she graduated at the optics research group. The title of her graduation work was: ‘Automatic analysis of digital images from a phase-stepped holographic interferometer’. The goal of the research was to investigate the amount and location of damage to buildings as a result of a blast-wave that typically occurs during an explosion.

Experiments were carried out on scale models of houses in a tunnel in which shock waves could be created. The recording of images with the existing experimental setup had to be automatised, the automatic analysis of the images was realised and a comparison between the calculated and the measured pressure was made. During her study Silvia did her practical work at the Laboratory for Ballistic Research, which is part of TNO. The title of her research there was: ‘Optical representation and quantification of pressure waves in gelatine during the impact of projectiles’. Since September 1999 Silvia has been working on her Ph.D. project at the Optics Research Group in Delft University of Technology on ‘Fluid Jet Polishing’.

Selection of (co-) publications

Publications within the university:

- Practical work report: ‘Optische weergave en kwantificatie van drukgolven in gelatine bij inslag van een projectiel,’ August 1998
- M.Sc. report: ‘Automatic analysis of digital images from a phase-stepped holographic interferometer,’ May 1999

Conference proceedings:

- ‘New developments in measuring techniques at TNO-PML,’ Louk H.J. Absil, Jaap Weerheijm, Rolf M.M. van Wees, and Silvia M. Booij, 16th international symposium military aspects of blast and shock, paper 85, pp. 283-292, 10-15 September 2000

- 'A mathematical model for machining spot in Fluid Jet Polishing,' Silvia M. Booij, Hedser van Brug and Oliver W. Föhnle, Optical Fabrication and Testing, OSA technical digest (Optical Society of America, Washington DC), Quebec, June 2000, pp.70-72
- 'Quantitative surface characterization using a Nomarski microscope,' H. van Brug, S.M. Booij, R.M. van der Bijl, and O.W. Föhnle, Optical Fabrication and Testing, OSA technical digest (Optical Society of America, Washington DC), Quebec, June 2000, pp. 91-93
- 'Nanometer accurate shaping with Fluid Jet Polishing,' Silvia M. Booij, Hedser van Brug, Mandeep Singh, and Joseph J.M. Braat, SPIE's 46th Annual meeting, International symposium on optical science and technology, 29 July-3 August 2001, San Diego, CA. pp.222-232
- 'Computational model for prediction of shaping with FJP and experimental validation,' Silvia M. Booij, Indro Partosoebroto, Joseph J.M. Braat, Hedser van Brug, and Oliver W. Föhnle, OSA Optical Fabrication & Testing conference, Tucson, pp.52-54, June 2002
- 'In-process measurements of material removal in fluid jet polishing,' Hedser van Brug, Mietta Groeneveld, Silvia M. Booij, and Joseph J.M. Braat, 47th Annual Meeting of the SPIE, July 2002, pp. 243-250
- 'Jules Verne - a new polishing technique related to FJP,' Silvia M. Booij, Oliver W. Föhnle, Joseph J.M. Braat, 48th Annual Meeting of the SPIE, August 2003
- 'Optimization of polishing processes by using iTIRM for in-situ monitoring of surface quality,' Oliver W. Föhnle, Mark Meeder, Torsten Wons, Silvia M. Booij, and Joseph J.M. Braat, 48th Annual Meeting of the SPIE, August 2003

Part of a book:

- Jahrbuch für Optik und Feinmechanik 2002, 'In situ Messmethode zum Monitoren der Qualität optischer Oberflächen während des Polierens auf der Maschine und Ihre Anwendung zum Klassifizieren von Polierprozessen,' Oliver Föhnle, Torsten Wons, Evelyn Koch, Sébastien Debruyne, Silvia Booij, Mark Meeder, Hedser v. Brug, Joseph Braat, p. 103-113, 47e Jahrgang, Herausgeber: dr. ing. Wolf-Dieter Prenzel, Schiele & Schoen Berlin, ISBN 3794906632, 2002
- Jahrbuch für Optik und Feinmechanik 2003, 'Politur und Formkorrektur optischer Elemente mittels Fluid Jet Polishing,' Oliver Föhnle, Torsten Wons, Mark Meeder, Silvia Booij und Joseph Braat, 2003

Reviewed journals:

- 'iTIRM as a tool for qualifying polishing processes,' Oliver W. Föhnle, Torsten Wons, Evelyn Koch, Sébastien Debruyne, Mark Meeder, Silvia M. Booij, and Joseph J.M. Braat, Appl. Opt., Vol. 41, No. 19, pp.4036-4038, July 1st 2002
- 'Nanometer deep shaping with Fluid Jet Polishing,' Silvia M. Booij, Hedser van Brug, Joseph J.M. Braat, and Oliver W. Föhnle, Opt. Eng., Vol. 41, No. 8, August 2002, pp.1926-1931

Handout for courses:

- Handout 'Optical Fabrication and Testing,' TN3321, Delft University of Technology, 2002-2003

